Estimation of the Total Solidification Time of a Liquid Phase Change Material Enclosed In Cylindrical and Spherical Containers

by

Levent BİLİR

A Dissertation Submitted to the
Graduate School in Partial Fulfillment of the
Requirements for the Degree of

MASTER OF SCIENCE

Department: Mechanical Engineering
Major: Mechanical Engineering

İzmir Institute of Technology
İzmir, Turkey

September, 2003

We approve the thesis of **Levent BİLİR**

Date of Signature

..... **01.09.2003**

Prof. Dr. Zafer İLKEN

Supervisor

Department of Mechanical Engineering

..... **01.09.2003**

Assist. Prof. Dr. Aytunç EREK

Dokuz Eylül University

Department of Mechanical Engineering

..... **01.09.2003**

Assist. Prof. Dr. Hüseyin GÜNERHAN

Ege University

Department of Mechanical Engineering

..... **01.09.2003**

Assoc. Prof. Dr. Barış ÖZERDEM

Head of Department

ACKNOWLEDGEMENTS

The author would like to express his sincere gratitude to his supervisor, Prof. Dr. Zafer İlken, for his valuable advises and continual support through the project.

The author also wishes to express his thanks to his family for their help and support during his studies.

ABSTRACT

This study investigates the inward solidification process of a phase change material (PCM) encapsulated in a spherical and cylindrical container with a third kind of boundary condition as well as the complete solidification and complete charging time of a cool storage tank which consists of spherical containers filled with a PCM.

The phase change problem inside the containers is modeled in spherical and cylindrical coordinates and solved numerically by using enthalpy method with control volume approach. Computer programs are written in Basic language to determine the dimensionless total solidification time of the PCM held in a spherical and cylindrical container. These programs are run many times by varying the affecting parameters to obtain data sets of the dimensionless total solidification time of PCM. These data sets are then used to derive correlations which express the dimensionless total solidification time of the PCM in terms of the affecting parameters by applying multiple regression analysis.

Another program is written to simulate a cool storage tank with spherical containers. The complete solidification and complete charging time of the tank are calculated by using this program. A parametric study is realized for the cool storage tank by varying the design parameters and the influence of these variations on the complete solidification and complete charging time is investigated.

ÖZ

Bu çalışmada küresel ve silindirik kaplar içerisinde bulunan faz değişim malzemesinin (FDM) üçüncü çeşit sınır koşulu altında içe doğru katılaşması ve içerisinde faz değişim malzemesi bulunan küresel kaplardan oluşmuş bir soğu depolama tankı için toplam katılaşma ve şarj olma süreleri incelenmektedir.

Kaplardaki içe doğru faz değişim problemi silindirik ve küresel koordinatlarda modellenmiş ve sayısal olarak entalpi metodu ve kontrol hacmi yaklaşımı kullanılarak çözülmüştür. Küresel ve silindirik kap içerisinde bulunan FDM'nin toplam katılaşma süresini boyutsuz olarak belirlemek için Basic dilinde programlar yazılmıştır. Bu programlar katılaşma süresi üzerinde etkili olan parametreler değiştirilerek birçok kere çalıştırılmış ve FDM'nin boyutsuz toplam katılaşma süresi için data setleri oluşturulmuştur. Elde edilen bu data setleri FDM'nin boyutsuz toplam katılaşma süresini sonuç üzerinde etkisi olan parametreler cinsinden veren korelasyonların çoklu regresyon analizi yöntemiyle türetilmesinde kullanılmıştır.

Bir başka program da küresel kaplardan oluşmuş soğu depolama tankının simülasyonu için yazılmıştır. Tank için toplam katılaşma ve şarj olma süreleri bu program yardımıyla hesaplanmaktadır. Soğu depolama tankının dizayn parametreleri değiştirilerek bir parametrik çalışma gerçekleştirilmiş ve bu değişimlerin tank için toplam katılaşma ve şarj olma süreleri üzerindeki etkileri incelenmiştir.

TABLE OF CONTENTS

LIST OF FIGURES

LIST OF TABLES

NOMENCLATURE

a: Regression coefficient

A_{cst}: Cross sectional area of the cool storage tank (m^2)

b: Regression coefficient

Bi: Biot number $\left(= \frac{h r_0}{k_s} \right)$

c: Regression coefficient

c_p: Specific heat (j/kgK)

C^*: Dimensionless specific heat $\left(= \frac{c_{p_l}}{c_{p_s}} \right)$

C^+: Dimensionless specific heat $\left(= \frac{c_{p_l}}{c_{p_s}} \right)$

d: Regression coefficient

d_{cst}: Diameter of the cool storage tank (m)

d_{ex}: External diameter of the spherical shell (m)

f: Weighting factor

f_e: Length ratio

h: Convective heat transfer coefficient (W/m^2K)

H: Enthalpy (j/kg)

H^*: Dimensionless enthalpy $\left(= \frac{H}{c_{p_s}\left(T_{initial} - T_\infty\right)} \right)$

i: Nodal point

k: Thermal conductivity (W/mK)

k_{shell}: Thermal conductivity of spherical shell (W/mK)

K^*: Dimensionless Thermal Conductivity $\left(= \frac{k_l}{k_s}; 1 \right)$

K^+: Dimensionless Thermal Conductivity $\left(= \frac{k_l}{k_s} \right)$

L: Latent Heat of Solidification (j/kg)

$\dot{m}$: Mass flow rate (kg/s)

M: Total Number of Layers in the Cool Storage Tank

Nu: Average Nusselt number

Pr: Prandtl number

q: Heat flux (W/m^2)

$\dot{Q}$: Heat transfer rate (W)

r: Radius, Radial position (m)

r_{ex}: External shell radius (m)

r_{in}: Internal shell radius (m)

r_0: Radius of the spherical or cylindrical container (m)

R: Dimensionless radial position $\left(=\frac{r}{r_0}\right)$, Correlation coefficient

Re: Reynolds number

s: Interface position (m)

spcl: Number of spherical containers in a layer

Ste: Stefan number $\left(=\frac{c_{p_s}\left(T_{initial}-T_\infty\right)}{L}\right)$

T: Temperature $\left(°C\right)$

$T_{initial}$: Initial temperature of PCM $\left(°C\right)$

T_m: Phase change temperature $\left(°C\right)$

T_0: Surface temperature $\left(°C\right)$

T_s: Surface temperature of the spherical container $\left(°C\right)$

T_w: Temperature of the Inner Surface of the spherical shell $\left(°C\right)$

T_∞: Coolant fluid temperature $\left(°C\right)$

$\overline{u}$: Mean velocity of working fluid (m/s)

$\dot{V}$: Volumetric flow rate (m^3/h)

x: Position in cartesian coordinates (m), Linear interpolation factor, Independent variable

X: Dimensionless Linear Interpolation Factor

$\hat{y}$: Dependent variable

α: Thermal diffusivity (m^2/s)

δx: x direction distance between two adjacent grid points (m)

Δr: Radial distance between grid points (m)

ΔR: Dimensionless radial distance between grid points

Δt : Time step (s)

Δx : x direction width of the control volume (m)

$\Delta \tau$: Dimensionless time step

ε : Void fraction

μ : Dynamic viscosity (kg/ms)

θ : Dimensionless temperature $\left(= \dfrac{T - T_\infty}{T_{initial} - T_\infty} \right)$

θ_m : Dimensionless phase change temperature $\left(= \dfrac{T_m - T_\infty}{T_{initial} - T_\infty} \right)$

ρ : Density (kg/m^3)

τ : Dimensionless time $\left(= \dfrac{\alpha_s t}{r_0^2} \right)$

τ_{total} : Dimensionless total solidification time

Subscripts

e: Control volume face between P and E

E: Neighbour grid point on the east side

l: liquid phase

L: layer number

P: Central grid point under consideration

s: Solid phase, Interface

w: Control volume face between P and W

W: Neighbour grid point on the west side

wf: Working fluid

Superscript

k: Time level

CHAPTER 1

INTRODUCTION

In 1973, the major oil producing countries in the Middle East established an oil embargo. This action made it very evident that the economic well being of the industrial countries of the world and their inhabitants depended on their energy sources which were controlled by other countries. Consequently, the industrial countries such as the United States and Western Europe etc. started to study the ways in which they could reduce their energy source dependence on others. As the result of these studies it is recommended to develop alternative energy sources (such as solar, wind and geothermal energy) to oil and natural gas, and also to use the present energy sources effectively. At this point it is realized that energy storage devices could greatly assist in improving the overall efficiency of large energy producing units through load leveling, decrease energy demands through the use of waste heat recovery and allow alternative sources of energy to be utilized more effectively. An example of these energy storage devices is the storage tanks used in thermal applications which increase the efficiency of thermal systems. These tanks temporary hold the thermal energy for later use. For example, solar energy systems can use a storage tank to store the heat energy collected to be used when there is no sun, which is the energy source of the system. Similarly, cool storage tanks are used in air conditioning systems to store the cool generated in off-peak periods to be used in on-peak periods. In this thesis, cool storage is focused on and will be described briefly.

1.1 COOL STORAGE SYSTEMS

Cool storage systems remove heat from a thermal storage medium during periods of low cooling demand. The stored cool is later used to meet an air conditioning or process-cooling load. The cool storage medium can be chilled water, ice or eutectic salt phase change material.

These systems help to reduce the peak demand on the generation and distribution systems of electric utility companies as for many utilities the peak demand is driven by the air conditioning load on the hottest days of the year. This reduction is

accomplished by shifting the on-peak energy consumption to off-peak periods. In this way, more peak capacity is available for other uses and off-peak capacity of utilities is more fully used. To promote the shifting of on-peak energy consumption to off-peak periods utility companies generally apply higher and lower electricity rates during on-peak and off-peak hours, respectively. Cool storage systems permit such a shift by decoupling chiller operation from instantaneous loads [1].

The main advantages of cool storage systems over conventional air conditioning systems are [2];

- Compared with a conventional air conditioning system, the refrigeration plant capacity can be substantially reduced, as it no longer has to cope with the peak building load.
- The chiller plant operates at 100% of its rated capacity, throughout its period of operation in the cool storage system, therefore the plant works at its optimum efficiency unlike conventional systems, which operate on part load for most of their working life.
- Cool storage systems shift the refrigeration electricity load to the nighttime and the ambient temperatures at night are substantially lower than in the daytime. Consequently, there is an improvement in chiller efficiency and a constant generating load can be maintained, ensuring efficient use of the plant, compared with the daytime operation.
- The larger air temperature difference offered by some cool storage technologies over the air handling units allows a reduction in circulated air volume, results in smaller air handling units, piping and air handlers, less electrical equipment and wiring and also reduces the size and cost of ductwork.
- The installation of the cool storage systems in buildings will significantly reduce chiller plant capacities and consequently the size of the refrigerant gas charges, thereby reducing the emission of harmful CFCs into the atmosphere, which helps reduce both the depletion of the ozone layer and the formation of the greenhouse effect.

1.1.1 Operating Strategies

Some operating strategies are available to decouple chiller operation from instantaneous loads. These are often classified as either full storage or partial storage. These terms refer to the amount of on-peak cooling load that is shifted to off-peak Additional variations on these strategies are possible by base loading or other sequencing of multiple chillers.

(a) Full Storage

A full storage or load shifting strategy shifts the entire peak-cooling load to off-peak hours as shown in figure 1.1. The system operates at full capacity during all non-peak hours on the hottest days to charge storage. Full storage systems fully decouple the operation of the cooling generating equipment from the peak-cooling load. The peak-cooling load is met through the use of storage while the refrigeration equipment does not run. This strategy is most attractive when peak demand charges are high or the peak period is relatively short [3].

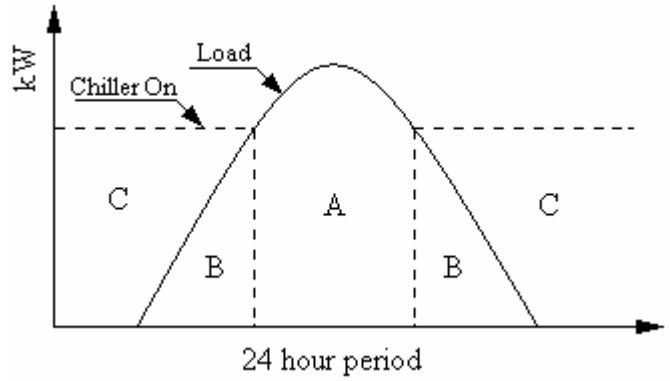

Fig 1.1 Full Storage Operating Strategy

(A:Storage meets the load, B:Chiller meets the load directly, C:Chiller charging storage)

(b) Partial Storage

In a partial storage method, part of the on peak-cooling load is met from storage while the rest of the load is met by the chiller. The chiller is sized at a smaller capacity than the design load. Partial storage operating strategies can be subdivided into load leveling (figure (1.2a)) and demand limiting (figure (1.2b)) operations.

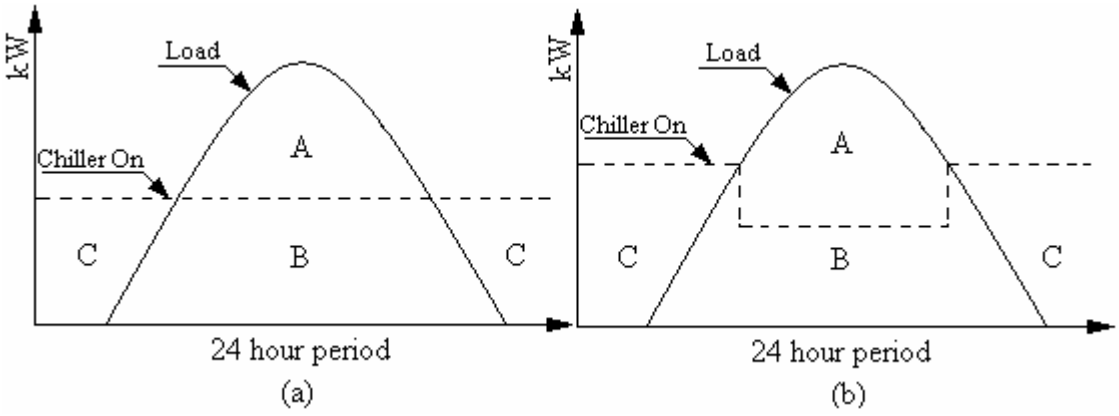

Fig 1.2 Partial Storage (a) Load Leveling (b) Demand Limiting

In a load leveling system the chiller runs at its full capacity for 24 hours on the hottest days. The strategy is most effective where the peak-cooling load is much higher than the average load.

In a demand limiting system the chiller runs at reduced capacity during peak hours. The demand limiting approach represents a middle ground between load shifting and load leveling [3].

1.1.2 Types of Cool Storage Systems

(a) Chilled Water Storage Systems

In these systems sensible heat capacity of water is used to store cooling. Water is cooled by a chiller and stored in a tank in stratified layers. The cooling capacity of the system depends on the temperature differential across the stratified storage tank. The disadvantage of this method is that the tanks used for chilled water storage are often very large and may be difficult to site due to space limitations. The outside and inside view of a chilled water storage tank are shown in figure (1.3) and (1.4)

Fig 1.3 Outside view of a chilled water storage tank

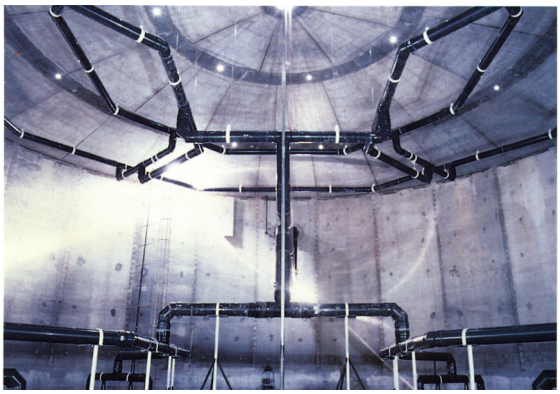

Fig 1.4 Inside view of a chilled water storage tank

These systems use conventional water chillers, because chilled water storage tanks are charged with water at 4-7 °*C* [1].

(b) Ice Harvesting Systems

These systems consist of a special evaporator section which is installed above an open tank. In this tank a combination of water and ice is stored. Water is pumped out of the storage tank and distributed over the evaporator surfaces where it is chilled or frozen.

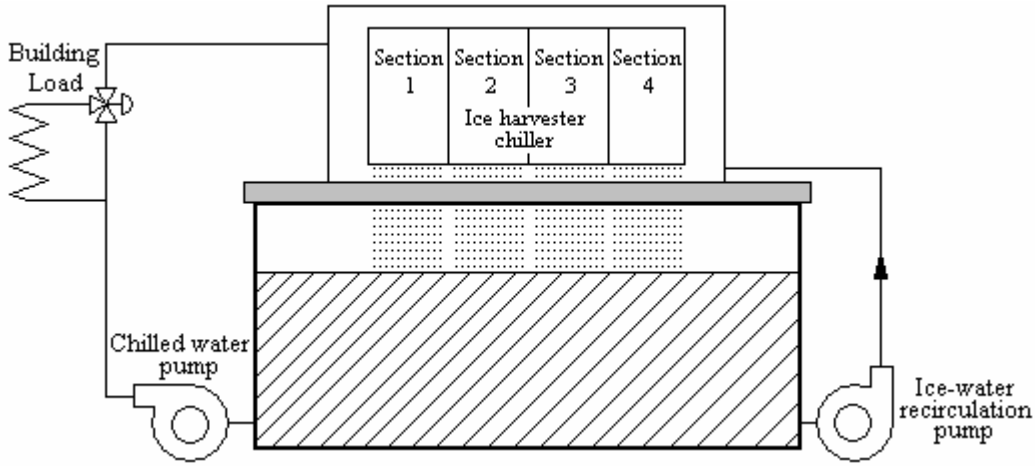

Fig 1.5 Ice Harvesting System

If water is near the freezing temperature when it enters the evaporator ice making mode is selected automatically and the layer of ice formed on evaporator surfaces is dropped periodically into the storage tank by activating a defrost cycle. When the temperature of the water is above the freezing point it is only chilled and falls into the storage tank.

The discharge of the cool storage tank is done by circulating the ice water taken from the tank to the building load [1].

(c) External Melt Ice-On-Coil Storage Systems

In these systems ice is built and stored on the surface of a heat exchange coil surrounded with water in a tank. Figure (1.6) illustrates an external melt storage tank and internal piping.

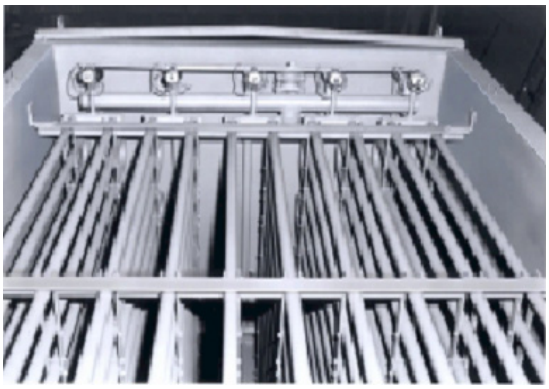

Fig 1.6 External Melt Storage Tank and Internal Piping

Ice is formed on the outside of the heat exchange tubes by circulating liquid refrigerant or a secondary coolant inside the tubes. When the warm return water is circulated through the tank, the ice on the tubes melts and chills the passing water which is then used to meet the building load. These systems require a chiller capable of generating charging temperatures of –3 to $-12\,°C$ depending on the thickness of ice to be formed [1].

(d) Internal Melt Ice-On-Coil Storage Systems

A secondary coolant fluid is circulated through the tubes submerged in a water tank to form ice on the tubes in internal melt ice on coil systems. Figure 1.7 illustrates an internal melt storage tank.

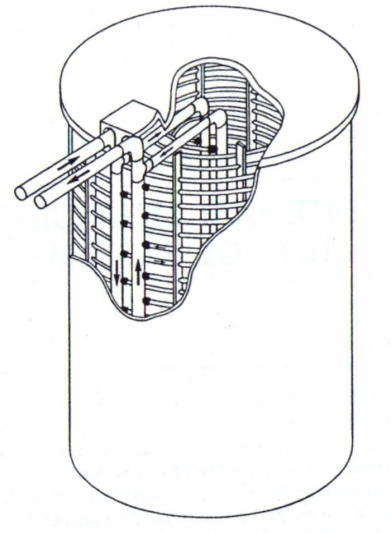

Fig 1.7 Internal Melt Ice Storage Tank

Discharging of the stored cool is realized by circulating warm secondary coolant through the tubes which causes the ice layer formed on the tubes to melt. These systems require chillers capable of producing charging temperatures of –6 to –3 $°C$ [1].

(e) Encapsulated Phase Change Material Systems

Encapsulated phase change material systems store the phase change material in a number of spherical or cylindrical containers placed inside a storage tank as shown in figure (1.8)

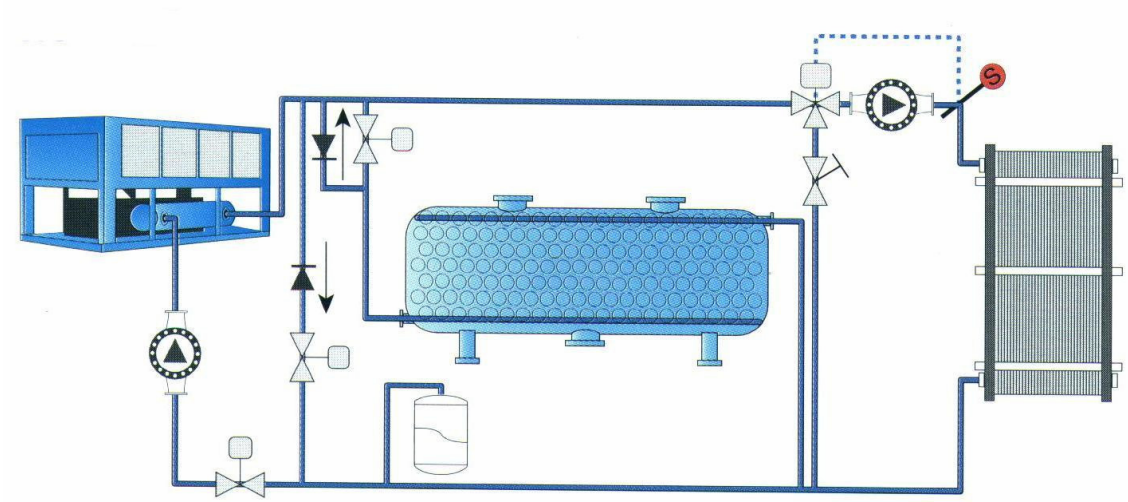

Fig 1.8 Schematic View of an Encapsulated Phase Change Material Storage System

The charging of the storage tank is accomplished by circulating a secondary coolant such as ethylene glycol through the tank, which cause the phase change material inside the containers to give its latent heat and freezes. During discharge, the warm secondary coolant carrying heat from the load flows outside the containers, the solid phase change material held inside the containers melts and the temperature of the warm secondary coolant is decreased. Figure (1.9) illustrates the formation of solid PCM in spherical and cylindrical containers during charging and discharging [1].

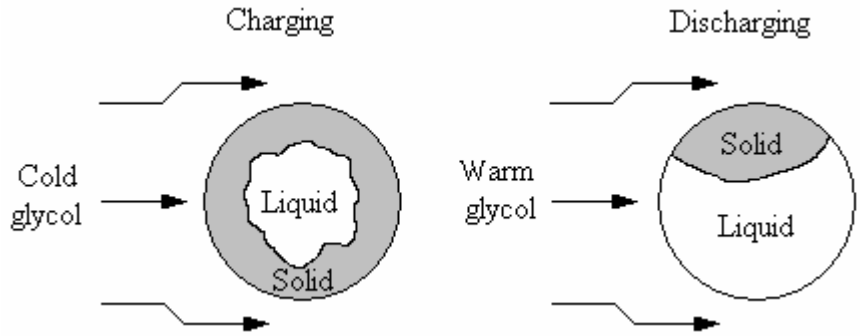

Fig 1.9 Charge and Discharge of Encapsulated Phase Change Material Storage System

CHAPTER 2

LITERATURE SURVEY

In this study, encapsulated phase change material systems described at the end of chapter 1 are investigated. Firstly, the total solidification time of a single spherical or cylindrical container, which are the basic elements of encapsulated storage systems, with a third kind boundary condition is determined. Secondly, an encapsulated storage tank which consists of spherical containers is investigated. To find the total solidification time of single containers, the inward solidification process inside the container is solved in spherical and cylindrical coordinates. Some of the studies related to this subject are summarized below;

Tao [4] presented a numerical method and graphs of generalized solutions for a moving interface problem of freezing a saturated liquid inside a cylindrical or a spherical container with a constant heat transfer coefficient, as well as melting a saturated solid. The graphical results of the position of the interface as a function of time, temperature profile at the instant of freezing at the center, the time required to freeze the center of a cylinder and a sphere are given for different dimensionless parameters. The generalized solutions can also be used for melting a solid inside a cylinder or a sphere by switching the notations of liquid and solid phases.

Cho and Sunderland [5] investigated both inward and outward phase changes of spherical bodies. The initial temperature of the system is assumed constant at the fusion temperature and the boundary surface temperature is assumed to change instantaneously. A simple approximation in which the temperature distribution is assumed to be similar to the exact solution for the one-dimensional Stefan problem is obtained and the interface position is found as a function of time. However this approximation is valid only for small time. Then a finite difference formulation is derived and evaluated to check the accuracy of the approximation.

Riley, Smith and Poots [6] presented an analytical study of the inward freezing of a sphere or a circular cylinder, initially molten and at the fusion temperature, when

the outside surface is suddenly cooled. The perturbation method is used in the solution and the treatment assumes constant thermal properties and that the ratio of the latent heat to the sensible heat of the substance is large. The major simplifying assumptions made are that the melt is always at its fusion temperature and that there exists at all times a sharply-defined line of division, the solidification front, between the solid and the liquid. These assumptions enable straightforward perturbation solutions for the temperature and the inward travel of the front to be derived. They presented a formula determining the time required for the cylinder or sphere to become totally solidified and the temperature profile at that moment.

Chuang and Szekely [7] used Green's Function Method to solve the cylindrical phase change problem under third kind of boundary condition. They investigated the melting (and initial solidification) of an iron rod immersed into an iron-carbon melt. The application of the fundamental Green's function to the moving boundary problem has converted the non-linear differential equations into a single transcendental equation which may be solved by simple numerical calculations. They present the movement of the interface during solidification and melting as a function of time.

Shih and Tsay [8] generated successive solutions for the instantaneous frozen layer thickness and temperature profile for the freezing of a saturated liquid inside cylindrical containers with constant heat transfer coefficient by the use of an analytical iteration technique. Successive solutions for freezing of a saturated liquid outside cylinders are also derived. The comparison of their results with experimental and numerical solutions shows satisfactory coincidence.

Pedroso and Domoto [9] applied the method of strained coordinates to obtain a perturbation solution for spherical solidification of a saturated liquid. The solution is uniformly valid and can be applied as the freezing front approaches the center where the regular perturbation solution is found to diverge. The wall temperature of the sphere is assumed constant. They present an equation which gives normalized freezing time of the sphere and normalized temperature distribution at the instant of freezing of the center.

Solomon [10] presented an analytical expression for the total melting time of a simple body (a slab, a cylinder and a sphere), initially at its critical temperature, subject to a convection boundary condition. Freezing time for an initially liquid PCM at the critical temperature can also be found from the expression proposed by substitution of the solid PCM properties.

Voller and Cross [11] developed a simple, explicit algorithm to produce accurate solutions of phase change problems in circular regions with spatially uniform boundary conditions. The governing equations are reformulated in terms of enthalpy and they relate the numerical value of the enthalpy at a node to the position of the phase change boundary. On study of numerically predicted results a single non-dimensional expression, which provides a prediction of the solidification/melting time of a circular cylinder is derived. This expression is subsequently used to provide upper and lower bounds on solidification/melting times for general symmetric cylindrically shaped regions with spatially uniform boundary conditions. The lower bound can be found by calculating the solidification time of a circular cylinder with a diameter value which is equal to the shortest possible straight line which passes through the cross section's center of gravity. The upper bound is determined by the calculation of the solidification time of a circular cylinder with the same cross-sectional area as the original cylinder.

Hill and Kucera [12] developed a new semi-analytical procedure for the problem of freezing a saturated liquid inside a spherical container and including the effect of radiation at the container surface. They give successive estimates of the time for complete solidification of the sphere. In addition an integral formulation is adopted to independently establish bounds for the time for complete solidification. The upper and lower bounds obtained are the standard order one corrected estimate of the time for complete solidification and the pseudo steady state estimate of the time for complete solidification, respectively. Numerical values of successive estimates for the complete solidification time indicate firstly satisfactory convergence and secondly that they are consistent with the bounds independently established.

Milanez [13] developed a correction factor which when applied to the exact solution of the semi-infinite slab will give a solution valid for the sphere. Exact solutions for the slab are compared with numerical solutions obtained for the sphere

under the same conditions and a correction factor is obtained. It is found that the ratio between the total solidification time for the sphere and for the plane increases with increasing Stefan number, but it is not affected by the Biot number. This fact suggested that the correction factor to be obtained can be a function only of the Stefan number, independently of the Biot number. A polynomial type expression is obtained for the dimensionless solidification time for the sphere.

Prud'Homme, Nguyen and Nguyen [14] applied the method of strained coordinates to study the inward solidification in slabs, cylinders and spheres. Constant thermal properties are assumed throughout the analysis for the liquid, which is initially at the fusion temperature. A unified approach is adopted that allows the simultaneous treatment of the problem in plane, cylindrical and spherical geometries for three different types of boundary condition. A general recurrence formula is derived for the determination of the series solutions up to any desired order of the Stefan number. A comparison is made with numerical and regular perturbation solutions in the plane case to illustrate the usefulness and the validity of the method.

Caldwell and Chan [15] applied a numerical scheme based on the enthalpy method to spherical solidification. The phase change material inside the spherical vessel is at its freezing temperature initially and a constant temperature boundary condition is applied on the surface. The method provides a means to track the position of the phase change front and is compared to the heat balance integral method, which is a front tracking method. The results show that the two methods compare well over a wide range of the Stefan number, except when the Stefan number is small.

Ismail and Henriquez [16] presented a numerical study of the solidification of phase change material enclosed in a spherical shell. The numerical solution is realized using the moving grid approach. The mathematical model is based on pure conduction in the PCM subject to boundary conditions of constant temperature or convective heat transfer on the external surface. The model is validated by comparison with available similar models. The model is then used to predict the effect of the size of the spherical shell, shell thickness, shell material and the external wall temperature on the solidified mass fraction and the time for complete solidification.

Günerhan [17] presented correlations for the dimensionless solid liquid interface position in cartesian and cylindrical geometries. In the study, physical relations between the velocities of the isotherms for two heat conduction problems, one of which has phase change while the other has not, with the same initial and boundary conditions are investigated. These relations are found mathematically depending on the physical properties of the phases and the common parameters of two different problems. In this way, it is possible to find the position of solid liquid interface by using the analytical solutions and the relation itself, not solving the phase change problem. One dimensional phase change problem is solved in cartesian and cylindrical coordinates for three different kind of boundary conditions via enthalpy method. The results are correlated with the analytical solutions of the problem having same geometry and conditions but without phase change and correlations with high correlation coefficients are obtained.

The studies given above are investigated the solidification of a single spherical and cylindrical container with simplified boundary conditions (first, second and third kind of boundary condition). So, their results cannot be used for the analysis of a cool storage tank having many spherical or cylindrical containers. Since in a cool storage tank with spherical or cylindrical containers the temperature of the coolant fluid passing over the containers and the convection coefficient between the coolant fluid and container are not constant, the results obtained for a single sphere or cylinder with a third kind of boundary condition are not appropriate for the whole cool storage tank. The studies taking into account this condition for the cool storage tanks using spherical and cylindrical containers are given below;

Saitoh and Hirose [18] presented a theoretical and experimental investigation of the transient thermal characteristics of a phase change thermal energy storage unit using spherical capsules. A simulation program that considers rigorously transient aspects of both the surrounding heat transfer fluid and the phase change material packed inside the spherical capsule is developed. In the simulation model the following major assumptions and restrictions are made;

- Quasi-steady approximation is valid for heat transmission inside the spherical capsule.
- Phase change occurs only at melting and freezing temperature.

- Spherically symmetric freezing or melting is assumed, i.e. heat conduction is dominant.
- Volumetric change due to phase change is negligible.
- Liquid is initially at melting temperature.

The coupled equations are solved numerically by the ordinary three-point explicit difference method.

The overall thermal response of the thermal energy storage unit is described with variation of the capsule diameter, the flow rate, the kind of PCM etc. It is found that the capsule diameter plays a dominant role on the performance of the unit. The effect of the temperature difference between the inlet temperature of heat transfer fluid and freezing temperature is also investigated and it is stated that the small temperature difference leads to a small Stefan number, thereby requiring a long time to finish solidification. Varying the capsule material shows that for a capsule with stainless steel, aluminium and plastic shells almost the same results are obtained, so it is recommended that the plastic material, which is also cost effective and corrosion resistant, can be considered as a promising candidate for practical applications. The simulation results are then compared with experimental observations.

Green and Vliet [19] presented an analytical and experimental investigation of the transient thermal response of a latent heat storage unit. The unit consists of a phase change material encapsulated in rectangular slabs, cylindrical tubes or spherical shells and a rectangular tank. In the analysis two coupled governing partial differential equations that describe the model are derived and then non-dimensionalized and solved numerically. The PCM solid-liquid front is assumed to progress uniformly from the containment walls, all thermophysical and transport properties are assumed constant, sensible heat storage in PCM and its container is assumed to be negligible and one dimensional heat conduction is assumed to exist in PCM. Initially the PCM and heat transfer fluid are at the saturation temperature. Analytical results are presented in terms of phase change material quality and heat transfer fluid temperature. In the experimentation, a baffled shell and tube type heat exchanger was fabricated to provide data for a preliminary evaluation of the model. A comparison of experimental and analytical results shows that while the analysis predicts slightly conservative results, it appears to be a very promising tool for designing and sizing latent heat storage units.

Beasley, Ramanarayanan and Torab [20] presented a computational model of the transient thermal response of a packed bed of spheres containing a phase change material. A one dimensional separate phases formulation is used to develop a numerical analysis of the dynamic response of the bed which is subject to the flow of a heat transfer fluid, for arbitrary initial conditions and inlet fluid temperature temporal variations. Phase change models are developed for both isothermal and non isothermal melting behaviours. Axial thermal dispersion effects are modelled, including intraparticle conduction effects. Results from the model for a commercial sized thermal storage bed for both the energy storage and recovery periods are presented. Experimental measurement of transient temperature distributions in a randomly packed bed of uniform spheres containing a PCM for a step change in inlet air temperature are reported for a range of Reynolds number.

Chen, Chen, Tin, Lee and Ke [21] experimentally investigated the thermal performance and the pressure drop of an encapsulated thermal storage tank during the charging process. A PVC hollow cylinder is used as the thermal storage tank. The cylindrical capsules inside the thermal storage tank utilize water added with nucleation agents as the phase change material, and the coolant is the aqueous solution of ethylene glycol. A series of experiments were carried out to investigate the effects of the inlet coolant temperature and coolant flow rate on nucleation of capsules, heat transfer and pressure drop of the tank. The results indicate that cool energy can be fully stored in the form of latent heat when the inlet coolant temperature is set below the temperature with 100% nucleation probability (-1 $^{\circ}C$ for this case). If the inlet temperature is greater than this value, increasing flow rate does not have any effect on crystallization of the PCM and it remains subcooled in liquid phase in capsules. On the contrary, the larger flow rate can reduce the time of crystallization under the condition of inlet coolant temperature with 100% probability of nucleation. The lower the inlet coolant temperature and the larger the coolant flow rate, the more efficient the storage tank. A correlation for the pressure drop of coolant during a charging process is also developed.

Cho and Choi [22] investigated the thermal characteristics of paraffin in spherical capsules in a storage tank during freezing and melting processes. Experiments were performed with paraffin, i.e., n-tetradecane and a mixture of n-tetradecane (40%) and n-hexadecane (60%) and water. The parameters were Reynolds number and the

inlet temperature during the freezing process and initial temperature during the melting process for a PCM thermal storage system. The phase change period for the capsule at the edge of a storage tank was shorter than that at the center due to smaller porosity at the center than the edge of the storage tank. Water showed a bigger subcooling than paraffin. It took longer for water to reach the dimensionless thermal storage capacity of 1 during the freezing process and shorter during the melting process than that of paraffin. The average heat transfer coefficients were affected by the inlet or initial temperature and Reynolds number more during the melting process than during the freezing process due to a natural convection effect during the melting process. The average heat transfer coefficients for paraffin were larger by a maximum of 40% than those for water during the freezing and melting processes.

Ismail and Henriquez [23] investigated a storage system with spherical capsules filled with phase change material. The capsules are packed in a cylindrical tank. In th estudy the cylindrical tank is divided into layers whose height is equal to a spherical capsule diameter. The solidification of PCM inside the capsules is treated by using a one dimensional phase change model with convective boundary condition. The convection present in the liquid phase of the PCM is treated by using an effective heat conduction coefficient in the liquid region of the PCM. The solution of the differential equations is realized by the finite difference approximation and a moving grid inside the spherical capsules. The geometrical and operational parameters of the system are investigated both numerically and experimentally and their influence on the charging and discharging times was investigated.

CHAPTER 3

CONTROL VOLUME FORMULATION AND ENTHALPY METHOD IN PHASE CHANGE PROBLEMS

In this chapter, control volume formulation which is used to discretize differential equations and enthalpy method which is a numerical solution method for phase change problems are explained in detail. The application of control volume formulation and enthalpy method is firstly explained for rectangular coordinates and then the changes to be made when they are used in spherical and cylindrical coordinates are described.

3.1 CONTROL VOLUME FORMULATION

Control volume formulation is a useful method to discretize a differential equation. The calculation domain is divided into a number of nonoverlapping control volumes such that there is one control volume surrounding each grid point. The differential equation is integrated for each control volume [24].

Unsteady one dimensional heat conduction equation for rectangular coordinates will be analysed as an example;

$$\rho c_p \frac{\partial T}{\partial t} = \frac{\partial}{\partial x}\left(k \frac{\partial T}{\partial x} \right) \tag{3.1}$$

where k is the thermal conductivity and T is the temperature.

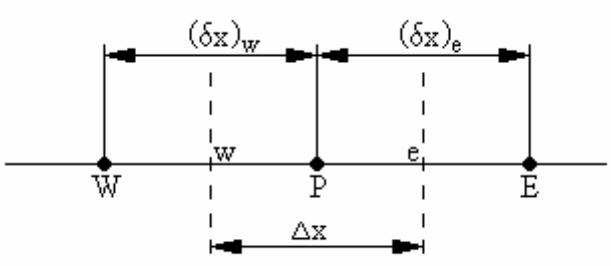

Fig 3.1 Grid Point Cluster

The grid point cluster shown in figure (3.1) is employed to derive the discretization equation. The grid point P, which has grid points E and W as its

neighbours (E denotes the east side, i.e., the positive x direction, while W stands for west or negative x direction), is focused. The dashed lines show the faces of the control volume and their exact locations are not important for the time being. The letters e and w denote these faces. For the one-dimensional problem under consideration, a unit thickness in the y and z directions will be assumed. Thus, the volume of the control volume shown in figure (3.1) is $\Delta x \times 1 \times 1$.

If ρ and c_p are assumed to be constant and equation (3.1) is integrated over the control volume and over the time interval from t to $t + \Delta t$, the discretization equation is obtained as;

$$\rho c_p \int_{\Delta V} \int_{t}^{t+\Delta t} \frac{\partial T}{\partial t} dt dV = \int_{t}^{t+\Delta t} \int_{\Delta V} \frac{\partial}{\partial x}\left(k \frac{\partial T}{\partial x} \right) dV dt \qquad , \qquad dV = dx \times 1 \times 1 \tag{3.2}$$

$$\rho c_p \int_{x_w}^{x_e} \int_{t}^{t+\Delta t} \frac{\partial T}{\partial t} dt dx = \int_{t}^{t+\Delta t} \int_{x_w}^{x_e} \frac{\partial}{\partial x}\left(k \frac{\partial T}{\partial x} \right) dx dt \tag{3.3}$$

For the representation of the term $\frac{\partial T}{\partial t}$, it is assumed that the grid point value of T prevails throughout the control volume. Then,

$$\rho c_p \int_{x_w}^{x_e} \int_{t}^{t+\Delta t} \frac{\partial T}{\partial t} dt dx = \rho c_p \left(T_P^{k+1} - T_P^{k} \right) \left(\underbrace{x_e - x_w}_{\Delta x} \right) \tag{3.4}$$

where k and k+1 represent successive time levels.

If equation (3.4) is replaced in equation (3.3);

$$\rho c_p \left(T_P^{k+1} - T_P^{k} \right) \Delta x = \int_{t}^{t+\Delta t} \left[\left(k \frac{\partial T}{\partial x} \right)_{x=x_e} - \left(k \frac{\partial T}{\partial x} \right)_{x=x_w} \right] dt \tag{3.5}$$

$$\rho c_p \left(T_P^{k+1} - T_P^{k} \right) \Delta x = \int_{t}^{t+\Delta t} \left[\left(k_e \frac{T_E - T_P}{(\delta x)_e} \right) - \left(k_w \frac{T_P - T_W}{(\delta x)_w} \right) \right] dt \tag{3.6}$$

At this point an assumption should be made about how T_P, T_E and T_W vary with time from t to $t + \Delta t$. Many assumptions are possible and some of them can be generalized by proposing;

$$\int_{t}^{t+\Delta t} T_P dt = \left[f T_P^{k+1} + (1-f) T_P^k \right] \Delta t \tag{3.7}$$

where f is a weighting factor between 0 and 1.

Using similar formulas for the integrals of T_E and T_W, equation (3.8) can be derived from equation (3.6);

$$\begin{aligned} \rho c_p \left(T_P^{k+1} - T_P^k \right) \frac{\Delta x}{\Delta t} = f & \left[\left(k_e \frac{T_E^{k+1} - T_P^{k+1}}{(\delta x)_e} \right) - \left(k_w \frac{T_P^{k+1} - T_W^{k+1}}{(\delta x)_w} \right) \right] \\ + (1-f) & \left[\left(k_e \frac{T_E^k - T_P^k}{(\delta x)_e} \right) - \left(k_w \frac{T_P^k - T_W^k}{(\delta x)_w} \right) \right] \end{aligned} \tag{3.8}$$

f = 0 leads to explicit scheme and f = 1 to the fully implicit scheme.

In equation (3.8), the thermal conductivity k_e has been used to represent the value of k pertaining to the control volume face e; similarly, k_w refers to the interface w. When the conductivity is a function of x, the value of k is often known at the grid points W, P, E and so on. A prescription is then needed for evaluating the interface conductivity in terms of these grid point values.

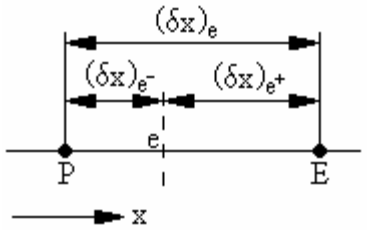

Fig 3.2 Distances Associated with Interface e

The most straightforward procedure for obtaining the interface conductivity k_e is to assume a linear variation of k between points P and E. Then,

$$k_e = f_e k_P + (1 - f_e) k_E \tag{3.9}$$

where the interpolation factor f_e is a ratio defined in terms of the distances shown in figure (3.2)

$$f_e = \frac{(\delta x)_{e^+}}{(\delta x)_e} \tag{3.10}$$

If the interface e is the midway between grid points, f_e is 0.5 and k_e is equal to the arithmetic mean of k_P and k_E.

An alternative to this approach, which is based on the steady, one-dimensional situation in which conductivity varies in a stepwise fashion from one control volume to the next, is developed. The heat flux at the interface e in this situation is;

$$q_e = k_e \frac{T_P - T_E}{(\delta x)_e} \tag{3.11}$$

If it is assumed that the control volume surrounding the grid point P is filled with a material of uniform conductivity k_P, and the one around E with a material of uniform conductivity k_E the heat flux can be written as;

$$q_e = \frac{T_P - T_E}{\frac{(\delta x)_{e^-}}{k_P} + \frac{(\delta x)_{e^+}}{k_E}} \tag{3.12}$$

Combination of equations (3.11) and (3.12) yields;

$$k_e = \left(\frac{1 - f_e}{k_P} + \frac{f_e}{k_E} \right)^{-1} \tag{3.13}$$

When the interface e is placed midway between P and E $(f_e = 0.5)$;

$$k_e^{-1} = 0.5\left(k_P^{-1} + k_E^{-1}\right) \tag{3.14a}$$

or

$$k_e = \frac{2k_P k_E}{k_P + k_E}$$

(3.14b)

Equation (3.14b) shows that k_e is the harmonic mean of k_P and k_E.

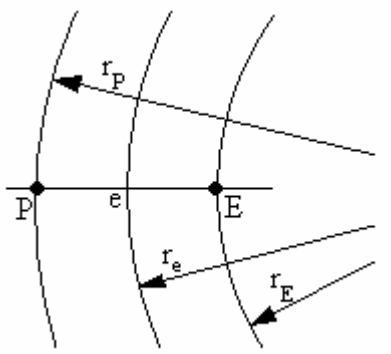

Fig 3.3 Distances Associated with Interface e in Spherical and Cylindrical Coordinates

If this method is applied for spherical coordinates;

The steady state heat flux in radial direction for the composite slab between P and E is [25];

$$q_e = k_e \frac{T_E - T_P}{r_e^2\left(\frac{1}{r_E} - \frac{1}{r_P}\right)}$$

(3.15)

or,

$$q_e = \frac{T_E - T_P}{r_e^2\left[\frac{1}{k_E}\left(\frac{1}{r_E} - \frac{1}{r_e}\right) + \frac{1}{k_P}\left(\frac{1}{r_e} - \frac{1}{r_P}\right)\right]} \tag{3.16}$$

From these two equations the thermal conductivity for the interface e can be found as;

$$k_e = \frac{\frac{1}{r_E} - \frac{1}{r_P}}{\frac{1}{k_E}\left(\frac{1}{r_E} - \frac{1}{r_e}\right) + \frac{1}{k_P}\left(\frac{1}{r_e} - \frac{1}{r_P}\right)} = \frac{r_e(r_P - r_E)k_E k_P}{r_P(r_e - r_E)k_P + r_E(r_P - r_e)k_E} \tag{3.17}$$

Similarly, for the cylindrical coordinates steady state heat flux can be written as [25];

$$q_e = k_e \frac{T_E - T_P}{r_e \ln\frac{r_P}{r_E}} \tag{3.18}$$

or,

$$q_e = \frac{1}{r_e} \frac{T_E - T_P}{\frac{\ln\left(r_P / r_e\right)}{k_P} + \frac{\ln\left(r_e / r_E\right)}{k_E}} \tag{3.19}$$

So, the thermal conductivity for the interface e in cylindrical coordinates is;

$$k_e = \frac{\ln\left(r_P / r_E\right)}{\frac{\ln\left(r_P / r_e\right)}{k_P} + \frac{\ln\left(r_e / r_E\right)}{k_E}} = \frac{k_P k_E \ln\left(r_P / r_E\right)}{k_E \ln\left(r_P / r_e\right) + k_P \ln\left(r_e / r_E\right)} \tag{3.20}$$

3.2 ENTHALPY METHOD

The enthalpy method is a simple and flexible technique for solving heat transfer problems involving phase change. Instead of working entirely in terms of the temperature of a material, an enthalpy function is defined which represents the total heat content per unit mass of the material. The advantage of such a reformulation is that the necessity to carefully track the location of the solid-liquid interface is removed [26].

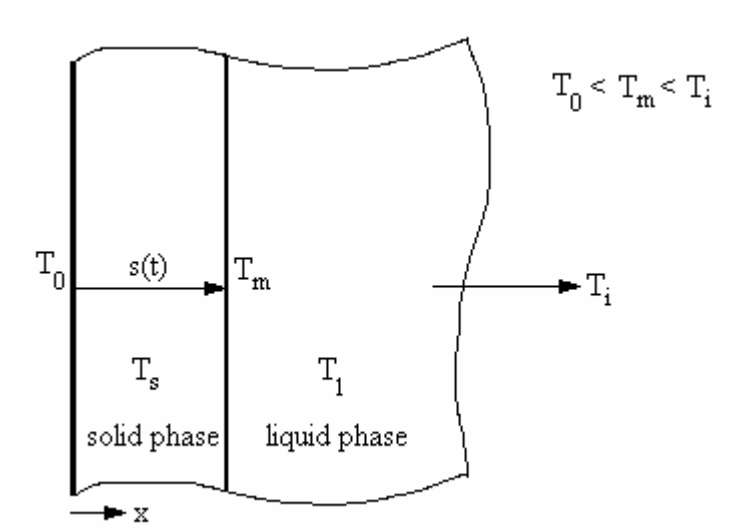

Fig 3.4 Heat Conduction with Phase Change Problem for Half Space

As an example, the problem of heat conduction with phase change for half space is considered. The material which fills the half space $x \geq 0$, is initially in liquid phase at a constant temperature T_i which is higher than T_m (phase change temperature). At time t=0 the temperature of the surface x=0 is instantaneously lowered and maintained at

$T(0,t)=T_0$ which is lower than T_m. This will cause a layer of solid to be formed adjacent to the surface x=0 and as time increases this layer will be expand into the liquid. Assuming that the heat transfer is only due to conduction the problem can be described by a pair of Fourier heat conduction equations;
one for the solid,

$$\frac{\partial}{\partial x}\left(k_s \frac{\partial T_s}{\partial x}\right) = \rho c_{p_s} \frac{\partial T_s}{\partial t} \qquad , \qquad 0 \le x < s(t) \tag{3.21a}$$

and the other for the liquid,

$$\frac{\partial}{\partial x}\left(k_l \frac{\partial T_l}{\partial x}\right) = \rho c_{p_l} \frac{\partial T_l}{\partial t} \qquad , \qquad s(t) \le x \tag{3.21b}$$

At the phase change boundary (i.e. the solid-liquid interface) the following conditions hold;

- $T_l = T_s = T_m \qquad , \qquad x = s(t)$

  (3.22)
- and the interface energy balance equation

$$k_s \frac{\partial T_s}{\partial x} - k_l \frac{\partial T_l}{\partial x} = \rho L \frac{ds(t)}{dt} \qquad , \qquad x = s(t) \tag{3.23}$$

where, L is the latent heat released on solidification.

Numerical schemes based on the equations (3.21)-(3.23) require the phase change boundary to be accurately traced. This necessity renders a large proportion of the available numerical schemes difficult to implement. However, if enthalpy of PCM is defined as;

$$H(T) = \begin{cases} c_{p_s}\left(T - T_m\right) & , \quad T < T_m \ (for\ solid\ phase) \\ c_{p_l}\left(T - T_m\right) + L & , \quad T > T_m \ (for\ liquid\ phase) \end{cases} \tag{3.24}$$

the equations (3.21)-(3.23) reduce to a single equation;

$$\rho \frac{\partial H}{\partial t} = \frac{\partial}{\partial x}\left(k \frac{\partial T}{\partial x}\right) \tag{3.25}$$

The temperature is related to the enthalpy via;

$$T = \begin{cases} \dfrac{H}{c_{p_s}} + T_m & for\ H < 0 \\ T_m & for\ 0 \le H \le L \\ \dfrac{H - L}{c_{p_l}} + T_m & for\ H > L \end{cases} \tag{3.26}$$

The advantages of this approach are [27];

- There are no conditions to be satisfied at x=s(t) (the phase change boundary).
- There is no need to accurately track the phase change boundary.
- There is no need to consider the regions on either side of the phase change boundary separately.

However, finite difference discretizations of the enthalpy method have a tendency to oscillate numerically in temperature and phase front position. To overcome this unsatisfactory aspect of the enthalpy method, Voller & Cross [27] have suggested an algorithm which bypasses the oscillations.

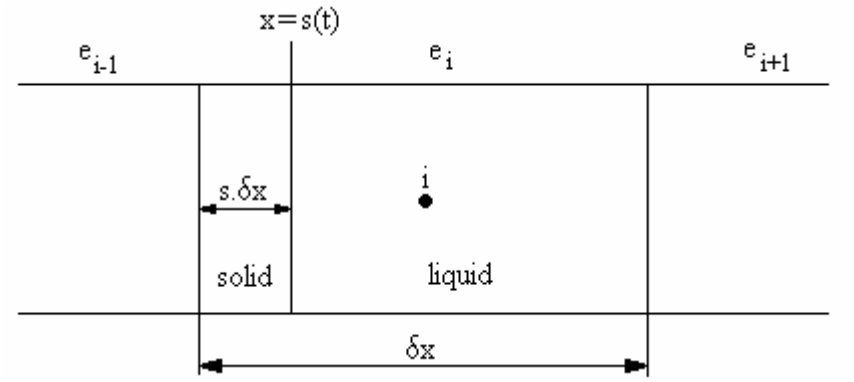

Fig 3.5 The Element with Phase Change Front

Let i be a node in a discretized region which is being frozen and let e_i be the element associated with that node point. The total heat in the element e_i at any time is approximated as $H_i.\delta x$ where H_i is the nodal enthalpy and δx is the length of the element. If at time t the freezing front is in element e_i and moving towards element e_{i+1} the total heat in the element may be approximated as the sum of the heat in the solid and liquid parts of the element;

$$H_i \delta x = \left[\left(c_{p_s}\left(T_i - T_m\right)\right)s + \left(c_{p_l}\left(T_i - T_m\right) + L\right)\left(1 - s\right)\right]\delta x \tag{3.27}$$

where s is the fraction of element which is solid.

When the freezing front reaches the node i then $s = \frac{1}{2}$ and $T_i = T_m$ and equation (3.27) yields,

$$H_i = \frac{L}{2} \tag{3.28}$$

Hence whenever the nodal enthalpy in a discretized region is equal to half of the latent heat, the phase change boundary should be approximately on the node i.

From the interpretation of the enthalpy given above the following algorithm is proposed;

- The enthalpy and a "working" temperature is calculated at each time step from the explicit finite difference scheme of equation (3.25).
- Whenever the enthalpy at a node point is such that at time level k+1, $H_i^{k+1} < \frac{L}{2}$ and $H_i^k > \frac{L}{2}$ the phase change boundary has passed through the node i.
- Furthermore, assuming that the enthalpy changes linearly in any time interval, the time at which the phase change front is on the node i is given by,

  $$t_i = (k + x)\delta t \tag{3.29}$$

  where x is estimated via linear interpolation in time;

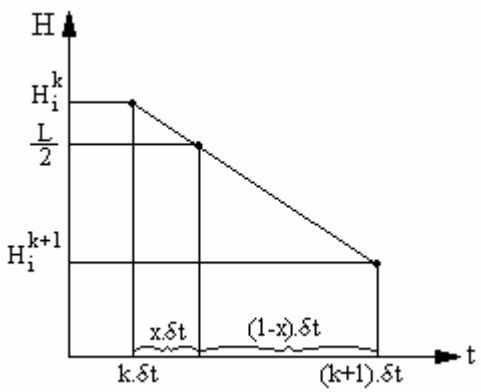

Fig 3.6 Enthalpy Values of the Node i

$$x = \frac{L/2 - H_i^k}{H_i^{k+1} - H_i^k} \tag{3.30}$$

At time t_i the temperature at node i is T_m. The temperatures at the other node points are easily estimated by using a linear interpolation;

$$T_j^{k+x} = x\left(T_j^{k+1} - T_j^k\right) + T_j^k \qquad , \qquad (j \neq i) \tag{3.31}$$

This algorithm can also be applied in spherical and cylindrical coordinates with some modifications;

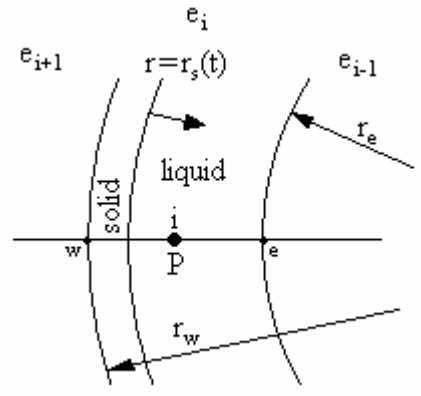

Fig 3.7 The Control Volume with Phase Change Front in Spherical and Cylindrical Coordinates

- for spherical coordinates;

The total heat in the control volume e_i is defined as $H_i.V_{e_i}$ where V_{e_i} is the volume of the control volume. The freezing front is moving towards the control volume e_{i-1} in the spherical container. So, the equation (3.27) becomes;

$$H_i V_{e_i} = \left[c_{p_s}\left(T_i - T_m\right)V_s + \left(c_{p_l}\left(T_i - T_m\right) + L\right)V_l\right] \tag{3.32}$$

where, V_s is the volume of solid and V_l is the volume of liquid in the control volume.

Equation (3.32) can also be expressed as;

$$H_i \frac{4}{3}\pi\left(r_w^3 - r_e^3\right) = \left[c_{p_s}\left(T_i - T_m\right)\frac{4}{3}\pi\left(r_w^3 - r_s^3\right) + \left(c_{p_l}\left(T_i - T_m\right) + L\right)\frac{4}{3}\pi\left(r_s^3 - r_e^3\right)\right] \tag{3.33}$$

When the freezing front is on the node i, $r_s = \frac{r_w + r_e}{2}$ and $T_i = T_m$, so the enthalpy value at this time is;

$$H_i = \frac{L}{8}\frac{r_w^3 + 3r_w^2 r_e + 3r_w r_e^2 - 7r_e^3}{r_w^3 - r_e^3} \tag{3.34}$$

So, for spherical coordinates when $H_i^{k+1} < \frac{L}{8}\frac{r_w^3 + 3r_w^2 r_e + 3r_w r_e^2 - 7r_e^3}{r_w^3 - r_e^3}$ and $H_i^k > \frac{L}{8}\frac{r_w^3 + 3r_w^2 r_e + 3r_w r_e^2 - 7r_e^3}{r_w^3 - r_e^3}$ the phase change front has passed through the node i and the linear interpolation defined in equation (3.30) becomes;

$$x = \frac{\frac{L}{8}\frac{r_w^3 + 3r_w^2 r_e + 3r_w r_e^2 - 7r_e^3}{r_w^3 - r_e^3} - H_i^k}{H_i^{k+1} - H_i^k} \tag{3.35}$$

- for cylindrical coordinates;

Equation (3.32) can also be written for cylindrical coordinates, but this time it becomes;

$$H_i\left(\pi\left(r_w^2 - r_e^2\right)l\right) = \left[c_{p_s}\left(T_i - T_m\right)\left(\pi\left(r_w^2 - r_s^2\right)l\right) + \left(c_{p_l}\left(T_i - T_m\right) + L\right)\left(\pi\left(r_s^2 - r_e^2\right)l\right)\right] \tag{3.36}$$

where l, is depth of the cylinder.

Similar to the spherical coordinates, when the freezing front is on the node i, $r_s = \frac{r_w + r_e}{2}$ and $T_i = T_m$, and the enthalpy value is;

$$H_i = \frac{L}{4}\frac{r_w^2 + 2r_w r_e - 3r_e^2}{r_w^2 - r_e^2} \tag{3.37}$$

Finally, in cylindrical coordinates when $H_i^{k+1} < \frac{L}{4}\frac{r_w^2 + 2r_w r_e - 3r_e^2}{r_w^2 - r_e^2}$ and $H_i^k > \frac{L}{4}\frac{r_w^2 + 2r_w r_e - 3r_e^2}{r_w^2 - r_e^2}$, the phase change front has passed through the node i and the linear interpolation defined in equation (3.30) becomes;

$$x = \frac{\frac{L}{4}\frac{r_w^2 + 2r_w r_e - 3r_e^2}{r_w^2 - r_e^2} - H_i^k}{H_i^{k+1} - H_i^k} \tag{3.38}$$

CHAPTER 4

NUMERICAL MODELLING OF SOLIDIFICATION OF A PHASE CHANGE MATERIAL INSIDE A SPHERICAL AND CYLINDRICAL CONTAINER

In this chapter the inward solidification in spherical and cylindrical coordinates is investigated. The total solidification time of a phase change material (PCM) inside a spherical and cylindrical container, which are subjected to convection on the external boundary is determined by using a numerical solution method named enthalpy method, which is explained in detail in Chapter 3. Dimensionless form of the differential enthalpy equation is obtained and control volume formulation is used to discretize the equation. Then, the solution algorithm described in Chapter 3 is used to find the dimensionless total solidification time of the PCM.

4.1 SOLIDIFICATION OF A PCM INSIDE A SPHERICAL CONTAINER

4.1.1 Definition and Formulation of the Problem

The schematic view of a spherical container is given in figure (4.1). A phase change material at a temperature $T_{initial}$, which is higher than its solidification temperature T_m, fills the container. At the external boundary of the container there is a coolant fluid at T_∞, which is lower than T_m and heat exchange between the coolant and PCM takes place by convection. As a result of the heat exchange, the PCM starts to solidify from the outer boundary of the container and the phase change front moves towards the center. The time at which phase change front reaches the center of the container is defined as the total solidification time of the PCM.

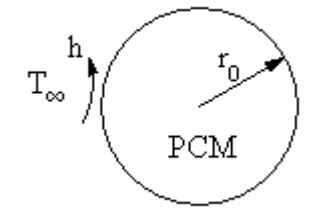

Fig 4.1 Schematic View of a Spherical Container Filled with PCM

Major assumptions in the formulation are;

- The temperature of the coolant fluid (T_∞) and the heat transfer coefficient (h) are constant.
- The heat transfer process inside the container is only by conduction in radial direction.
- The densities of solid and liquid phases of PCM are equal.

The enthalpy equation in spherical coordinates is;

$$\rho \frac{\partial H}{\partial t} = \frac{1}{r^2} \frac{\partial}{\partial r} \left(k.r^2 \frac{\partial T}{\partial r} \right) \tag{4.1}$$

Enthalpy values are defined in equation (3.24) and the temperature- enthalpy relation is defined in equation (3.26).

Initial condition; $$T(r,0) = T_{initial} \tag{4.2}$$

The boundary condition at $r = r_0$; $$-k \frac{\partial T}{\partial r} = h.\left((T)_{r=r_0} - T_\infty \right) \tag{4.3}$$

If the following dimensionless variables are introduced;

- Dimensionless enthalpy: $$H^* = \frac{H}{c_{p_s} \left(T_{initial} - T_\infty \right)} \tag{4.4a}$$
- Dimensionless temperature: $$\theta = \frac{T - T_\infty}{T_{initial} - T_\infty} \tag{4.4b}$$
- Dimensionless radial position: $R = \frac{r}{r_0}$ (4.4c)
- Dimensionless time: $$\tau = \frac{\alpha_s .t}{r_0^2} \tag{4.4d}$$
- Dimensionless thermal conductivity: $K^* = \frac{k}{k_s}$ (4.4e)

where, $\begin{cases} k = k_s & , \quad for\ solid\ phase \\ k = k_l & , \quad for\ liquid\ phase \end{cases}$

- Dimensionless specific heat: $C^* = \frac{c_{P_l}}{c_{p_s}}$ (4.4f)

- Stefan number: $$Ste = \frac{c_{p_s}.(T_{initial} - T_\infty)}{L} \quad (4.4g)$$

- Biot number; $$Bi = \frac{h.r_0}{k_s} \quad (4.4h)$$

The dimensionless enthalpy equation is obtained as;

$$\frac{\partial H^*}{\partial \tau} = \frac{1}{R^2}\frac{\partial}{\partial R}\left(K^*.R^2\frac{\partial \theta}{\partial R}\right) \quad (4.5)$$

The enthalpy expression defined in equation (3.24) is in dimensionless form as;

$$H^*(\theta) = \begin{cases} \theta - \theta_m & for\ \ \theta < \theta_m \\ C^*.(\theta - \theta_m) + \dfrac{1}{Ste} & for\ \ \theta > \theta_m \end{cases} \quad (4.6)$$

The enthalpy temperature relation defined in equation (3.26) becomes;

$$\theta = \begin{cases} H^* + \theta_m & for\ H^* < 0 \\ \theta_m & for\ 0 \le H^* \le \dfrac{1}{Ste} \\ \dfrac{H^* - \dfrac{1}{Ste}}{C^*} + \theta_m & for\ H^* > \dfrac{1}{Ste} \end{cases} \quad (4.7)$$

where, θ_m is the dimensionless solidification temperature

The initial and boundary conditions defined in equations (4.2) and (4.3) are in dimensionless form as;

Initial condition; $$\theta(R,0) = 1 \quad (4.8)$$

The boundary condition at R=1; $$K^*\frac{\partial \theta}{\partial R} = -Bi(\theta)_{R=1} \quad (4.9)$$

4.1.2 Numerical Formulation

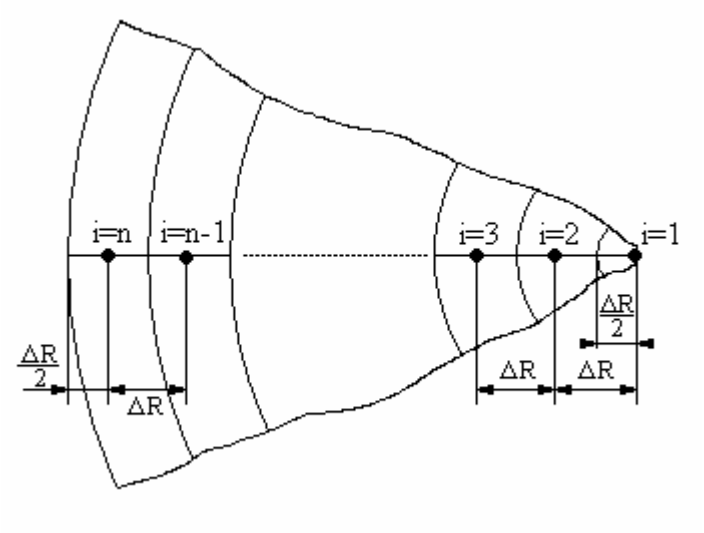

Fig 4.2 Control Volumes and Nodal Points Inside the Spherical Container

The spherical volume is divided into small control volumes as shown in figure (4.2). The interfaces are placed at the midway between nodes. If the control volume formulation is applied to the dimensionless enthalpy equation and explicit scheme is used following equations are obtained.

- for i=1;

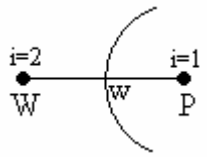

Fig 4.3 First Control Volume of the Spherical Container

$$R_p = 0 \quad , \quad R_w = \frac{\Delta R}{2} \quad , \quad R_W = \Delta R$$

$$\int_{\Delta V}\int_{\tau}^{\tau+\Delta\tau} \frac{\partial H^*}{\partial \tau} d\tau . dV = \int_{\tau}^{\tau+\Delta\tau}\int_{\Delta V} \frac{1}{R^2}\frac{\partial}{\partial R}\left(K^* R^2 \frac{\partial \theta}{\partial R}\right) dV . d\tau \qquad , \qquad dV = 4\pi R^2 dR \tag{4.10a}$$

$$\int_{R_P}^{R_w}\int_{\tau}^{\tau+\Delta\tau} \frac{\partial H^*}{\partial \tau} d\tau . 4\pi R^2 dR = \int_{\tau}^{\tau+\Delta\tau}\int_{R_P}^{R_w} \frac{1}{R^2}\frac{\partial}{\partial R}\left(K^* R^2 \frac{\partial \theta}{\partial R}\right) 4\pi R^2 dR d\tau \tag{4.10b}$$

$$\left(H_P^{*k+1} - H_P^{*k}\right)\frac{R_w^3}{3} = \left(K^* R^2 \frac{\partial \theta}{\partial R}\right)_{R=R_w} \Delta\tau \tag{4.10c}$$

$$H_P^{*k+1} = H_P^{*k} + \frac{3.\Delta\tau}{R_w} K_w^* \frac{\theta_W^k - \theta_P^k}{\Delta R} \tag{4.10d}$$

For the thermal conductivity at the interface w, the arithmetic mean of the nodal thermal conductivities is taken $\left(K_w^* = \frac{K_P^* + K_W^*}{2} \right)$, so;

$$H_1^{*k+1} = H_1^{*k} + \frac{3\Delta\tau}{(\Delta R)^2}\left(K_1^* + K_2^*\right)\left(\theta_2^k - \theta_1^k\right) \tag{4.10e}$$

- for i=2,3,…,n-1

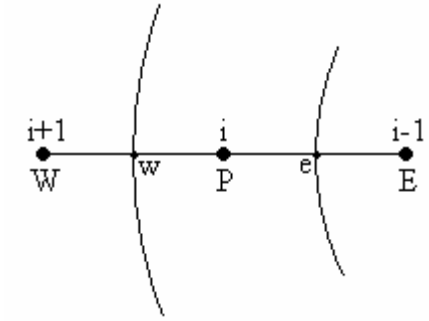

Fig 4.4 Internal Control Volumes of the Spherical Container

$$R_W = i.\Delta R \ , \ R_w = (i-0.5)\Delta R \ , \ R_P = (i-1)\Delta R \ , \ R_e = (i-1.5)\Delta R \ , \ R_E = (i-2)\Delta R$$

Equation (4.10a) can be written for internal control volumes as;

$$\int_{R_e}^{R_w}\int_{\tau}^{\tau+\Delta\tau} \frac{\partial H^*}{\partial\tau} d\tau . 4\pi R^2 dR = \int_{\tau}^{\tau+\Delta\tau}\int_{R_e}^{R_w} \frac{1}{R^2}\frac{\partial}{\partial R}\left(K^* R^2 \frac{\partial\theta}{\partial R}\right) 4\pi R^2 dR d\tau \tag{4.11a}$$

$$\left(H_P^{*k+1} - H_P^{*k}\right)\frac{R_w^3 - R_e^3}{3} = \left[\left(K^* R^2 \frac{\partial\theta}{\partial R}\right)_{R=R_w} - \left(K^* R^2 \frac{\partial\theta}{\partial R}\right)_{R=R_e}\right]\Delta\tau \tag{4.11b}$$

Since, $R_w^3 - R_e^3 = \left(\underbrace{R_w - R_e}_{\Delta R} \right)\left(R_w^2 + R_w R_e + R_e^2\right)$;

$$H_P^{*k+1} = H_P^{*k} + \frac{3\Delta\tau}{\left(R_w^2 + R_w R_e + R_e^2\right)} \frac{\left[\left(K_w^* R_w^2 \frac{\theta_W^k - \theta_P^k}{\Delta R}\right) - \left(K_e^* R_e^2 \frac{\theta_P^k - \theta_E^k}{\Delta R}\right)\right]}{\Delta R} \tag{4.11c}$$

The dimensionless form of the thermal conductivity at the interface defined in equation (3.17) is;

$$K_e^* = \frac{R_e.(R_P - R_E).K_E^*.K_P^*}{R_P.(R_e - R_E).K_P^* + R_E.(R_P - R_e).K_E^*} \tag{4.12}$$

If the dimensionless radius values are replaced in equation (4.12);

$$K_e^* = \frac{(i-1.5)K_E^* K_P^*}{0.5(i-1)K_P^* + 0.5(i-2)K_E^*} \tag{4.13a}$$

$$K_w^* = \frac{(i-0.5)K_P^* K_W^*}{0.5i.K_W^* + 0.5(i-1)K_P^*} \tag{4.13b}$$

However for i=2 the thermal conductivity at the interface e is taken as the arithmetic average of the nodal thermal conductivities $\left(K_e^* = \frac{K_E^* + K_P^*}{2} \right)$.

So, for i=2;

$$H_2^{*k+1} = H_2^{*k} + \frac{3\Delta\tau}{\left(1.5^2 + 1.5\times 0.5 + 0.5^2\right)(\Delta R)^2} \times \frac{\left[\left(\frac{1.5K_P^*K_W^*}{0.5K_P^* + K_W^*} 1.5^2 (\Delta R)^2 \frac{\theta_W^k - \theta_P^k}{\Delta R}\right) - \left(\frac{K_E^* + K_P^*}{2} 0.5^2 (\Delta R)^2 \frac{\theta_P^k - \theta_E^k}{\Delta R}\right)\right]}{\Delta R} \tag{4.14a}$$

$$H_2^{*k+1} = H_2^{*k} + \frac{3\Delta\tau}{3.25(\Delta R)^2}\left[\frac{1.5^3 K_2^* K_3^*}{0.5K_2^* + K_3^*}\left(\theta_3^k - \theta_2^k\right) - \frac{K_1^* + K_2^*}{2} 0.5^2 \left(\theta_2^k - \theta_1^k\right)\right] \tag{4.14b}$$

for i=3,4,…,n-1;

$$H_i^{*k+1} = H_i^{*k} + \frac{3\Delta\tau}{\left((i-0.5)^2 + (i-0.5)(i-1.5) + (i-1.5)^2\right)(\Delta R)^2} \times \tag{4.15a}$$

$$\frac{\left[\left(\frac{(i-0.5)K_P^*K_W^*}{0.5iK_W^* + 0.5(i-1)K_P^*}(i-0.5)^2(\Delta R)^2 \frac{\theta_W^k - \theta_P^k}{\Delta R}\right) - \frac{(i-1.5)K_E^*K_P^*}{0.5(i-1)K_P^* + 0.5(i-2)K_E^*}(i-1.5)^2(\Delta R)^2 \frac{\theta_P^k - \theta_E^k}{\Delta R}\right]}{\Delta R}$$

$$H_i^{*k+1} = H_i^{*k} + \frac{3\Delta\tau}{(3i^2 - 6i + 3.25)(\Delta R)^2} \times$$

$$\left[\frac{(i-0.5)^3 K_i^* K_{i+1}^*}{0.5iK_{i+1}^* + 0.5(i-1)K_i^*} (\theta_{i+1}^k - \theta_i^k) - \frac{(i-1.5)^3 K_{i-1}^* K_i^*}{0.5(i-1)K_i^* + 0.5(i-2)K_{i-1}^*} (\theta_i^k - \theta_{i-1}^k) \right] \quad (4.15b)$$

- for i=n;

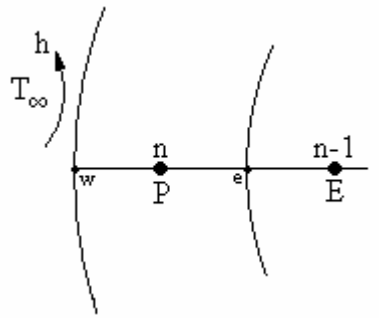

Fig 4.5 Last Control Volume of the Spherical Container

$$R_w = 1 \ , \ R_P = (n-1)\Delta R \ , \ R_e = (n-1.5)\Delta R \ , \ R_E = (n-2)\Delta R$$

When integration in equation (4.10a) is done for the last control volume, the following expression can be obtained;

$$H_P^{*k+1} = H_P^{*k} + \frac{3\Delta\tau}{(R_w^2 + R_w R_e + R_e^2)} \frac{\left[\left(K^* R^2 \frac{\partial\theta}{\partial R} \right)_{R=R_w} - \left(K^* R^2 \frac{\partial\theta}{\partial R} \right)_{R=R_e} \right]}{\Delta R} \quad (4.16a)$$

If the dimensionless boundary condition defined in equation (4.9) is replaced in equation (4.16a);

$$H_P^{*k+1} = H_P^{*k} + \frac{3\Delta\tau}{(\Delta R)(1 + (n-1.5)\Delta R + (n-1.5)^2(\Delta R)^2)} \left[\begin{array}{r} -Bi(\theta)_{R=1} \\ -K_e^* R_e^2 \frac{\theta_P^k - \theta_E^k}{\Delta R} \end{array} \right] \quad (4.16b)$$

The dimensionless temperature at the boundary, $(\theta)_{R=1}$, can be found also from the dimensionless boundary condition as;

$$K_P^* \frac{(\theta)_{R=1} - \theta_P}{\Delta R / 2} = -Bi(\theta)_{R=1} \quad (4.17a)$$

$$(\theta)_{R=1} = \frac{2K_P^*}{2K_P^* + Bi\Delta R}\theta_P \tag{4.17b}$$

The thermal conductivity at the interface e can be determined from equation (4.13a) as;

$$K_e^* = \frac{(n-1.5)K_E^* K_P^*}{0.5(n-1)K_P^* + 0.5(n-2)K_E^*} \tag{4.18}$$

When equation (4.17b) and (4.18) are substituted in equation (4.16b);

$$H_n^{*k+1} = H_n^{*k} + \frac{3\Delta\tau}{\left(\Delta R + (n-1.5)(\Delta R)^2 + (n-1.5)^2(\Delta R)^3\right)} \times \left[-\frac{2BiK_n^*}{2K_n^* + Bi\Delta R}\theta_n^k - \frac{(n-1.5)^3 K_{n-1}^* K_n^*}{0.5(n-1)K_n^* + 0.5(n-2)K_{n-1}^*}\Delta R(\theta_n^k - \theta_{n-1}^k) \right] \tag{4.19}$$

4.1.3 Solution Algorithm

A program with Q Basic language is written to determine dimensionless solidification time of a PCM inside a spherical container. The position of the phase change front is determined by controlling if the enthalpy value of the last and internal nodes is greater than dimensionless form of the value given by equation (3.34) at time level k and lower at time level k+1 as described in Chapter 3.

The dimensionless form of equation (3.34) is;

$$H_i^* = \frac{1}{8.Ste}\frac{R_w^3 + 3R_w^2 R_e + 3R_w R_e^2 - 7R_e^3}{R_w^3 - R_e^3} \tag{4.20}$$

If the dimensionless radius values of the internal nodes are replaced in equation (4.20), the following expression is obtained;

$$H_i^* = \frac{1}{8.Ste}\frac{(i-0.5)^3 + 3(i-0.5)^2(i-1.5) + 3(i-0.5)(i-1.5)^2 - 7(i-1.5)^3}{(i-0.5)^3 - (i-1.5)^3} \tag{4.21}$$

and the interpolation given in equation (3.35) to find the time at which the phase change front is on the node is in dimensionless form as;

$$X = \frac{\frac{1}{8.Ste}\frac{(i-0.5)^3 + 3(i-0.5)^2(i-1.5) + 3(i-0.5)(i-1.5)^2 - 7(i-1.5)^3}{(i-0.5)^3 - (i-1.5)^3} - H_i^{*k}}{H_i^{*k+1} - H_i^{*k}} \tag{4.22}$$

However to find the time at which the phase change front reaches the first node, the value used for internal nodes given in equation (4.21) is not valid, because the first control volume is a half volume.

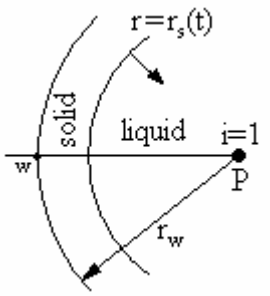

Fig 4.6 The First Control Volume with Phase Change Front

When the equation (3.32) is considered for the first control volume it can be found that the enthalpy value should be 0 when the phase change front is on the first node, because in this case the liquid volume (V_l) is equal to 0. The dimensionless form of this enthalpy value is also 0. So, the same controlling operation is done with this enthalpy value for the first node. The interpolation defined in equation (4.22) for the internal nodes also changes for the first node as;

$$X = \frac{H_i^{*k}}{H_i^{*k} - H_i^{*k+1}} \tag{4.23}$$

The nodal thermal conductivities are also determined by controlling the same enthalpy values for the nodes. It is assumed that the nodal thermal conductivity of the node is equal to the thermal conductivity value of liquid PCM until the phase change front reaches the node $(so, K_i^* = K^+)$, while it is equal to the thermal conductivity of solid phase after this time $(so, K_i^* = 1)$.

The spherical container program is given in Appendix A.

The algorithm of the program is summarized by the following flow chart;

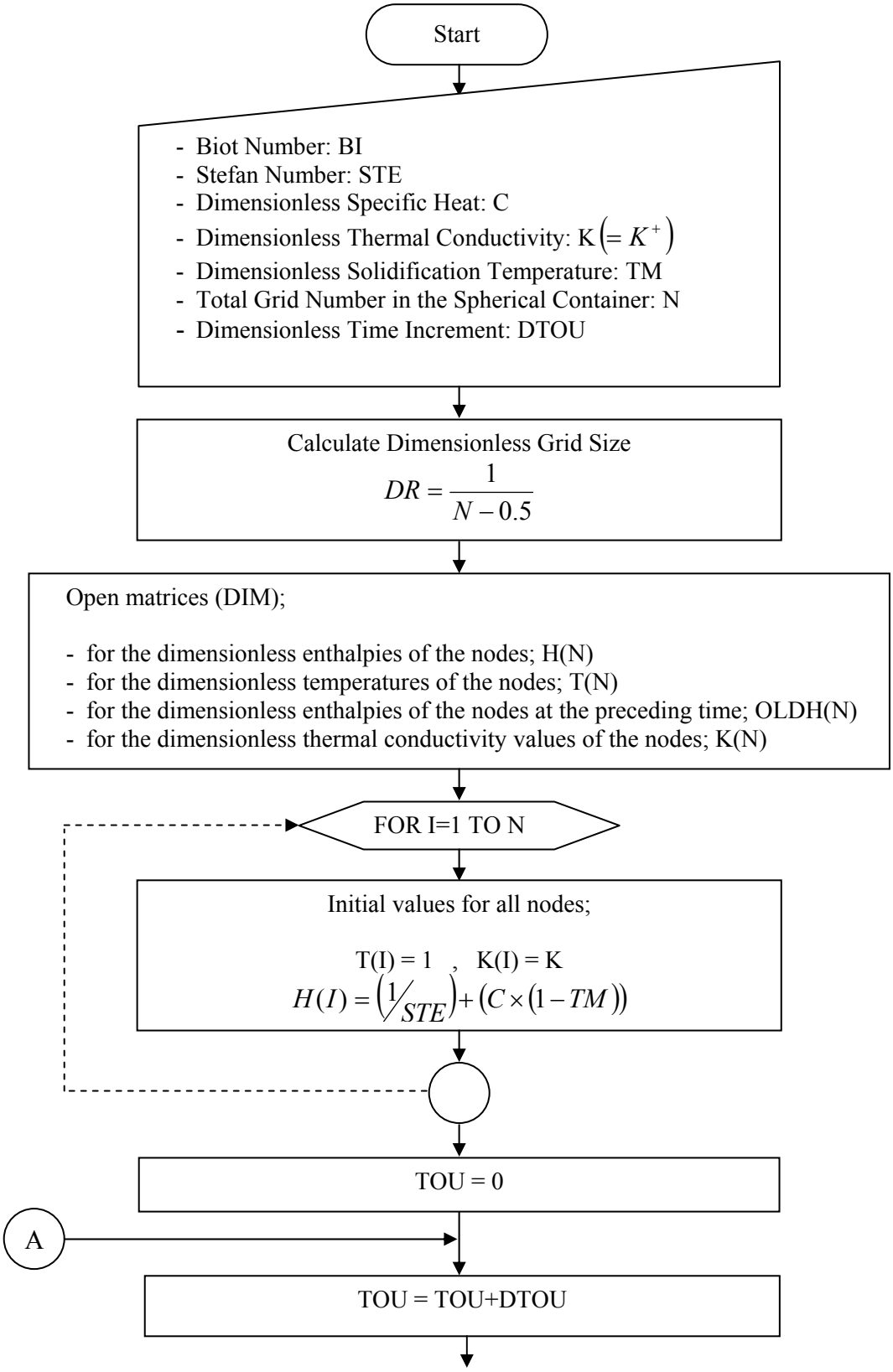
Start
- Biot Number: BI
- Stefan Number: STE
- Dimensionless Specific Heat: C
- Dimensionless Thermal Conductivity: K $(= K^{+})$
- Dimensionless Solidification Temperature: TM
- Total Grid Number in the Spherical Container: N
- Dimensionless Time Increment: DTOU
Calculate Dimensionless Grid Size
$DR = \frac{1}{N - 0.5}$
Open matrices (DIM);
- for the dimensionless enthalpies of the nodes; H(N)
- for the dimensionless temperatures of the nodes; T(N)
- for the dimensionless enthalpies of the nodes at the preceding time; OLDH(N)
- for the dimensionless thermal conductivity values of the nodes; K(N)
FOR I=1 TO N
Initial values for all nodes;
T(I) = 1 , K(I) = K
$H(I) = \left(1/STE\right) + \left(C \times \left(1 - TM\right)\right)$
TOU = 0
A
TOU = TOU+DTOU

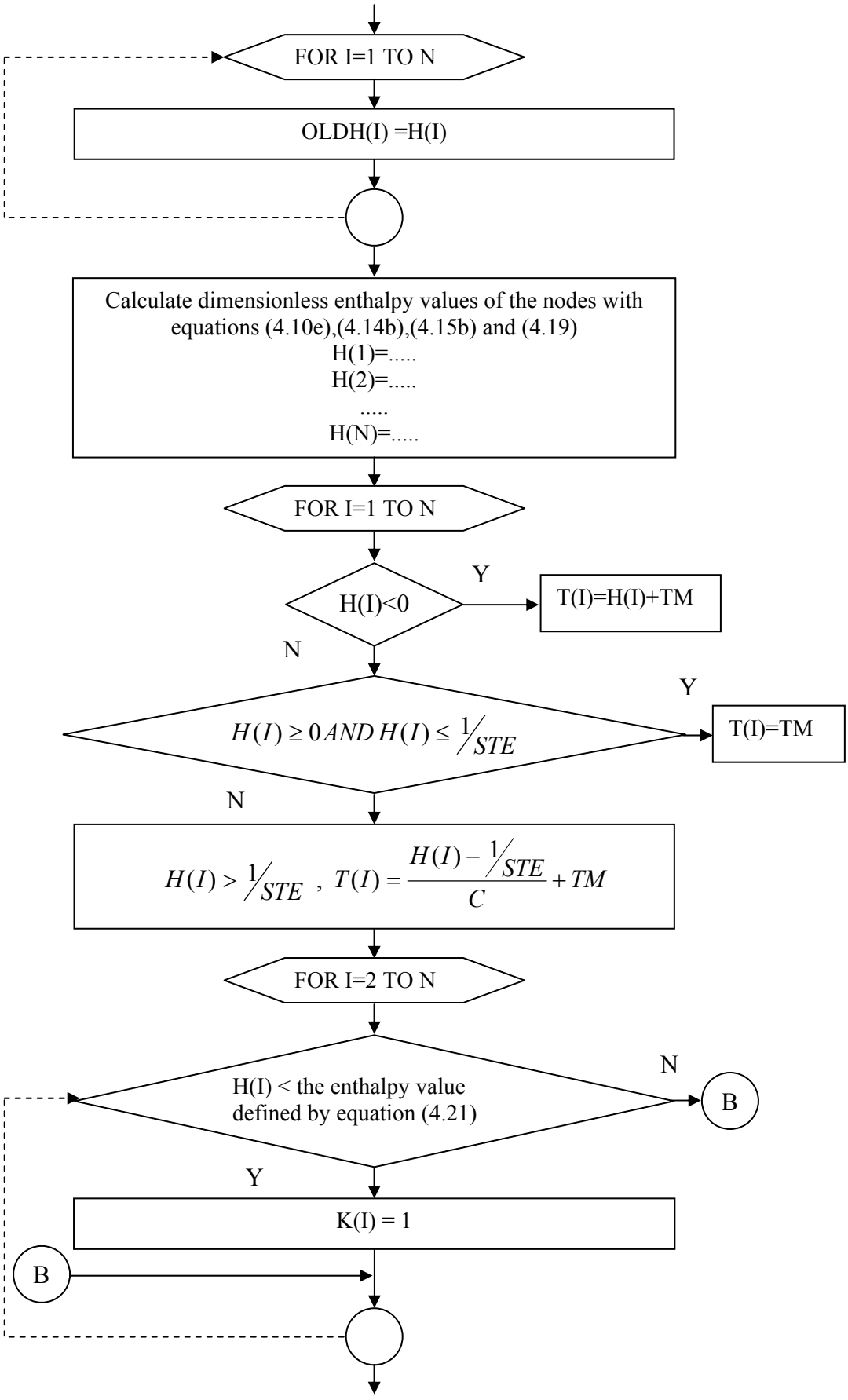
FOR I=1 TO N
OLDH(I) =H(I)
Calculate dimensionless enthalpy values of the nodes with equations (4.10e),(4.14b),(4.15b) and (4.19)
H(1)=.....
H(2)=.....
.....
H(N)=.....
FOR I=1 TO N
H(I)<0
Y
T(I)=H(I)+TM
N
$H(I) \geq 0 \, AND \, H(I) \leq 1/STE$
Y
T(I)=TM
N
$H(I) > 1/STE \;,\; T(I) = \frac{H(I) - 1/STE}{C} + TM$
FOR I=2 TO N
H(I) < the enthalpy value defined by equation (4.21)
N
B
Y
K(I) = 1
B

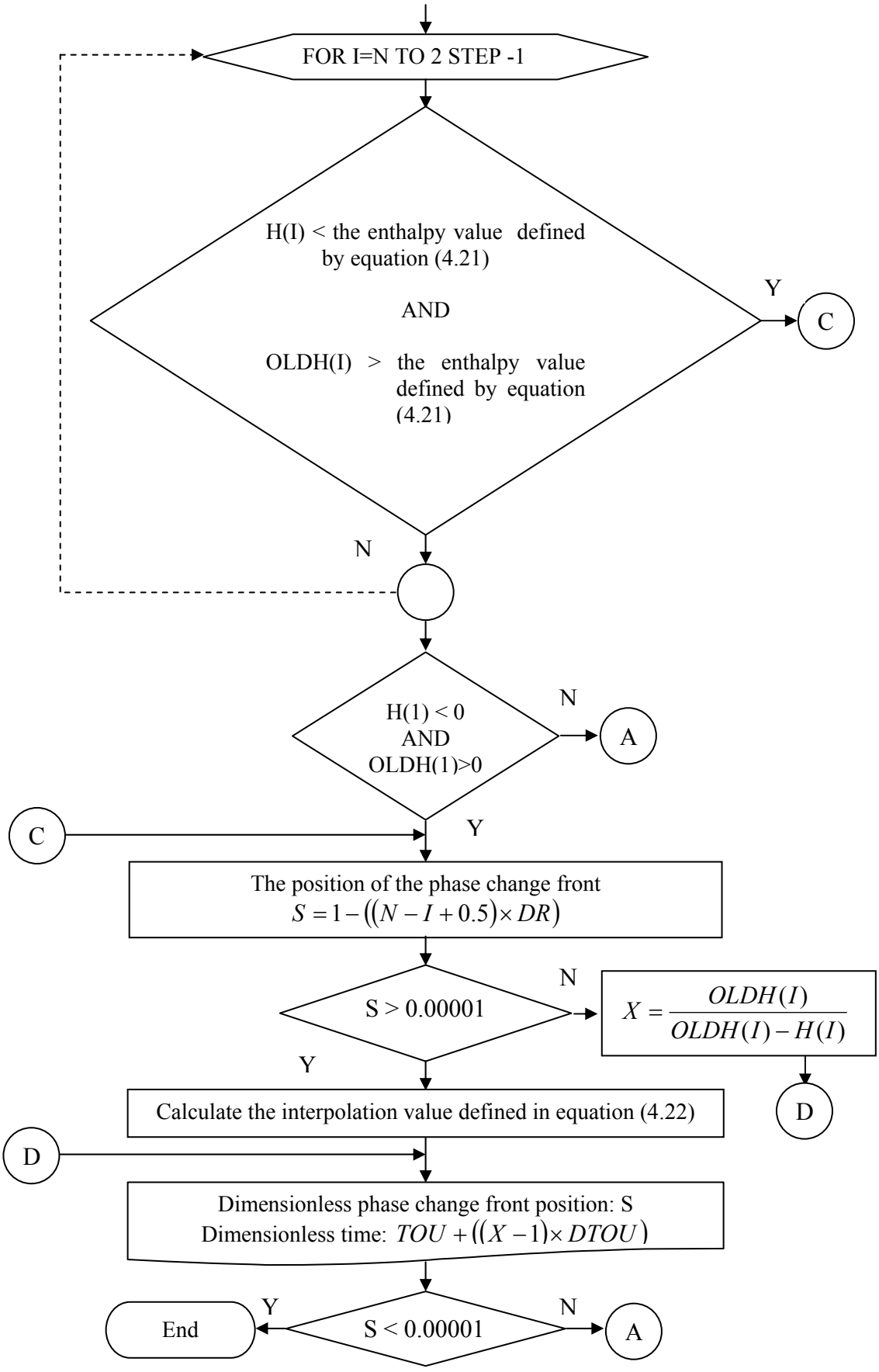
FOR I=N TO 2 STEP -1
H(I) < the enthalpy value defined by equation (4.21)
AND
OLDH(I) > the enthalpy value defined by equation (4.21)
Y
C
N
H(1) < 0
AND
OLDH(1)>0
N
A
C
Y
The position of the phase change front
$S = 1 - ((N - I + 0.5) \times DR)$
S > 0.00001
N
$X = \frac{OLDH(I)}{OLDH(I) - H(I)}$
Y
D
Calculate the interpolation value defined in equation (4.22)
D
Dimensionless phase change front position: S
Dimensionless time: $TOU + ((X - 1) \times DTOU)$
End
Y
S < 0.00001
N
A

4.2 SOLIDIFICATION OF A PCM INSIDE A CYLINDRICAL CONTAINER

4.2.1 Definition and Formulation of the Problem

The schematic view of a cylindrical container is given in figure (4.7). The problem considered is the same as the solidification inside a spherical container. The phase change material at $T_{initial}\ (> T_m)$ inside the container solidifies by the effect of the convective heat transfer to the coolant fluid at $T_\infty\ (< T_m)$. The solidification starts from the outer boundary of the container and the phase change front moves towards the center. The total solidification time of the PCM is the time at which phase change front reaches the center of the container. The assumptions made for the solidification inside the spherical container are also valid in this section.

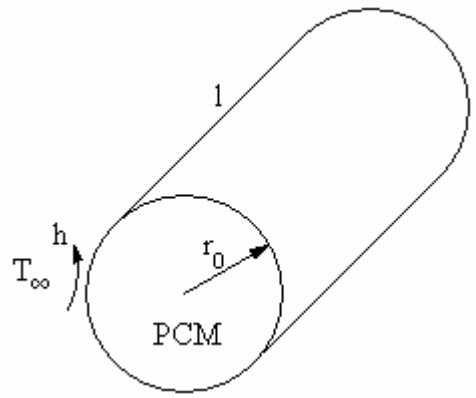

Fig 4.7 Schematic View of a Cylindrical Container Filled with PCM

The enthalpy equation in cylindrical coordinates is;

$$\rho \frac{\partial H}{\partial t} = \frac{1}{r} \frac{\partial}{\partial r} \left(k.r \frac{\partial T}{\partial r} \right) \tag{4.24}$$

Enthalpy values are defined in equation (3.24) and the temperature- enthalpy relation is defined in equation (3.26).

The boundary condition on the external surface and the initial condition are the same as those of the spherical containers given in equation (4.2) and (4.3).

The dimensionless enthalpy equation in cylindrical coordinates is obtained by using the dimensionless variables defined by equations (4.4a,b,c,d,e,f,g and h) as;

$$\frac{\partial H^*}{\partial \tau} = \frac{1}{R}\frac{\partial}{\partial R}\left(K^* R \frac{\partial \theta}{\partial R}\right) \tag{4.25}$$

The dimensionless form of enthalpy temperature relation is given by equations (4.6) and (4.7) and dimensionless initial and boundary conditions are defined in equation (4.8) and (4.9).

4.2.2 Numerical Formulation

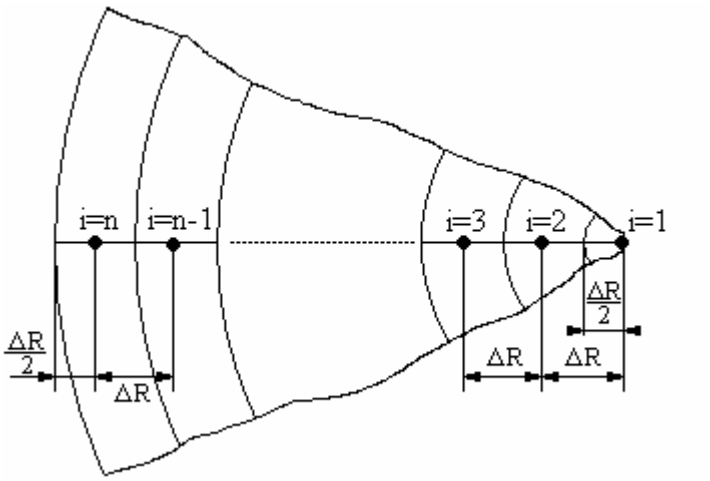

Fig 4.8 Control Volumes and Nodal Points Inside the Cylindrical Container

Similar to the spherical container, the cylindrical container volume is divided into small control volumes as shown in figure (4.8). The interfaces in this case are also placed at the midway between nodes. The following numerical equations for cylindrical container are found by the application of control volume formulation and explicit scheme;

- for i=1;

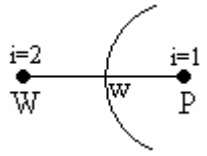

Fig 4.9 First Control Volume of the Cylindrical Container

$$R_p = 0 \quad , \quad R_w = \frac{\Delta R}{2} \quad , \quad R_W = \Delta R$$

$$\int_{\Delta V}\int_{\tau}^{\tau+\Delta\tau}\frac{\partial H^*}{\partial\tau}d\tau.dV=\int_{\tau}^{\tau+\Delta\tau}\int_{\Delta V}\frac{1}{R}\frac{\partial}{\partial R}\left(K^*R\frac{\partial\theta}{\partial R}\right)dVd\tau \quad , \quad dV=2\pi RdR \tag{4.26a}$$

$$\int_{R_P}^{R_w}\int_{\tau}^{\tau+\Delta\tau}\frac{\partial H^*}{\partial\tau}d\tau.2\pi RdR=\int_{\tau}^{\tau+\Delta\tau}\int_{R_P}^{R_w}\frac{1}{R}\frac{\partial}{\partial R}\left(K^*R\frac{\partial\theta}{\partial R}\right)2\pi RdRd\tau \tag{4.26b}$$

$$\left(H_P^{*k+1}-H_P^{*k}\right)\frac{R_w^2}{2}=\left(K^*R\frac{\partial\theta}{\partial R}\right)_{R=R_w}\Delta\tau \tag{4.26c}$$

$$H_P^{*k+1}=H_P^{*k}+\frac{2\Delta\tau}{R_w}K_w^*\frac{\theta_W^k-\theta_P^k}{\Delta R} \tag{4.26d}$$

The interface thermal conductivity is taken as the arithmetic mean of the nodal thermal conductivities, so;

$$H_1^{*k+1}=H_1^{*k}+\frac{2\Delta\tau}{(\Delta R)^2}\left(K_1^*+K_2^*\right)\left(\theta_2^k-\theta_1^k\right) \tag{4.26e}$$

- for i=2,3,…,n-1

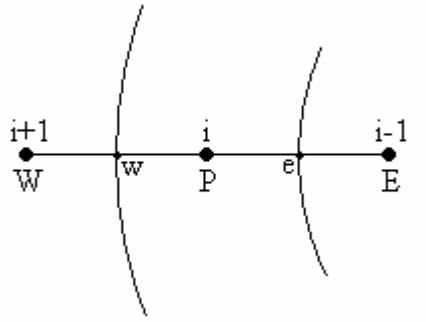

Fig 4.10 Internal Control Volumes of the Cylindrical Container

$$R_W=i.\Delta R \ , \ R_w=(i-0.5)\Delta R \ , \ R_P=(i-1)\Delta R \ , \ R_e=(i-1.5)\Delta R \ , \ R_E=(i-2)\Delta R$$

For internal control volumes, equation (4.26a) can be written as;

$$\int_{R_e}^{R_w}\int_{\tau}^{\tau+\Delta\tau}\frac{\partial H^*}{\partial\tau}d\tau.2\pi RdR=\int_{\tau}^{\tau+\Delta\tau}\int_{R_e}^{R_w}\frac{1}{R}\frac{\partial}{\partial R}\left(K^*R\frac{\partial\theta}{\partial R}\right)2\pi RdRd\tau \tag{4.27a}$$

$$\left(H_P^{*k+1} - H_P^{*k}\right)\frac{R_w^2 - R_e^2}{2} = \left[\left(K^* R \frac{\partial\theta}{\partial R}\right)_{R=R_w} - \left(K^* R \frac{\partial\theta}{\partial R}\right)_{R=R_e}\right]\Delta\tau \tag{4.27b}$$

$$\text{As } \frac{R_w^2 - R_e^2}{2} = \left(\underbrace{\frac{R_w + R_e}{2}}_{=R_P}\right)\left(\underbrace{R_w - R_e}_{\Delta R}\right),$$

$$H_P^{*k+1} = H_P^{*k} + \frac{1}{R_P}\frac{\left[\left(K_w^* R_w \frac{\theta_W^k - \theta_P^k}{\Delta R}\right) - \left(K_e^* R_e \frac{\theta_P^k - \theta_E^k}{\Delta R}\right)\right]}{\Delta R}\Delta\tau \tag{4.27c}$$

The dimensionless form of the thermal conductivity in cylindrical coordinates defined in equation (3.20) is;

$$K_e^* = \frac{K_P^*.K_E^*.\ln\left(R_P / R_E\right)}{K_E^*.\ln\left(R_P / R_e\right) + K_P^*.\ln\left(R_e / R_E\right)} \tag{4.28}$$

When the dimensionless radius values are replaced in equation (4.28),

$$K_e^* = \frac{K_P^*.K_E^*.\ln\left(\frac{i-1}{i-2}\right)}{K_E^*.\ln\left(\frac{i-1}{i-1.5}\right) + K_P^*.\ln\left(\frac{i-1.5}{i-2}\right)} \tag{4.29a}$$

$$K_w^* = \frac{K_W^*.K_P^*.\ln\left(\frac{i}{i-1}\right)}{K_P^*.\ln\left(\frac{i}{i-0.5}\right) + K_W^*.\ln\left(\frac{i-0.5}{i-1}\right)} \tag{4.29b}$$

Since for i=2, the thermal conductivity at the interface e is taken the arithmetic mean value of nodal thermal conductivities, equation (4.27c) can be written for i=2 as;

$$H_2^{*k+1} = H_2^{*k} + \frac{\Delta\tau}{\Delta R} \times \frac{\left[\left(\frac{K_W^* K_P^* \ln 2}{K_P^* \ln\left(2/1.5\right) + K_W^* \ln 1.5} 1.5\Delta R \frac{\theta_W^k - \theta_P^k}{\Delta R}\right) - \left(\frac{K_P^* + K_E^*}{2}\frac{\Delta R}{2}\frac{\theta_P^k - \theta_E^k}{\Delta R}\right)\right]}{\Delta R} \tag{4.30a}$$

$$H_2^{*k+1} = H_2^{*k} + \frac{\Delta\tau}{(\Delta R)^2}\left[\frac{1.5K_2^*K_3^*\ln 2}{K_2^*\ln\left(2/1.5\right)+K_3^*\ln 1.5}\left(\theta_3^k-\theta_2^k\right)-\frac{K_1^*+K_2^*}{4}\left(\theta_2^k-\theta_1^k\right)\right] \qquad (4.30b)$$

for i=3,4,…,n-1;

$$H_i^{*k+1} = H_i^{*k} + \frac{\Delta\tau}{(i-1)\Delta R}\times \frac{\left[\left(\frac{K_W^*.K_P^*.\ln\left(i/i-1\right)}{K_P^*.\ln\left(i/i-0.5\right)+K_W^*.\ln\left(i-0.5/i-1\right)}(i-0.5)\Delta R\frac{\theta_W^k-\theta_P^k}{\Delta R}\right)-\left(\frac{K_P^*.K_E^*.\ln\left(i-1/i-2\right)}{K_E^*.\ln\left(i-1/i-1.5\right)+K_P^*.\ln\left(i-1.5/i-2\right)}(i-1.5)\Delta R\frac{\theta_P^k-\theta_E^k}{\Delta R}\right)\right]}{\Delta R} \qquad (4.31a)$$

$$H_i^{*k+1} = H_i^{*k} + \frac{\Delta\tau}{(i-1)(\Delta R)^2}\times \left[\frac{K_{i+1}^*.K_i^*.\ln\left(i/i-1\right)}{K_i^*.\ln\left(i/i-0.5\right)+K_{i+1}^*.\ln\left(i-0.5/i-1\right)}(i-0.5)\left(\theta_{i+1}^k-\theta_i^k\right)-\frac{K_i^*.K_{i-1}^*.\ln\left(i-1/i-2\right)}{K_{i-1}^*.\ln\left(i-1/i-1.5\right)+K_i^*.\ln\left(i-1.5/i-2\right)}(i-1.5)\left(\theta_i^k-\theta_{i-1}^k\right)\right] \qquad (4.31b)$$

- for i=n;

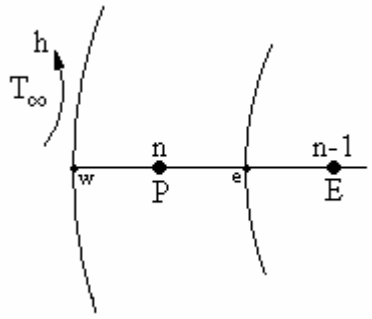

Fig 4.11 Last Control Volume of the Cylindrical Container

$$R_w = 1\ ,\ R_P = (n-1)\Delta R\ ,\ R_e = (n-1.5)\Delta R\ ,\ R_E = (n-2)\Delta R$$

For the last control volume, the result of the integration in equation (4.26a) yields,

$$H_P^{*k+1} = H_P^{*k} + \frac{\Delta\tau}{R_P}\frac{\left[\left(K^*R\frac{\partial\theta}{\partial R}\right)_{R=R_w}-\left(K^*R\frac{\partial\theta}{\partial R}\right)_{R=R_e}\right]}{\Delta R} \qquad (4.32a)$$

If the dimensionless boundary condition given in equation (4.9) and the dimensionless temperature value at the boundary given in equation (4.17b) is replaced in equation (4.32a);

$$H_n^{*k+1} = H_n^{*k} + \frac{\Delta\tau}{(n-1)(\Delta R)^2} \times \left[-\frac{2BiK_n^*}{2K_n^* + Bi\Delta R}\theta_n^k - \frac{(n-1.5)K_n^*K_{n-1}^* \ln\left(n-1/n-2\right)}{K_{n-1}^* \ln\left(n-1/n-1.5\right) + K_n^* \ln\left(n-1.5/n-2\right)}\left(\theta_n^k - \theta_{n-1}^k\right) \right] \quad (4.32b)$$

4.2.3 Solution Algorithm

The dimensionless solidification time of a PCM inside a cylindrical container is found by using a program written with Q Basic language. The cylindrical container program is given in Appendix B. Similar to the spherical container the phase change front position is determined by controlling if the internal and last nodal enthalpies is greater than the dimensionless form of the value given in equation (3.37) at time level k and lower at time level k+1.

The dimensionless form of equation (3.37) is;

$$H_i^* = \frac{1}{4.Ste}\frac{R_w^2 + 2R_wR_e - 3R_e^{\,2}}{R_w^2 - R_e^2} \quad (4.33)$$

If the dimensionless radius values of the internal nodes are replaced in equation (4.33), the following expression is obtained;

$$H_i^* = \frac{1}{4.Ste}\frac{(i-0.5)^2 + 2(i-0.5)(i-1.5) - 3(i-1.5)^2}{(i-0.5)^2 - (i-1.5)^2} \quad (4.34)$$

and the interpolation given in equation (3.38) to find the time at which the phase change front is on the node is in dimensionless form as;

$$X = \frac{\frac{1}{4.Ste}\frac{(i-0.5)^2 + 2(i-0.5)(i-1.5) - 3(i-1.5)^2}{(i-0.5)^2 - (i-1.5)^2} - H_i^{*k}}{H_i^{*k+1} - H_i^{*k}} \quad (4.35)$$

The time at which the phase change front reaches the center of the container is determined by checking if the first dimensionless nodal enthalpy value reached 0 at the interval of time levels k and k+1 for similar reasons as in spherical container and the interpolation expression for the first node is the same as the spherical container and given in equation (4.23).

The nodal thermal conductivity values are assumed to be equal to that of the liquid PCM until the phase change front reaches the node, while it is equal to that of the solid PCM after this time.

The method is summarized by the following algorithm;

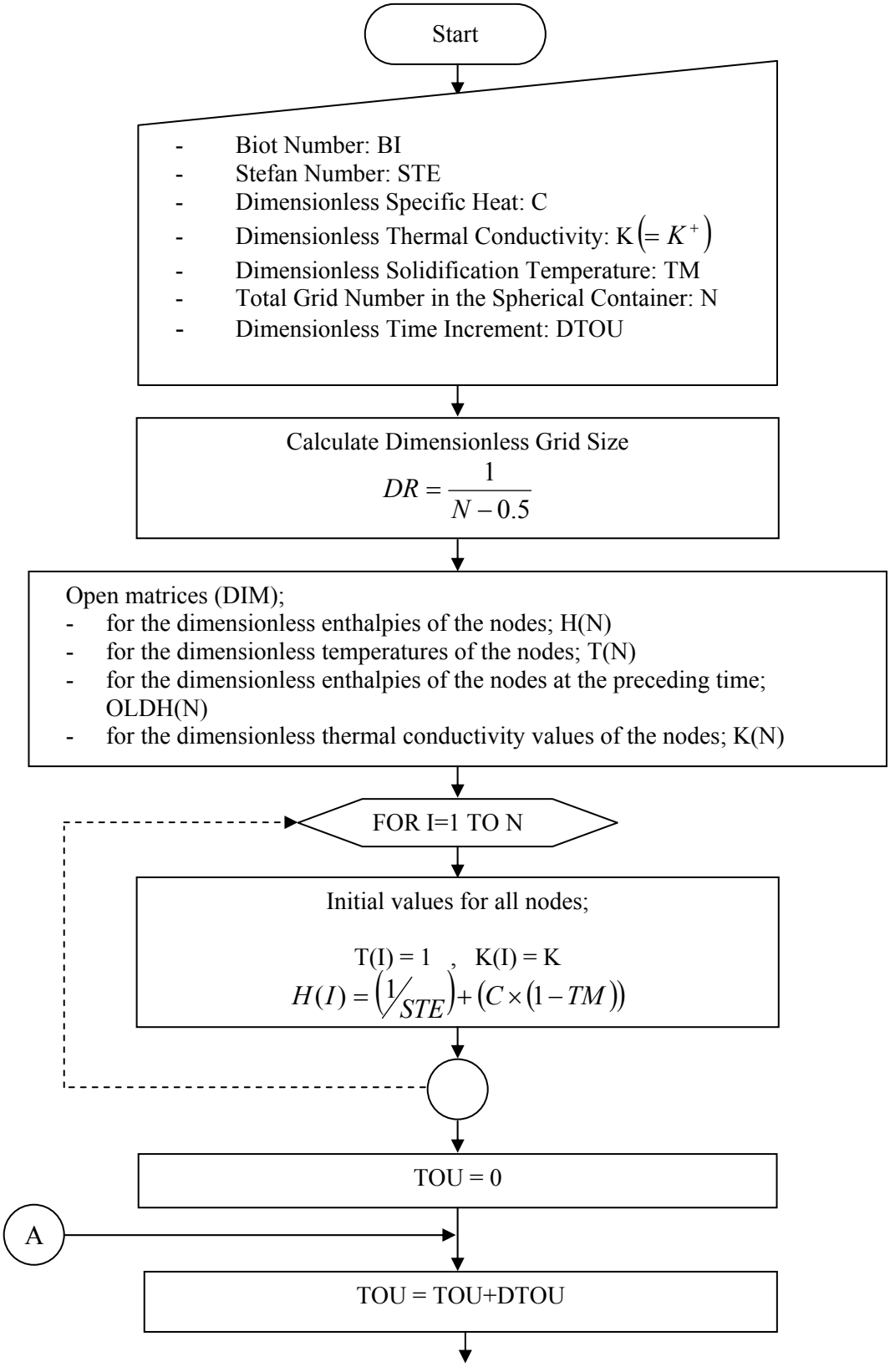

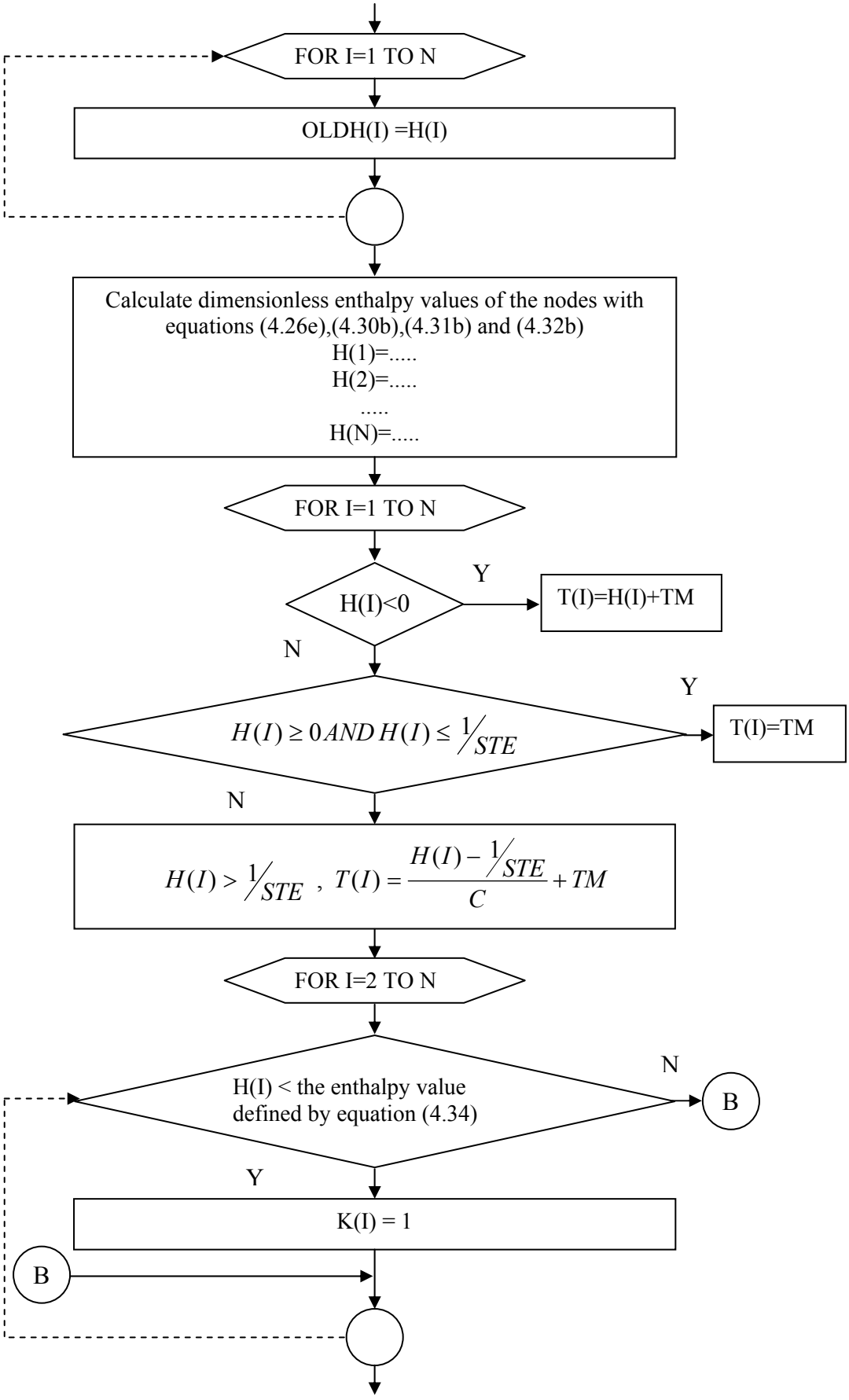
FOR I=1 TO N
OLDH(I) =H(I)
Calculate dimensionless enthalpy values of the nodes with equations (4.26e),(4.30b),(4.31b) and (4.32b)
H(1)=.....
H(2)=.....
.....
H(N)=.....
FOR I=1 TO N
H(I)<0
Y
T(I)=H(I)+TM
N
$H(I) \geq 0 \, AND \, H(I) \leq 1/STE$
Y
T(I)=TM
N
$H(I) > 1/STE \;,\; T(I) = \frac{H(I) - 1/STE}{C} + TM$
FOR I=2 TO N
H(I) < the enthalpy value defined by equation (4.34)
N
B
Y
K(I) = 1
B

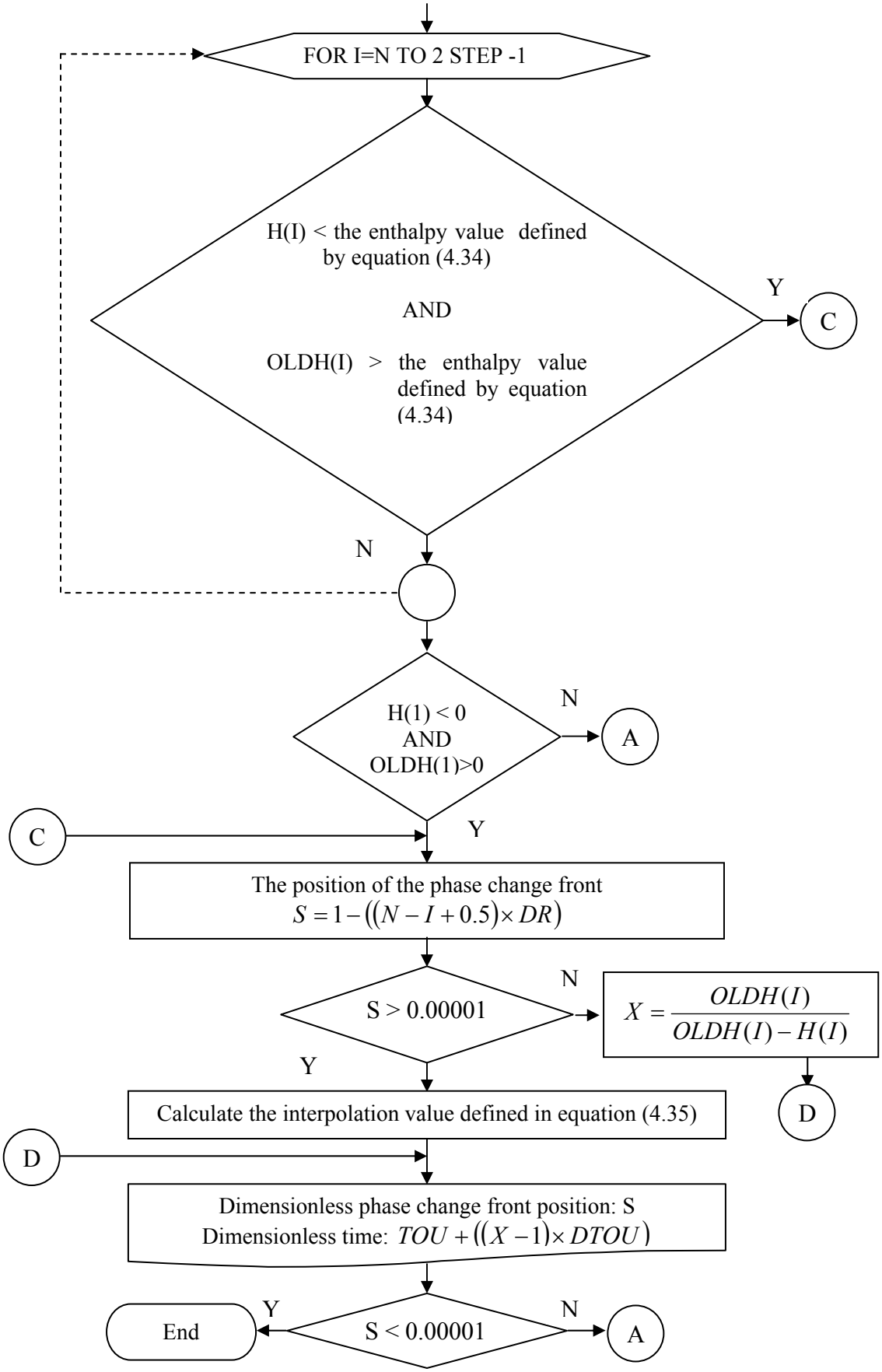
FOR I=N TO 2 STEP -1
H(I) < the enthalpy value defined by equation (4.34)
AND
OLDH(I) > the enthalpy value defined by equation (4.34)
Y
C
N
H(1) < 0
AND
OLDH(1)>0
N
A
C
Y
The position of the phase change front
$S = 1 - ((N - I + 0.5) \times DR)$
S > 0.00001
N
$X = \frac{OLDH(I)}{OLDH(I) - H(I)}$
Y
D
Calculate the interpolation value defined in equation (4.35)
D
Dimensionless phase change front position: S
Dimensionless time: $TOU + ((X - 1) \times DTOU)$
End
Y
S < 0.00001
N
A

CHAPTER 5

NUMERICAL MODELING OF A COOL STORAGE TANK

A numerical model is developed to simulate a storage system composed of spherical containers filled with phase change material (PCM) placed inside a cylindrical tank fitted with a working fluid circulation system to charge the storage tank. The simplified transient one-dimensional model is based on dividing the tank into a number of axial layers whose thickness is always equal to a container diameter. The numerical solution of the problem is realized by using a marching technique in which the phase change problem inside the spherical container is coupled with the energy balance equation between the spherical boundary and the working fluid. The solidification process inside the spherical container is solved by using enthalpy method with convective boundary condition on the external surface. The total solidification time of the spherical containers placed at the last layer and the charging time of the storage tank are investigated.

5.1 THE MATHEMATICAL MODEL

The physical system under study composed of a cylindrical tank filled with spherical containers containing PCM is shown in Figure (5.1).

In the mathematical model, the assumptions mentioned below are made for simplicity;

- The tank is fully insulated.
- The spherical containers form regular layers in the storage tank and the tank height is divided into M layers whose height is equal to the spherical containers' diameter.
- The temperature of working fluid at the entry of the cool storage tank is constant.
- Variation of working fluid temperature is only along the axial direction.
- The temperature of working fluid in a layer is uniform and equal to the average temperature of the layer.
- The heat exchange between each spherical container and the working fluid in a layer is equal.

- The assumptions, which are made in chapter 4, for the solidification process inside a spherical container are also valid in the cool storage tank model (except working fluid temperature, T_∞ and convection coefficient, h are not constant in this model).

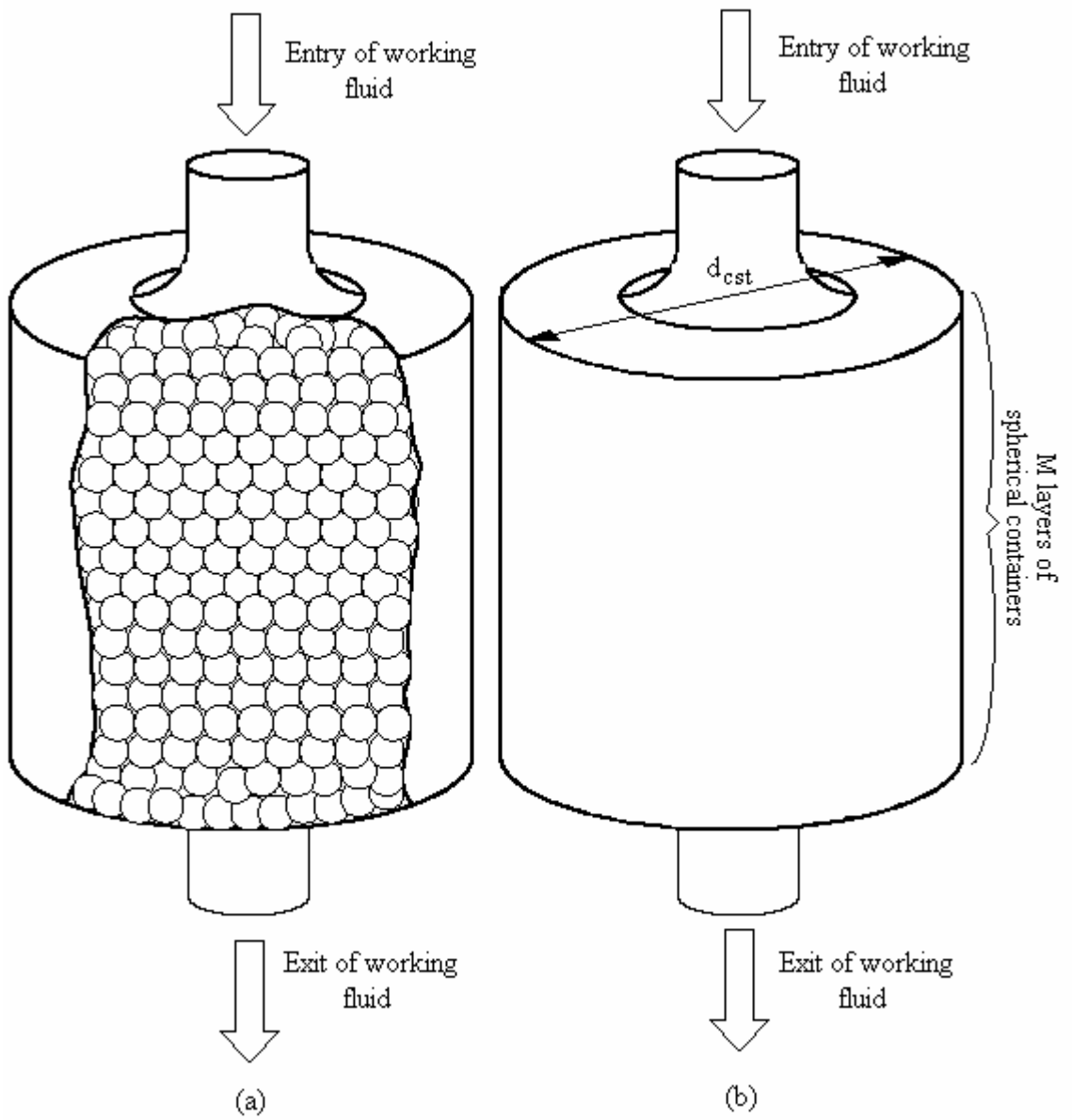

Fig 5.1 a) Layout of the Cool Storage Tank **b)** Dimensions of the Cool Storage Tank

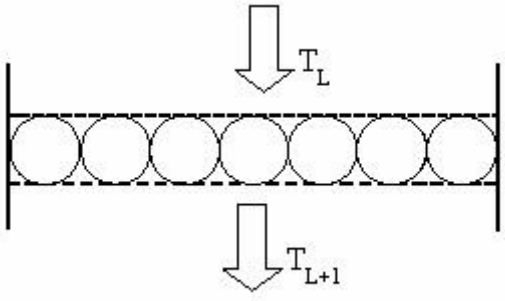

Fig 5.2 A Layer of the Cool Storage Tank

The energy balance for the working fluid in a layer of the cool storage tank shown in Figure 5.2 can be written as [23];

$$\dot{E}_{stored} = \dot{E}_{in} - \dot{E}_{out} + \dot{E}_{gen} \tag{5.1}$$

$$\rho_{wf} c_{p_{wf}} V_{wf} \frac{\partial T}{\partial t} = \dot{m} c_{p_{wf}} \left(T_L - T_{L+1}\right) + spcl.\dot{Q} \tag{5.2}$$

where V_{wf} is the volume of working fluid, spcl is the number of spherical containers in the layer and $\dot{Q}$ is the heat exchange between each spherical container and the working fluid.

Equation (5.2) can be written in finite difference as;

$$\rho_{wf} c_{p_{wf}} V_{wf} \left(\frac{T_j^{k+1} - T_j^k}{\Delta t} \right) = \dot{m} c_{p_{wf}} \left(T_L^k - T_{L+1}^k\right) + spcl.\dot{Q} \tag{5.3}$$

where T_j represents the working fluid temperature at the center of the layer while k and k+1 represent two successive time levels.

If it is assumed that temperature at the center of the layer T_j is the average value of entry (T_L) and exit (T_{L+1}) temperatures of the layer, equation (5.3) can be written as;

$$\rho_{wf} c_{p_{wf}} V_{wf} \left(\frac{\frac{T_{L+1}^{k+1} + T_L^{k+1}}{2} - \frac{T_{L+1}^k + T_L^k}{2}}{\Delta t} \right) = \dot{m} c_{p_{wf}} \left(T_L^k - T_{L+1}^k\right) + spcl.\dot{Q} \tag{5.4}$$

The temperature of working fluid at the exit of the layer at time level k+1 can be found from equation (5.4) as;

$$T_{L+1}^{k+1} = \frac{2.\dot{m}.\Delta t}{\rho_{wf}.V_{wf}} \left(T_L^k - T_{L+1}^k\right) + \frac{2.spcl.\dot{Q}.\Delta t}{\rho_{wf}.c_{p_{wf}}.V_{wf}} + T_L^k + T_{L+1}^k - T_L^{k+1} \tag{5.5}$$

The temperature at the entry of the first layer is known from the boundary condition and is considered constant $\left(T_{L=1}^{k+1} = T_{L=1}^k : cons\tan t\right)$, so the exit temperature of

the layer $\left(T_{L=2}^{k+1}\right)$ can be calculated from equation (5.5). The exit temperature of each layer is also the entry temperature for the next layer, so the exit temperature of all layers at time level k+1 can be found by using the same equation.

The complete charging time of the cool storage tank is determined by the exit temperature of the last layer. When the exit temperature of the last layer reaches the inlet temperature of the first layer (the inlet temperature to the cool storage tank), the charging process of the tank is finished and this time value is taken as the complete charging time of the cool storage tank.

5.1.1 Heat Exchange Between the Working Fluid and the Spherical Container

In the modeling of a cool storage tank, spherical containers with shells shown in Figure (5.3) are used.

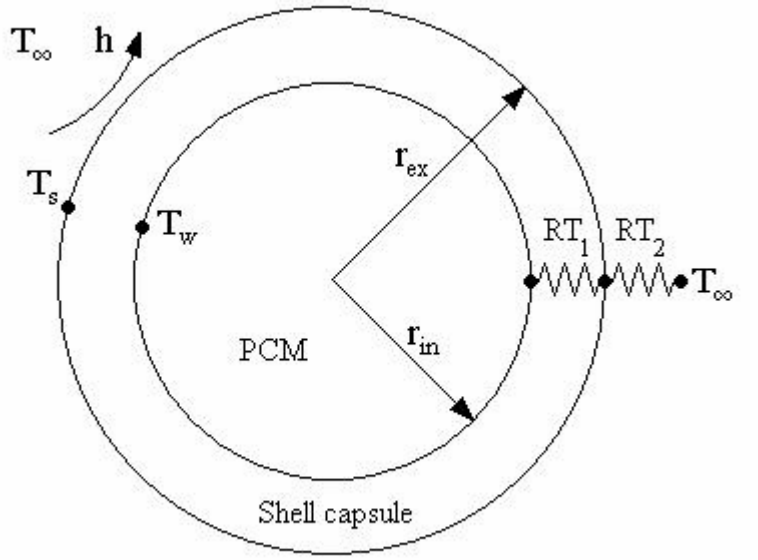

Fig 5.3 View of a Spherical Container with Shell

The heat exchange between the working fluid and the spherical container $\left(\dot{Q}\right)$ is obtained from an energy balance as below [25];

$$\dot{Q} = \frac{T_w - T_\infty}{RT_1 + RT_2} \tag{5.6}$$

$$\dot{Q} = \frac{T_w - T_\infty}{\left(\frac{r_{ex} - r_{in}}{4 \times \pi \times k_{shell} \times r_{ex} \times r_{in}} + \frac{1}{4 \times \pi \times r_{ex}^2 \times h}\right)} \tag{5.7}$$

The convection coefficient (h) on the external surface of the spherical containers is obtained from the relation proposed for the case of fluid flow in between the spheres arranged in a random form as below [23];

$$Nu = 3.22 \times \mathrm{Re}^{(1/3)} \times \mathrm{Pr}^{(1/3)} + 0.117 \times \mathrm{Re}^{0.8} \times \mathrm{Pr}^{0.8} \tag{5.8}$$

The thermophysical properties of the working fluid should be evaluated at the average of the surface temperature of the spherical container (T_s) and the mean temperature of entry and exit temperatures of the working fluid.

$$T = \frac{\frac{T_L + T_{L+1}}{2} + T_s}{2} \tag{5.9}$$

Reynolds number can be calculated from the following relation;

$$\mathrm{Re} = \frac{\rho_{wf} \times \bar{u} \times d_{ex}}{\mu_{wf}} \tag{5.10}$$

where ρ_{wf} is the density, μ_{wf} is the viscosity of the working fluid, d_{ex} is the external diameter of the sphere and $\bar{u}$ is the mean velocity in the bed.

The mass flow rate of the working fluid $(\dot{m})$ can be used to calculate the mean velocity in the bed of spheres of void fraction ε.

$$\dot{m} = \rho_{wf} \times \bar{u} \times (\varepsilon \times A_{cst}) \tag{5.11}$$

where, A_{cst} is the cross sectional area of the cool storage tank.

The void fraction is calculated as;

$$\varepsilon = \frac{volume\ of\ the\ cool\ storage \tan k - volume\ of\ the\ spherical\ containers}{volume\ of\ the\ cool\ storage \tan k}$$

$$\varepsilon = \frac{A_{cst} \times M \times d_{ex} - M \times spcl \times \left(\frac{4}{3}\pi . r_{ex}^3\right)}{A_{cst} \times M \times d_{ex}} \tag{5.12}$$

Finally, the convection heat transfer coefficient can be determined from the Nusselt number as;

$$h = \frac{k_{wf} \times Nu}{d_{ex}} \tag{5.13}$$

where k_{wf} is the thermal conductivity of working fluid.

5.1.2 Solidification Process Inside the Spherical Containers

Enthalpy method and control volume formulation are applied to solve the solidification problem of PCM inside the spherical containers as in chapter 4. However, since the containers used in cool storage tank have shells and the enthalpy equation used in chapter 4 is dimensionless, there are some differences in the numerical equations from the ones used in chapter 4. The spherical volume is divided into small control volumes as shown in Figure (5.4).

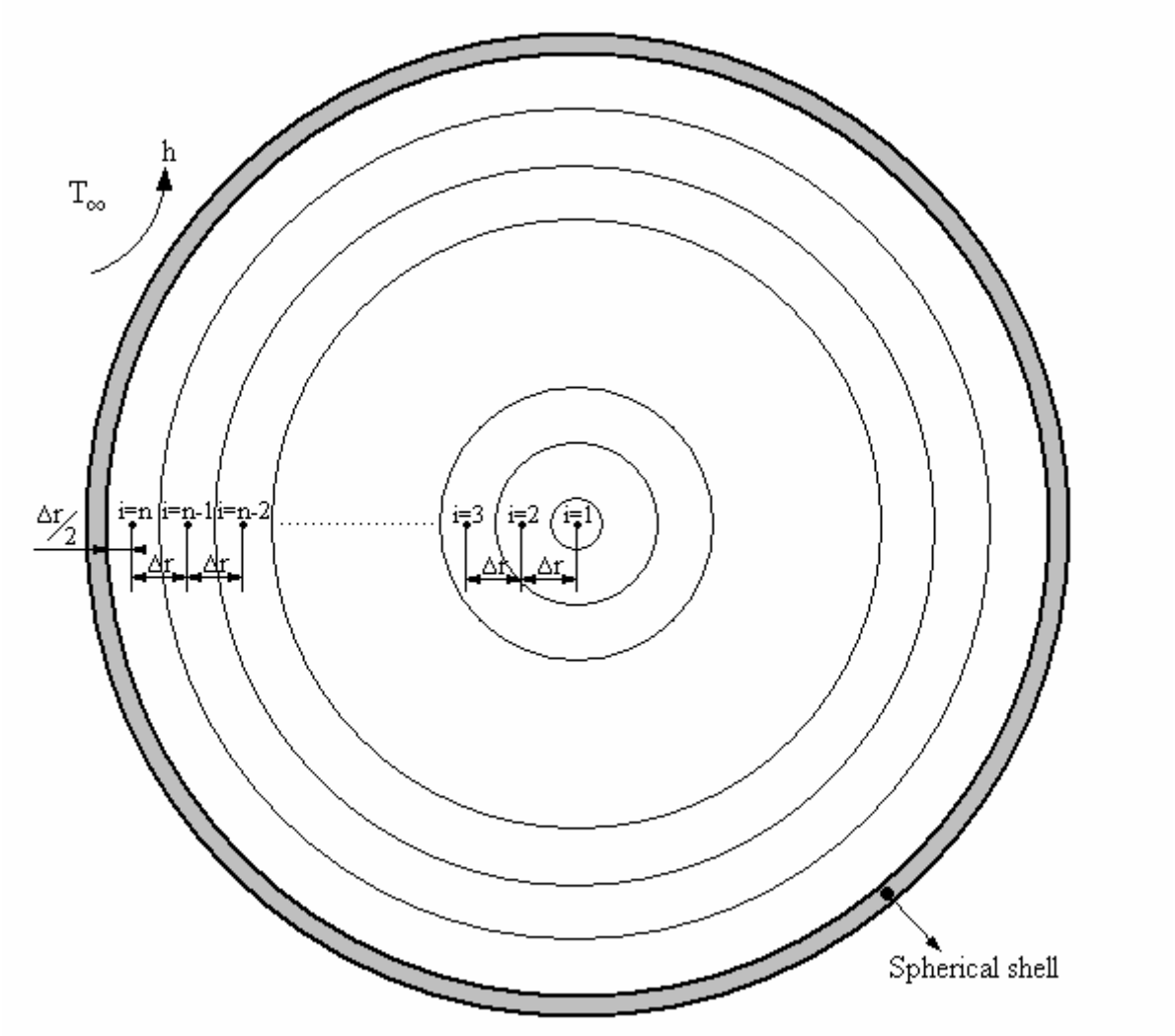

Fig 5.4 Control Volumes Inside a Spherical Container with Shell

The enthalpy equation for a spherical container is;

$$\rho \frac{\partial H}{\partial t} = \frac{1}{r^2} \frac{\partial}{\partial r} \left(k.r^2 . \frac{\partial T}{\partial r} \right) \tag{5.14}$$

The numerical equations obtained from the enthalpy equation by applying control volume formulation described in chapter 3 are;

- for i=1;

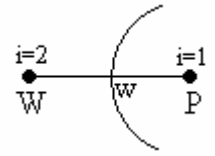

Fig 5.5 First Control Volume

$$r_P = 0 \ , \ r_w = \frac{\Delta r}{2} \ , \ r_W = \Delta r$$

For the first control volume if the enthalpy equation (eq 5.14) is integrated over the control volume and over the time interval;

$$\rho \int_{\Delta V} \int_{t}^{t+\Delta t} \frac{\partial H}{\partial t} dt dV = \int_{t}^{t+\Delta t} \int_{\Delta V} \frac{1}{r^2} \frac{\partial}{\partial r} \left(kr^2 \frac{\partial T}{\partial r} \right) dV dt \qquad , \quad dV = 4\pi r^2 dr \tag{5.15a}$$

$$\rho \int_{r_P}^{r_w} \int_{t}^{t+\Delta t} \frac{\partial H}{\partial t} dt 4\pi r^2 dr = \int_{t}^{t+\Delta t} \int_{r_P}^{r_w} \frac{1}{r^2} \frac{\partial}{\partial r} \left(kr^2 \frac{\partial T}{\partial r} \right) 4\pi r^2 dr dt \tag{5.15b}$$

$$\rho \left(H_P^{k+1} - H_P^k \right) \frac{r_w^3}{3} = \left(kr^2 \frac{\partial T}{\partial r} \right)_{r=r_w} \Delta t \tag{5.15c}$$

$$H_P^{k+1} = H_P^k + \frac{3\Delta t}{\rho . r_w} k_w \frac{T_W^k - T_P^k}{\Delta r} \tag{5.15d}$$

For the thermal conductivity value at the interface of the first two control volumes arithmetic average of the nodal thermal conductivities $\left(k_w = \left(k_P + k_W \right) \Big/ 2 \right)$ is taken.

$$H_1^{k+1} = H_1^k + \frac{3\Delta t}{\rho(\Delta r)^2}(k_1 + k_2)(T_2^k - T_1^k) \tag{5.15e}$$

- for i=2,3,.....,n-1

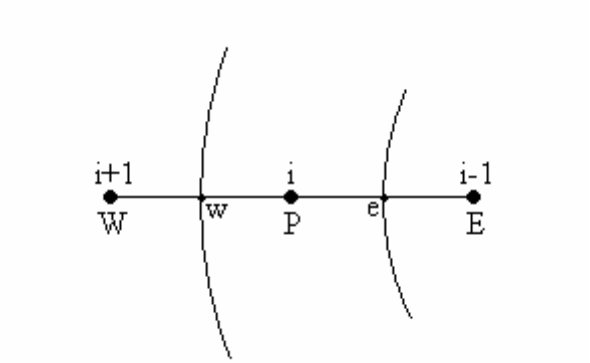

Fig 5.6 Control Volume for the Internal Points

$$r_W = i.\Delta r,\ r_w = (i-0.5).\Delta r,\ r_P = (i-1).\Delta r,\ r_e = (i-1.5).\Delta r,\ r_E = (i-2).\Delta r$$

The numerical equations for the internal nodes can be obtained by applying the same integration to the enthalpy equation;

$$\rho\int_{r_e}^{r_w}\int_{t}^{t+\Delta t}\frac{\partial H}{\partial t}dt\,4\pi r^2 dr = \int_{t}^{t+\Delta t}\int_{r_e}^{r_w}\frac{1}{r^2}\frac{\partial}{\partial r}\left(kr^2\frac{\partial T}{\partial r}\right)4\pi r^2 dt \tag{5.16a}$$

$$\rho\left(H_P^{k+1} - H_P^k\right)\left(\frac{r_w^3 - r_e^3}{3}\right) = \left[\left(kr^2\frac{\partial T}{\partial r}\right)_{r=r_w} - \left(kr^2\frac{\partial T}{\partial r}\right)_{r=r_e}\right]\Delta t \tag{5.16b}$$

Since, $r_w^3 - r_e^3 = \left(\underbrace{r_w - r_e}_{\Delta r}\right)\left(r_w^2 + r_w r_e + r_e^2\right)$;

$$H_P^{k+1} = H_P^k + \frac{3.\Delta t}{\rho.\left(r_w^2 + r_w r_e + r_e^2\right)}\frac{\left[\left(k_w r_w^2\frac{T_W^k - T_P^k}{\Delta r}\right) - \left(k_e r_e^2\frac{T_P^k - T_E^k}{\Delta r}\right)\right]}{\Delta r} \tag{5.16c}$$

The thermal conductivities at the interfaces are calculated as described in chapter 3;

$$k_e = \frac{r_e.(r_P - r_E).k_P.k_E}{r_E.(r_P - r_e).k_E + r_P.(r_e - r_E).k_P} \tag{5.17}$$

If the radius values are replaced in equation (5.17);

$$k_e = \frac{(i-1.5).k_P.k_E}{0.5(i-2).k_E + 0.5(i-1).k_P} \tag{5.18a}$$

$$k_w = \frac{(i-0.5).k_W.k_P}{0.5(i-1).k_P + 0.5i.k_W} \tag{5.18b}$$

However for i=2 the thermal conductivity at the interface of first and second control volumes is taken as the arithmetic average of the nodal thermal conductivities of the first and second nodes $\left(k_e = \frac{k_P + k_E}{2}\right)$.

So, for i=2;

$$H_2^{k+1} = H_2^k + \frac{3.\Delta t}{\rho.(1.5^2 + 1.5\times 0.5 + 0.5^2).(\Delta r)^2} \times \frac{\left[\left(\frac{1.5k_W.k_P}{0.5k_P + k_W} 1.5^2(\Delta r)^2 \frac{T_W^k - T_P^k}{\Delta r}\right) - \left(\frac{k_P + k_E}{2} 0.5^2(\Delta r)^2 \frac{T_P^k - T_E^k}{\Delta r}\right)\right]}{\Delta r} \tag{5.19a}$$

$$H_2^{k+1} = H_2^k + \frac{3.\Delta t}{3.25\rho(\Delta r)^2}\left[\frac{1.5^3 k_3.k_2}{0.5k_2 + k_3}\left(T_3^k - T_2^k\right) - \frac{k_1 + k_2}{2} 0.5^2\left(T_2^k - T_1^k\right)\right] \tag{5.19b}$$

for i=3,4,.....,n-1;

$$H_i^{k+1} = H_i^k + \frac{3.\Delta t}{\rho\left((i-0.5)^2 + (i-0.5)(i-1.5) + (i-1.5)^2\right).(\Delta r)^2} \times \frac{\left[\left(\frac{(i-0.5)k_W.k_P}{0.5(i-1)k_P + 0.5i.k_W}(i-0.5)^2(\Delta r)^2 \frac{T_W^k - T_P^k}{\Delta r}\right) - \left(\frac{(i-1.5)k_P k_E}{0.5(i-2)k_E + 0.5(i-1)k_P}(i-1.5)^2(\Delta r)^2 \frac{T_P^k - T_E^k}{\Delta r}\right)\right]}{\Delta r} \tag{5.20a}$$

$$H_i^{k+1} = H_i^k + \frac{3.\Delta t}{\rho\left(3i^2 - 6i + 3.25\right)\left(\Delta r\right)^2} \times$$

$$\left[\left(\frac{\left(i-0.5\right)^3 k_{i+1} k_i}{0.5\left(i-1\right)k_i + 0.5i.k_{i+1}}\left(T_{i+1}^k - T_i^k\right)\right) - \left(\frac{\left(i-1.5\right)^3 k_i k_{i-1}}{0.5\left(i-2\right)k_{i-1} + 0.5\left(i-1\right)k_i}\left(T_i^k - T_{i-1}^k\right)\right)\right] \tag{5.20b}$$

- for i=n

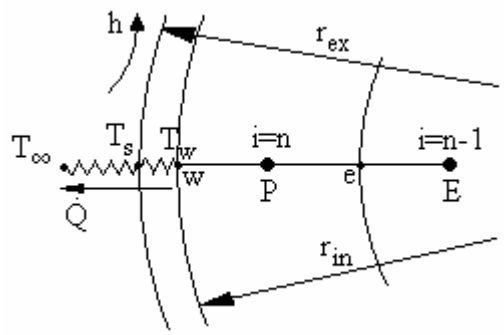

Fig 5.7 Last Control Volume

$$r_w = \left(n-0.5\right)\Delta r \ , \ r_P = \left(n-1\right)\Delta r \ , \ r_e = \left(n-1.5\right)\Delta r \ , \ r_E = \left(n-2\right)\Delta r$$

The main difference between the spherical containers investigated in chapter 4 and in the modeling of the cool storage tank is that the latter has shell, so the numerical equation written for the last node can be obtained as follows;

When the integration of the enthalpy equation (equation 5.16a) is done for the last control volume, the following equation is derived;

$$H_P^{k+1} = H_P^k + \frac{3.\Delta t}{\rho\left(r_w^2 + r_w r_e + r_e^2\right)} \frac{\left[\left(kr^2 \frac{\partial T}{\partial r}\right)_{r=r_w} - \left(kr^2 \frac{\partial T}{\partial r}\right)_{r=r_e}\right]}{\Delta r} \tag{5.21a}$$

$$H_P^{k+1} = H_P^k + \frac{3.\Delta t}{\rho\left(r_w^2 + r_w r_e + r_e^2\right)} \frac{\left[\left(k_w r_w^2 \frac{T_w^k - T_P^k}{\Delta r/2}\right) - \left(k_e r_e^2 \frac{T_P^k - T_E^k}{\Delta r}\right)\right]}{\Delta r} \tag{5.21b}$$

The thermal conductivity for the interface between the nodes P and E can be obtained from equation (5.17) as;

$$k_e = \frac{(n-1.5).k_P.k_E}{0.5(n-2)k_E + 0.5(n-1)k_P} \tag{5.22}$$

The thermal conductivity for the west side of the node P is;

$$k_w = k_P \tag{5.23}$$

So, the numerical equation for i=n is;

$$H_n^{k+1} = H_n^k + \frac{3.\Delta t}{\rho\left((n-0.5)^2 + (n-0.5)(n-1.5) + (n-1.5)^2\right)(\Delta r)^2} \times \tag{5.24a}$$

$$\frac{\left[\left(k_P.(n-0.5)^2(\Delta r)^2 \frac{T_w^k - T_P^k}{\Delta r/2}\right) - \left(\frac{(n-1.5).k_P.k_E}{0.5(n-2)k_E + 0.5(n-1)k_P}(n-1.5)^2(\Delta r)^2 \frac{T_P^k - T_E^k}{\Delta r}\right)\right]}{\Delta r}$$

$$H_n^{k+1} = H_n^k + \frac{3.\Delta t}{\rho\left(3n^2 - 6n + 3.25\right)(\Delta r)^2} \times \tag{5.24b}$$

$$\left[\left(2.k_n(n-0.5)^2\left(T_w^k - T_n^k\right)\right) - \left(\frac{(n-1.5)^3 k_n.k_{n-1}}{0.5(n-2)k_{n-1} + 0.5(n-1)k_n}\left(T_n^k - T_{n-1}^k\right)\right)\right]$$

The temperature of the inner surface of the spherical shell (T_w) can be found from the heat exchange between the working fluid and spherical container as follows;

$$\dot{Q} = \frac{T_w - T_\infty}{\frac{1}{4.\pi.r_{ex}^2.h} + \frac{r_{ex} - r_{in}}{4.\pi.k_{shell}.r_{ex}.r_{in}}} = -k.A.\left(\frac{dT}{dr}\right)_{r=r_{in}} \tag{5.25a}$$

$$\dot{Q} = \frac{T_w - T_\infty}{\frac{1}{4.\pi.r_{ex}^2.h} + \frac{r_{ex} - r_{in}}{4.\pi.k_{shell}.r_{ex}.r_{in}}} = -k_n.4.\pi.r_{in}^2 \frac{T_w - T_n}{\frac{\Delta r}{2}} \tag{5.25b}$$

$$T_w = \frac{2.k_n.r_{in}.\left(k_{shell}.r_{in} + r_{ex}.h.(r_{ex} - r_{in})\right).T_n + h.k_{shell}.r_{ex}^2.\Delta r.T_\infty}{h.k_{shell}.r_{ex}^2.\Delta r + 2.k_n.r_{in}.\left(k_{shell}.r_{in} + r_{ex}.h.(r_{ex} - r_{in})\right)} \tag{5.25c}$$

If equation (5.25c) is replaced in equation (5.24b);

$$H_n^{k+1} = H_n^k + \frac{3.\Delta t}{\rho\left(3n^2 - 6n + 3.25\right)\left(\Delta r\right)^2} \times \tag{5.26}$$

$$\left[\left(2.k_n.\left(n-0.5\right)^2\left(\frac{2.k_n.r_{in}.\left(k_{shell}.r_{in} + r_{ex}.h.\left(r_{ex} - r_{in}\right)\right)T_n^k + h.k_{shell}.r_{ex}^2.\Delta r.T_\infty}{h.k_{shell}.r_{ex}^2.\Delta r + 2.k_n.r_{in}.\left(k_{shell}.r_{in} + r_{ex}.h.\left(r_{ex} - r_{in}\right)\right)} - T_n^k\right)\right)\right.$$

$$\left. - \frac{\left(n-1.5\right)^3.k_n.k_{n-1}}{0.5\left(n-2\right).k_{n-1} + 0.5\left(n-1\right).k_n}\left(T_n^k - T_{n-1}^k\right)\right]$$

The enthalpy values of all nodes at time level k+1 can be calculated by using equations (5.15e), (5.19b), (5.20b) and (5.26). Then the new temperature values can be found from the enthalpies as described in chapter 3;

$$T = \begin{cases} \dfrac{H}{c_s} + T_m & for\ H < 0 \\ T_m & for\ 0 \le H \le L \\ \dfrac{H - L}{c_l} + T_m & for\ H > L \end{cases} \tag{5.27}$$

These new temperature values are used to find the enthalpy values for the next time level and the total solidification time of the container is determined by controlling if the enthalpy value of the first node (i=1) is less than 0 or not.

The complete solidification time for the cool storage tank is investigated in this chapter. Complete solidification is reached when the spherical containers of the last layer of the cool storage tank are fully solidified. This time value also indicates that solidification process for all of the containers inside the tank is finished. The complete solidification time is determined as described above by controlling the enthalpy value of the first node of the container in the last layer.

5.1.3 Surface temperature of the spherical container

The surface temperature of the spherical container (T_s) is necessary for the calculation of thermophysical properties of working fluid and is calculated from the heat exchange between the spherical container and working fluid.

$$\dot{Q} = \frac{T_w - T_\infty}{\frac{1}{4.\pi.r_{ex}^2.h} + \frac{r_{ex} - r_{in}}{4.\pi.k_{shell}.r_{ex}.r_{in}}} = \frac{T_w - T_s}{\frac{r_{ex} - r_{in}}{4.\pi.k_{shell}.r_{ex}.r_{in}}} \tag{5.28a}$$

$$T_s = \frac{k_{shell}.r_{in}.T_w + h.r_{ex}.(r_{ex} - r_{in}).T_\infty}{k_{shell}.r_{in} + r_{ex}.h.(r_{ex} - r_{in})} \tag{5.28b}$$

The surface temperature of a single spherical container with shell is determined for constant convective heat transfer coefficient (h) and constant coolant fluid temperature (T_∞) and some oscillations are encountered during the solidification process. The reason of these numerical oscillations is the approximation (which is similar to the harmonic mean approach in rectangular coordinates) used for the calculation of thermal conductivity values at the interfaces of control volumes. It is indicated that temperature predictions obtained with the harmonic and arithmetic mean approximation quite often show such oscillations [28]. However, when the total grid number inside the container is increased it is observed that there is a reduction in numerical fluctuations in the surface temperature. When the time step (Δt) is changed it is seen that there is no change in the oscillations as shown in figures (5.9), (5.10) and (5.11). Similar oscillations are also observed in the surface temperature of the containers used in cool storage program, but they are decreased to minimum by taking many grid points inside the container.

For the following figures convective heat transfer coefficient is taken as $100 W/m^2K$, the coolant fluid temperature is –20 $°C$, initial temperature of PCM is $10°C$, the inner and outer diameter of the spherical shell is 0.0745 m and 0.0765 m, respectively and the thermal conductivity of spherical shell is $0.35 W/mK$.

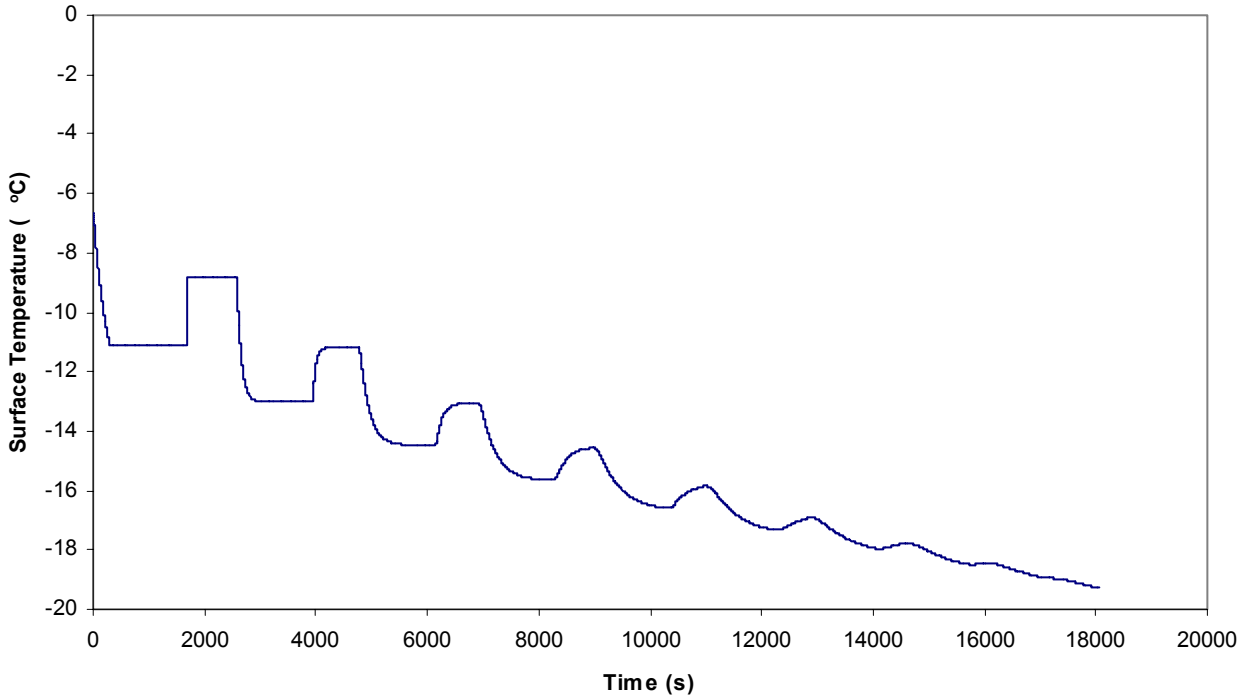

Fig 5.8 Surface Temperature for N=11, DT=0.2 (s)

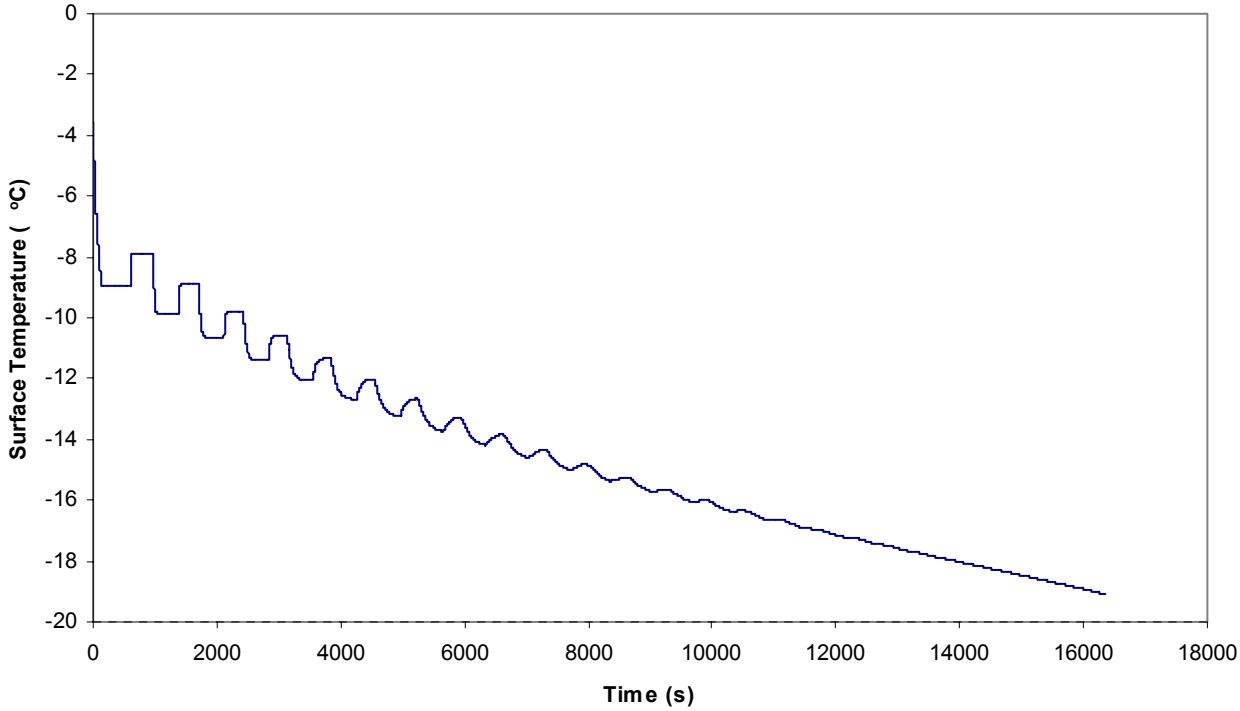

Fig 5.9 Surface Temperature for N=31, DT=0.2 (s)

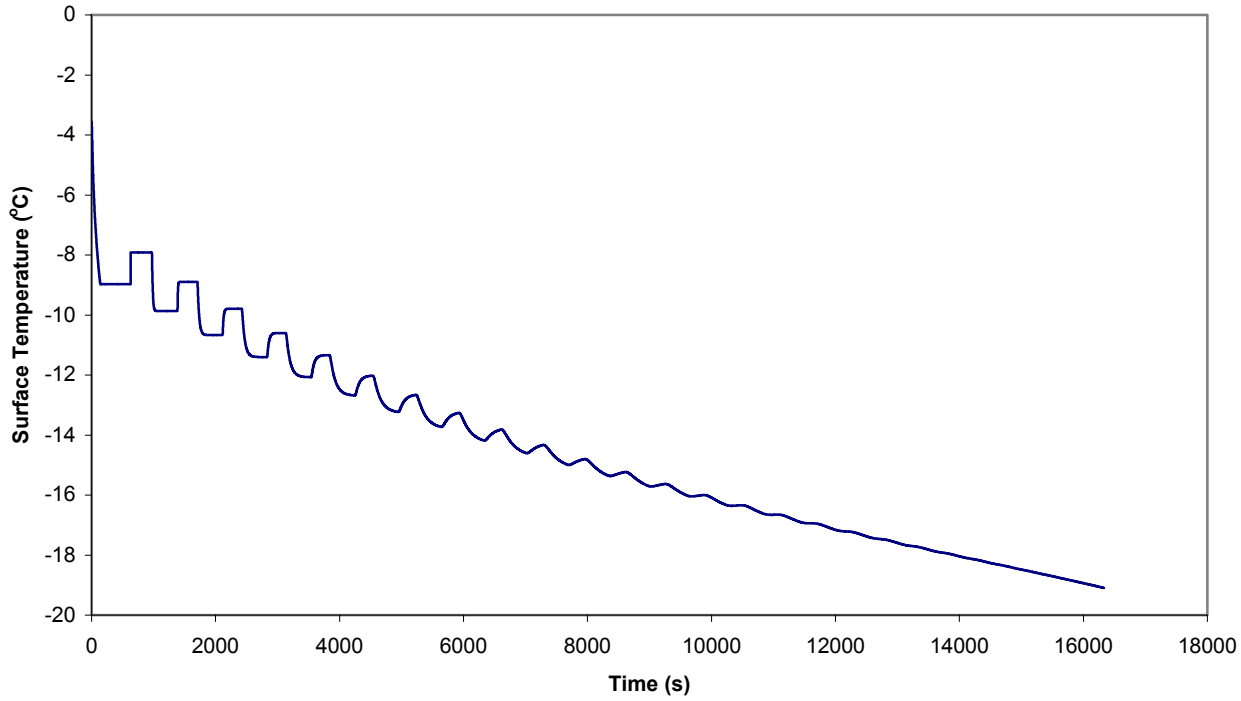

Fig 5.10 Surface Temperature for N=31, DT=0.1(s)

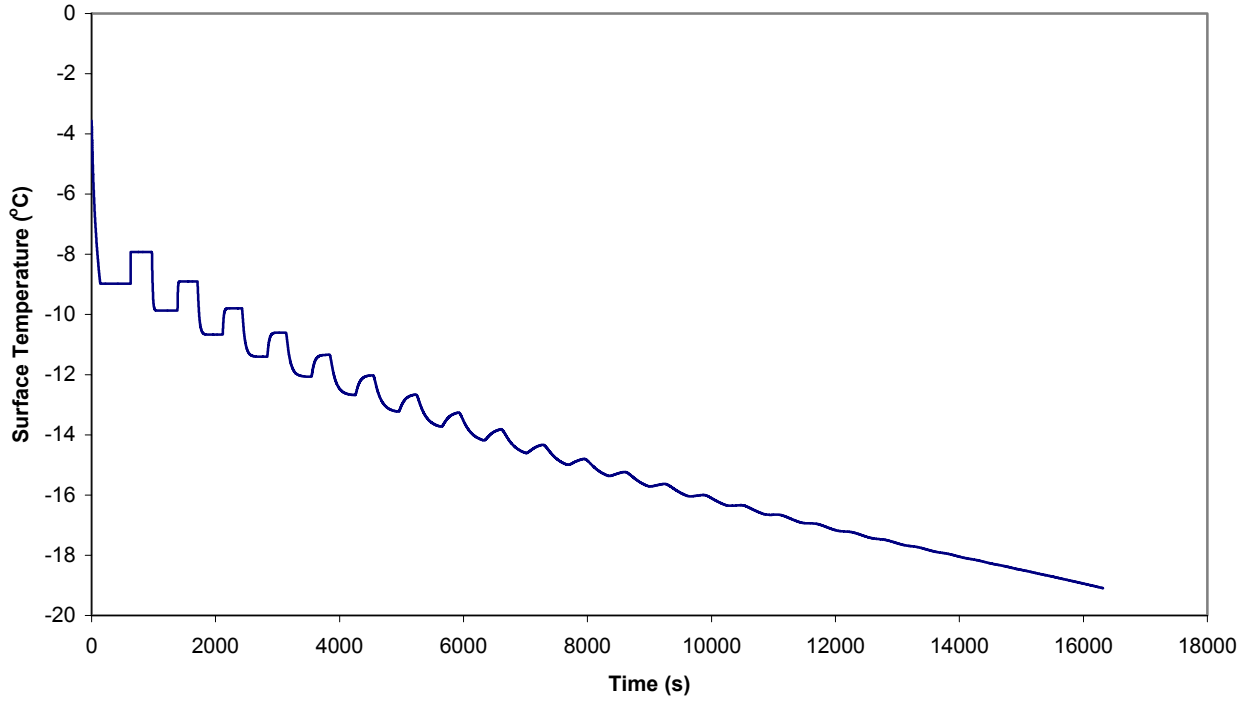

Fig 5.11 Surface Temperature for N=31, DT=0.05(s)

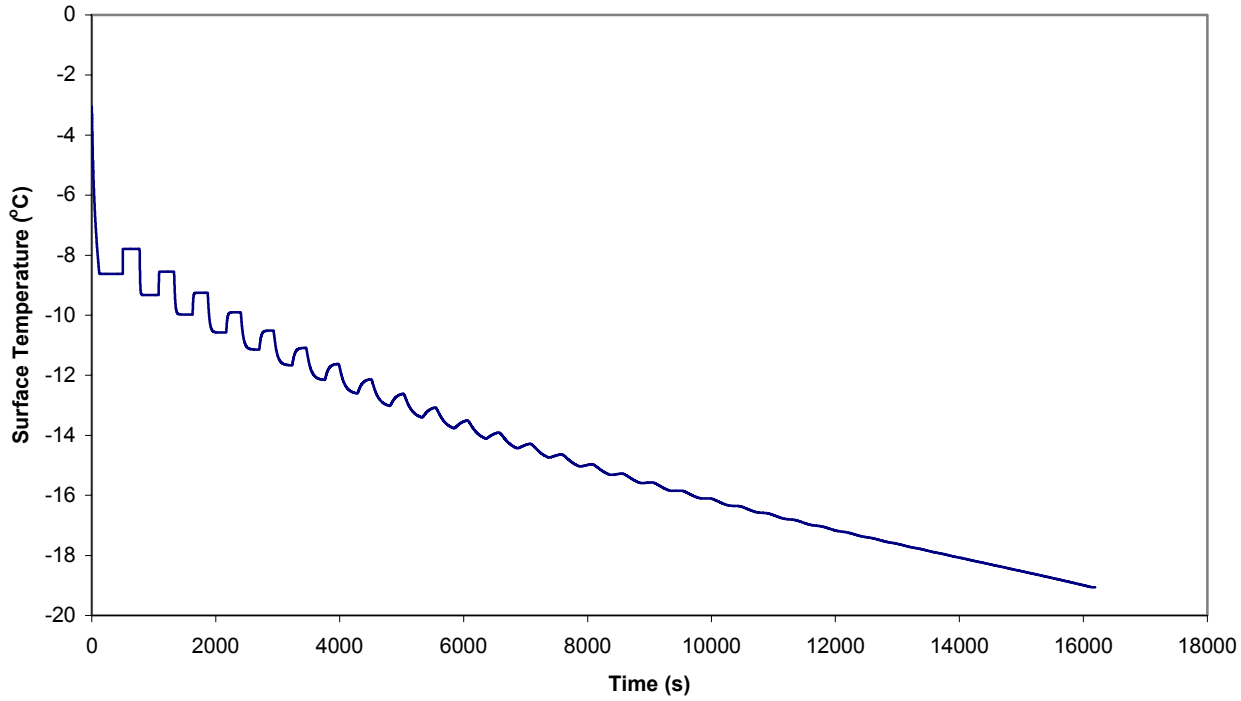

Fig 5.12 Surface Temperature for N=41, DT=0.2(s)

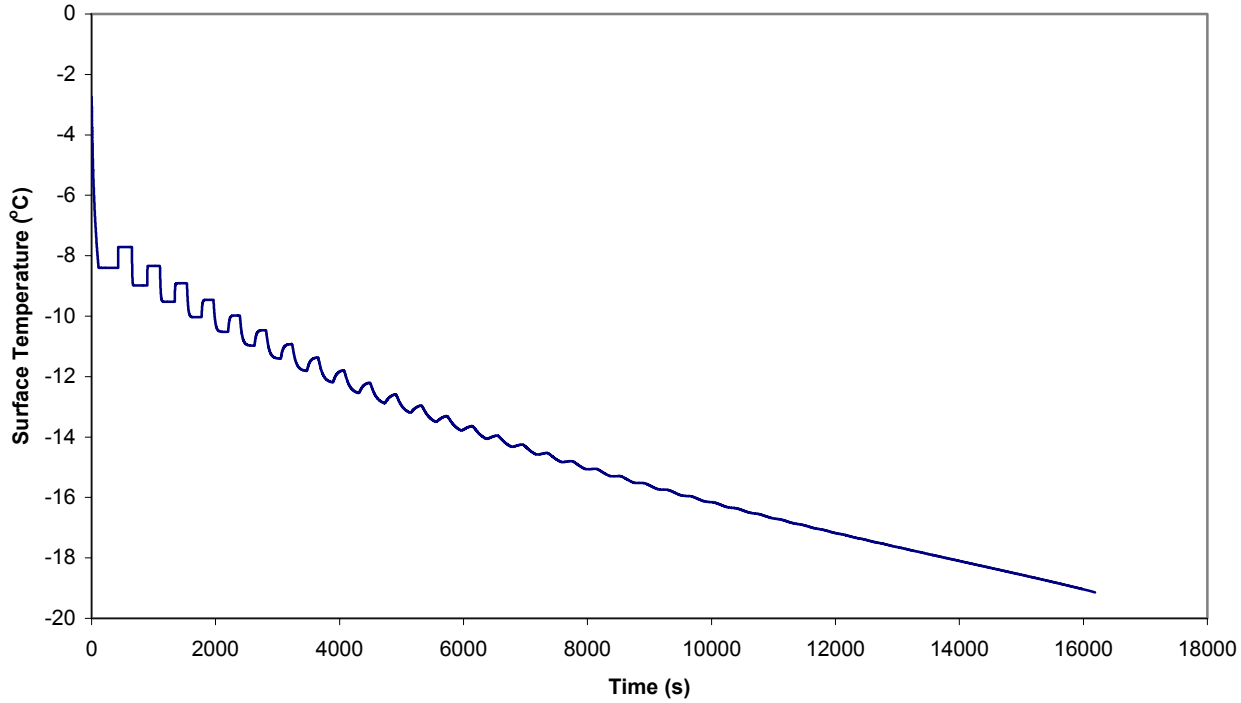

Fig 5.13 Surface Temperature for N=51, DT=0.2(s)

5.2 THE COOL STORAGE TANK PROGRAM

A program with Q Basic language is written to determine the complete solidification and charging time of the cool storage tank. The program is given in Appendix C. In the program, the solidification process inside the spherical containers and working fluid exit temperature of all layers inside the storage tank are solved simultaneously as described in the mathematical model. In the program, ethylene glycol of 30% volumetric concentration is used as the working fluid. Polynomial expressions are determined for the thermophysical properties of the ethylene glycol as;

$$\rho_{wf}\left(\frac{kg}{m^3}\right) = 0.0000001399\times T^3 - 0.0024417249\times T^2 - 0.2775594406\times T + 1051.7802564102 \quad (5.29a)$$

$$k_{wf}\left(\frac{W}{m^2.K}\right) = 0.0000000078\times T^3 - 0.0000065035\times T^2 + 0.0013500389\times T + 0.4290885781 \quad (5.29b)$$

$$c_{p_{wf}}\left(\frac{j}{kg.K}\right) = 0.000004662\times T^3 - 0.0005361305\times T^2 + 2.8526806527\times T + 3588.578088578 \quad (5.29c)$$

$$\mu_{wf}\left(\frac{kg}{m.s}\right) = -0.000000037\times T^3 + 0.000003635\times T^2 - 0.0001578089\times T + 0.0041800699 \quad (5.29d)$$

Prandtl number of working fluid is calculated as;

$$\mathrm{Pr}_{wf} = \frac{c_{p_{wf}}\times \mu_{wf}}{k_{wf}} \quad (5.29e)$$

The flow chart of the program is given as follows;

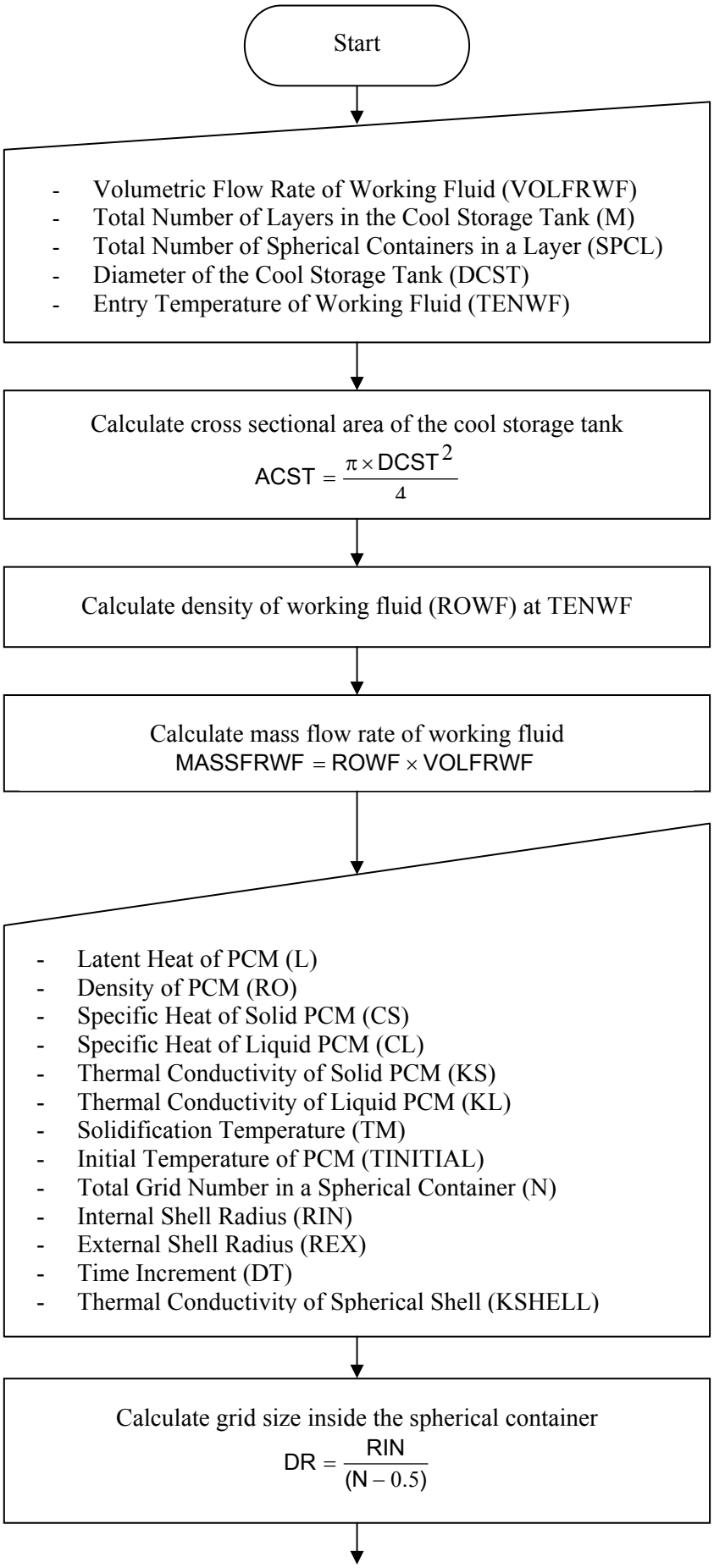
Start
- Volumetric Flow Rate of Working Fluid (VOLFRWF)
- Total Number of Layers in the Cool Storage Tank (M)
- Total Number of Spherical Containers in a Layer (SPCL)
- Diameter of the Cool Storage Tank (DCST)
- Entry Temperature of Working Fluid (TENWF)
Calculate cross sectional area of the cool storage tank
$ACST = \frac{\pi \times DCST^2}{4}$
Calculate density of working fluid (ROWF) at TENWF
Calculate mass flow rate of working fluid
$MASSFRWF = ROWF \times VOLFRWF$
- Latent Heat of PCM (L)
- Density of PCM (RO)
- Specific Heat of Solid PCM (CS)
- Specific Heat of Liquid PCM (CL)
- Thermal Conductivity of Solid PCM (KS)
- Thermal Conductivity of Liquid PCM (KL)
- Solidification Temperature (TM)
- Initial Temperature of PCM (TINITIAL)
- Total Grid Number in a Spherical Container (N)
- Internal Shell Radius (RIN)
- External Shell Radius (REX)
- Time Increment (DT)
- Thermal Conductivity of Spherical Shell (KSHELL)
Calculate grid size inside the spherical container
$DR = \frac{RIN}{(N - 0.5)}$

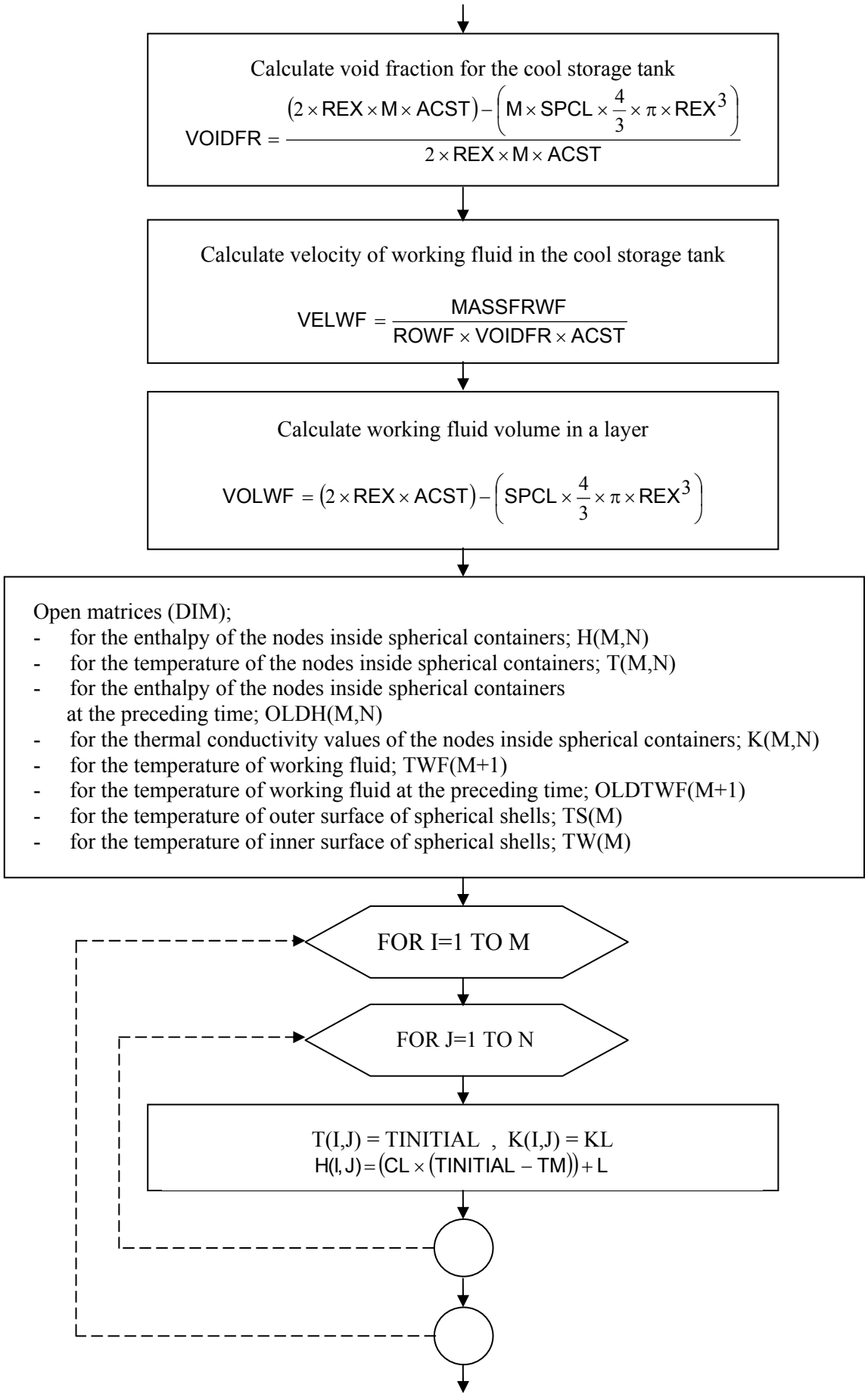
Calculate void fraction for the cool storage tank
$VOIDFR = \frac{(2 \times REX \times M \times ACST) - \left(M \times SPCL \times \frac{4}{3} \times \pi \times REX^3\right)}{2 \times REX \times M \times ACST}$
Calculate velocity of working fluid in the cool storage tank
$VELWF = \frac{MASSFRWF}{ROWF \times VOIDFR \times ACST}$
Calculate working fluid volume in a layer
$VOLWF = (2 \times REX \times ACST) - \left(SPCL \times \frac{4}{3} \times \pi \times REX^3\right)$
Open matrices (DIM);
- for the enthalpy of the nodes inside spherical containers; H(M,N)
- for the temperature of the nodes inside spherical containers; T(M,N)
- for the enthalpy of the nodes inside spherical containers at the preceding time; OLDH(M,N)
- for the thermal conductivity values of the nodes inside spherical containers; K(M,N)
- for the temperature of working fluid; TWF(M+1)
- for the temperature of working fluid at the preceding time; OLDTWF(M+1)
- for the temperature of outer surface of spherical shells; TS(M)
- for the temperature of inner surface of spherical shells; TW(M)
FOR I=1 TO M
FOR J=1 TO N
T(I,J) = TINITIAL , K(I,J) = KL
$H(I,J) = (CL \times (TINITIAL - TM)) + L$

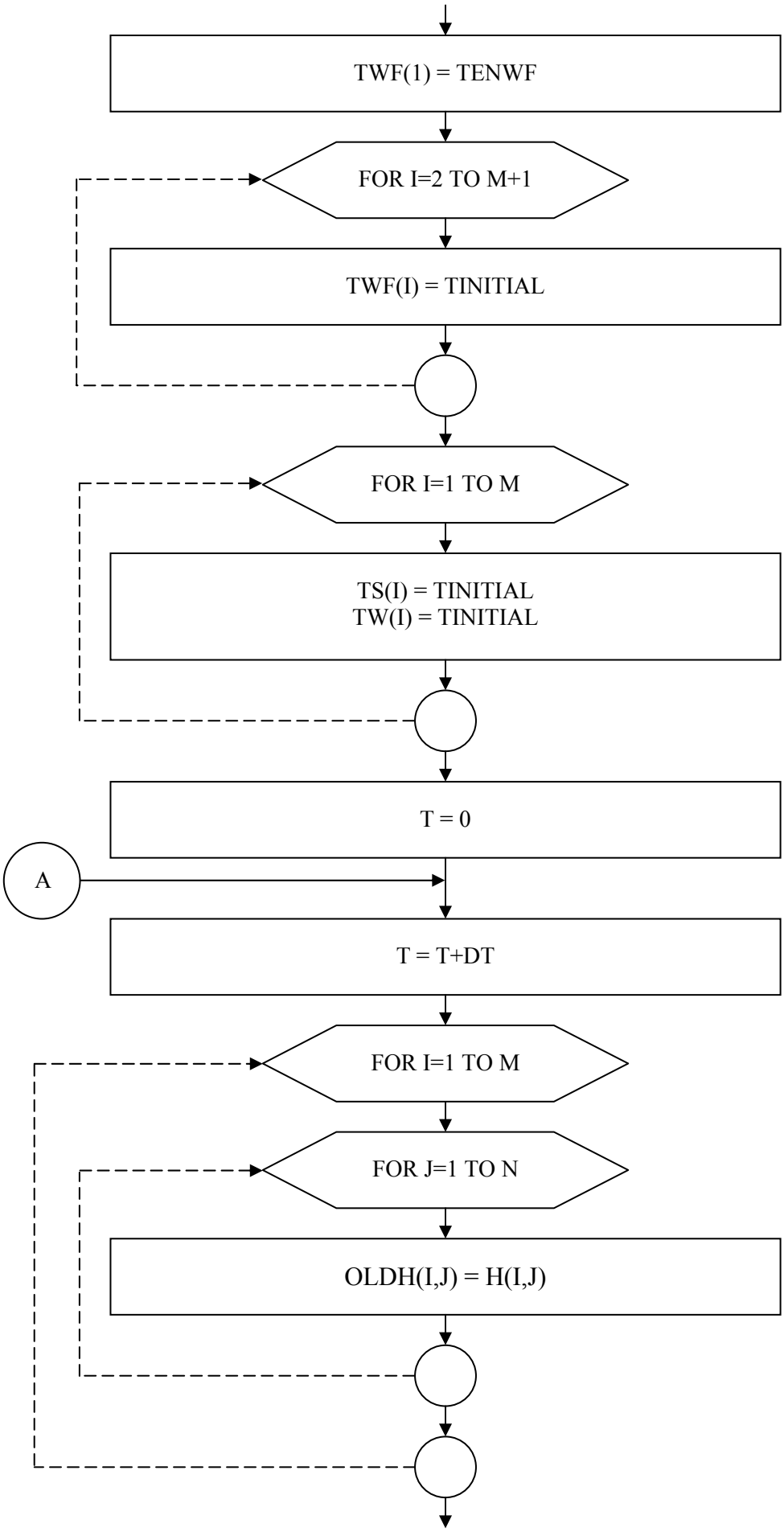
TWF(1) = TENWF
FOR I=2 TO M+1
TWF(I) = TINITIAL
FOR I=1 TO M
TS(I) = TINITIAL
TW(I) = TINITIAL
T = 0
A
T = T+DT
FOR I=1 TO M
FOR J=1 TO N
OLDH(I,J) = H(I,J)

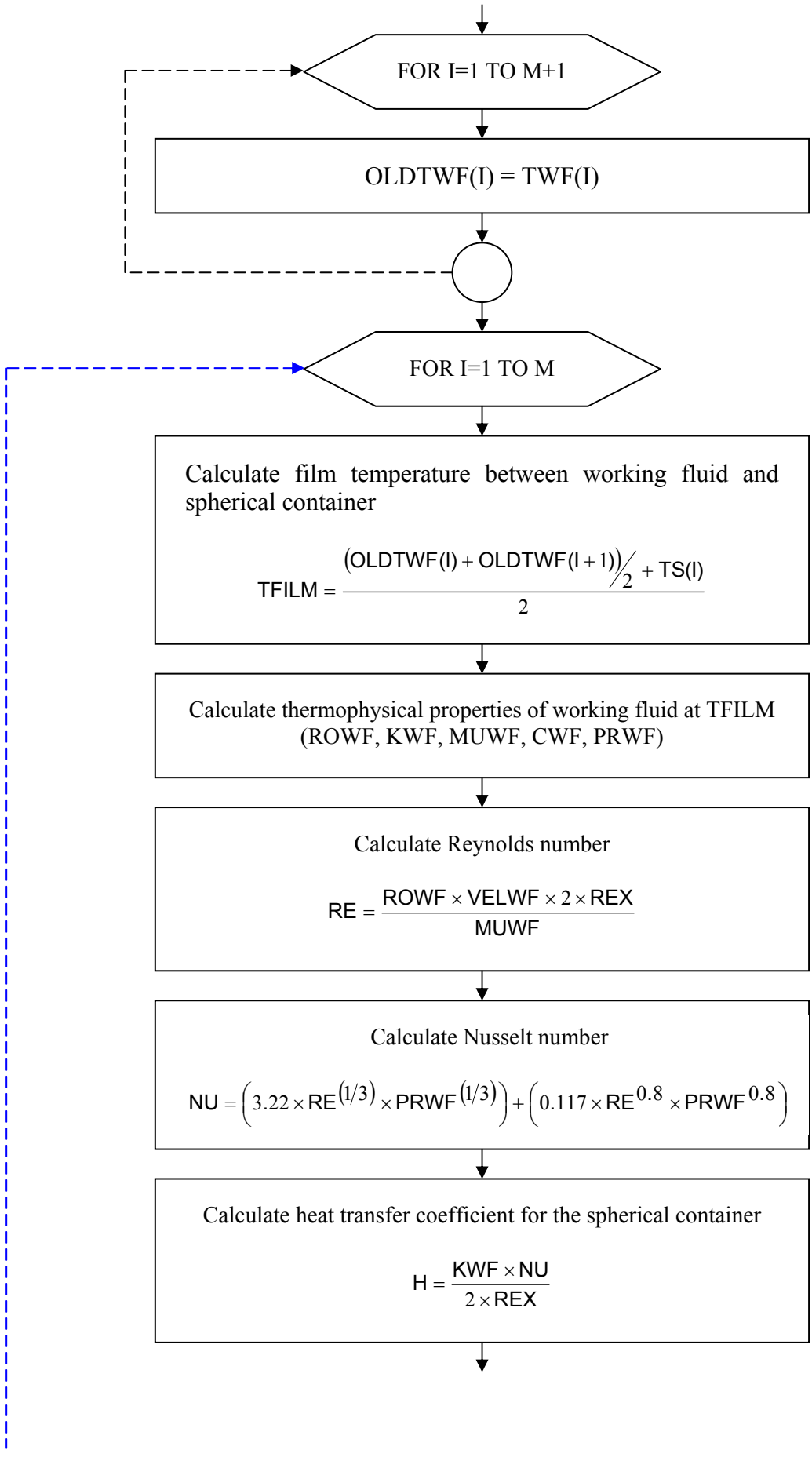
FOR I=1 TO M+1
OLDTWF(I) = TWF(I)
FOR I=1 TO M
Calculate film temperature between working fluid and spherical container
$TFILM = \frac{\left(OLDTWF(I) + OLDTWF(I+1)\right)/2 + TS(I)}{2}$
Calculate thermophysical properties of working fluid at TFILM (ROWF, KWF, MUWF, CWF, PRWF)
Calculate Reynolds number
$RE = \frac{ROWF \times VELWF \times 2 \times REX}{MUWF}$
Calculate Nusselt number
$NU = \left(3.22 \times RE^{(1/3)} \times PRWF^{(1/3)}\right) + \left(0.117 \times RE^{0.8} \times PRWF^{0.8}\right)$
Calculate heat transfer coefficient for the spherical container
$H = \frac{KWF \times NU}{2 \times REX}$

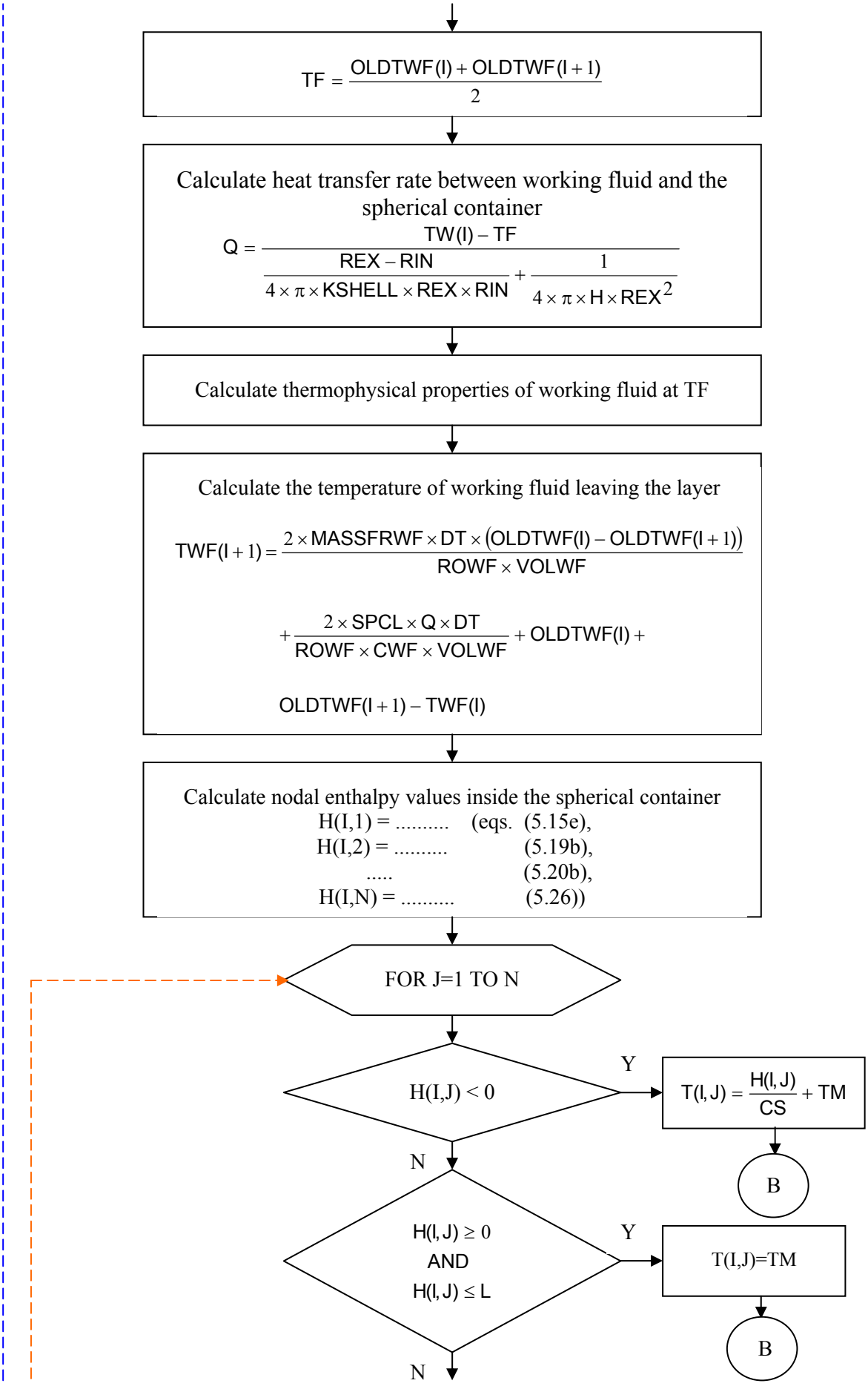
$TF = \frac{OLDTWF(I) + OLDTWF(I+1)}{2}$
Calculate heat transfer rate between working fluid and the spherical container
$Q = \frac{TW(I) - TF}{\frac{REX - RIN}{4 \times \pi \times KSHELL \times REX \times RIN} + \frac{1}{4 \times \pi \times H \times REX^2}}$
Calculate thermophysical properties of working fluid at TF
Calculate the temperature of working fluid leaving the layer
$TWF(I+1) = \frac{2 \times MASSFRWF \times DT \times (OLDTWF(I) - OLDTWF(I+1))}{ROWF \times VOLWF}$
$+ \frac{2 \times SPCL \times Q \times DT}{ROWF \times CWF \times VOLWF} + OLDTWF(I) +$
$OLDTWF(I+1) - TWF(I)$
Calculate nodal enthalpy values inside the spherical container
H(I,1) = ... (eqs. (5.15e),
H(I,2) = ... (5.19b),
..... (5.20b),
H(I,N) = ... (5.26))
FOR J=1 TO N
H(I,J) < 0
Y
$T(I,J) = \frac{H(I,J)}{CS} + TM$
B
N
H(I,J) ≥ 0
AND
H(I,J) ≤ L
Y
T(I,J)=TM
B
N

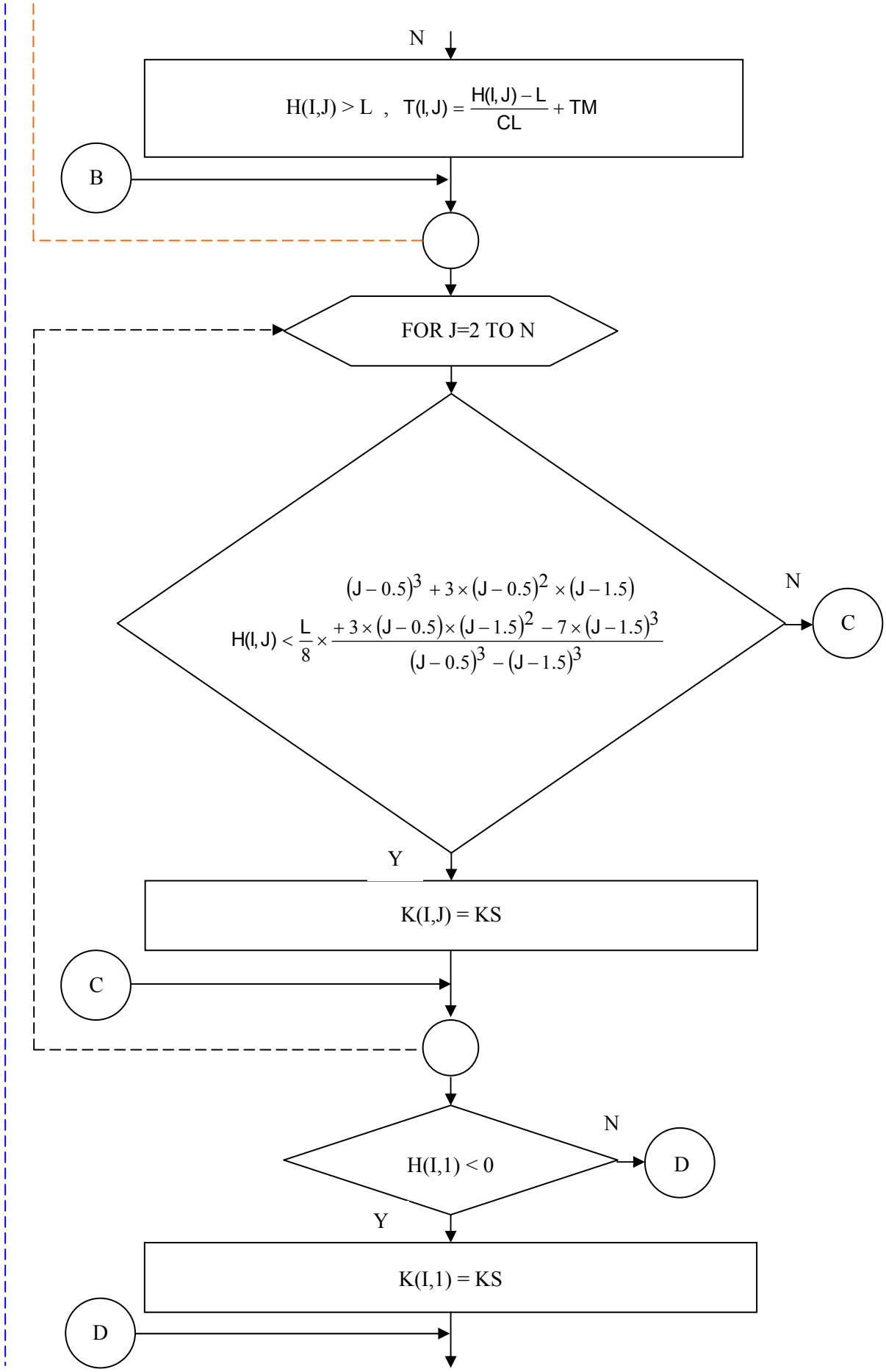
N
H(I,J) > L , T(I,J) = H(I,J) − L / CL + TM
B
FOR J=2 TO N
H(I,J) < L/8 × [(J − 0.5)^3 + 3 × (J − 0.5)^2 × (J − 1.5) + 3 × (J − 0.5) × (J − 1.5)^2 − 7 × (J − 1.5)^3] / [(J − 0.5)^3 − (J − 1.5)^3]
N
C
Y
K(I,J) = KS
C
H(I,1) < 0
N
D
Y
K(I,1) = KS
D

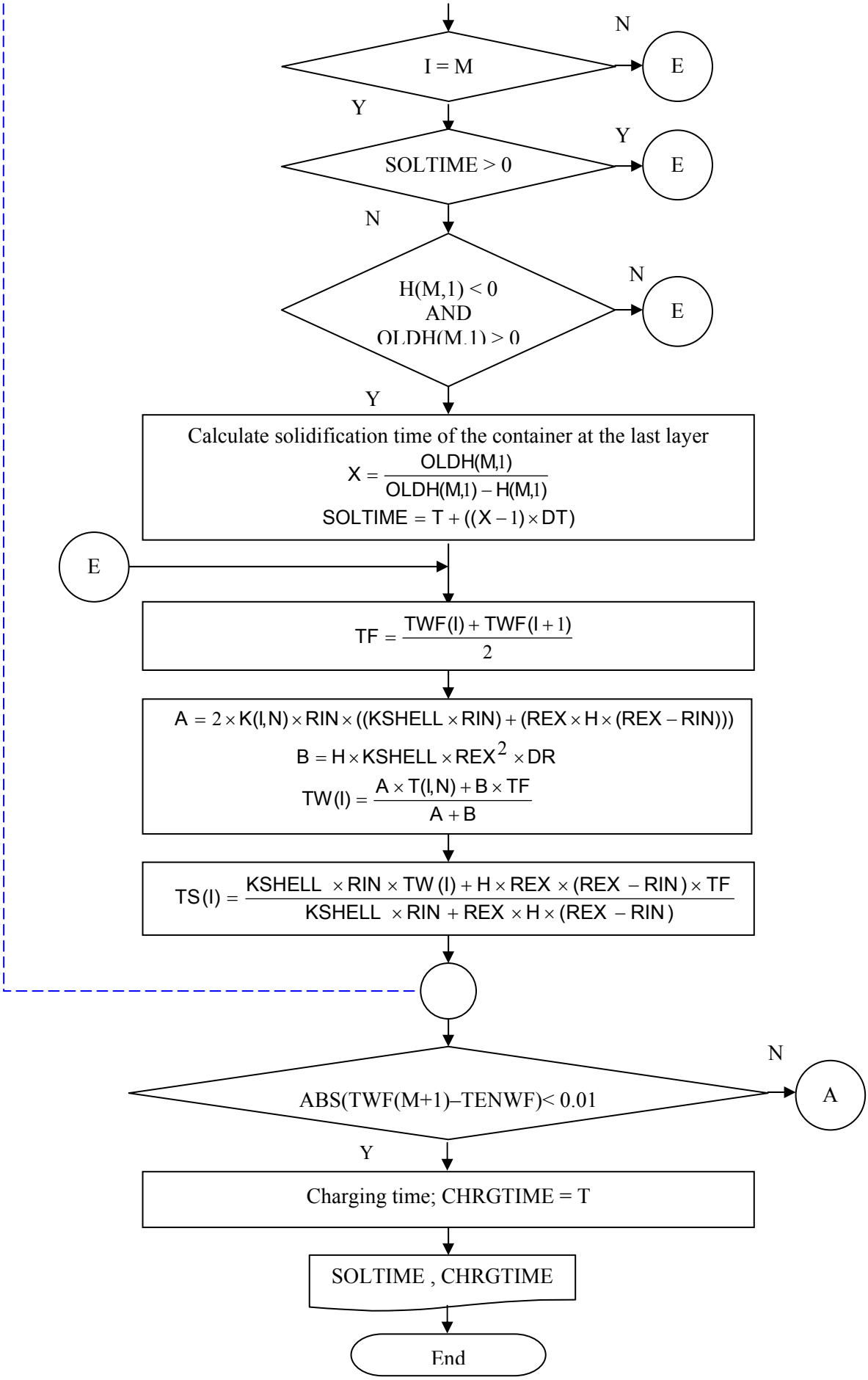
I = M
N
E
Y
SOLTIME > 0
Y
E
N
H(M,1) < 0
AND
OLDH(M,1) > 0
N
E
Y
Calculate solidification time of the container at the last layer
$X = \frac{OLDH(M,1)}{OLDH(M,1) - H(M,1)}$
$SOLTIME = T + ((X-1) \times DT)$
E
$TF = \frac{TWF(I) + TWF(I+1)}{2}$
$A = 2 \times K(I,N) \times RIN \times ((KSHELL \times RIN) + (REX \times H \times (REX - RIN)))$
$B = H \times KSHELL \times REX^2 \times DR$
$TW(I) = \frac{A \times T(I,N) + B \times TF}{A + B}$
$TS(I) = \frac{KSHELL \times RIN \times TW(I) + H \times REX \times (REX - RIN) \times TF}{KSHELL \times RIN + REX \times H \times (REX - RIN)}$
ABS(TWF(M+1)–TENWF)< 0.01
N
A
Y
Charging time; CHRGTIME = T
SOLTIME , CHRGTIME
End

CHAPTER 6

RESULTS AND DISCUSSION

6.1 VERIFICATION OF THE PROGRAMS

In order to verify the programs written to find the total solidification time of a spherical and cylindrical container and the complete solidification and charging time of a cool storage tank with spherical containers, some comparisons are made with available similar models.

6.1.1 Verification of the Spherical Container Program

In order to validate the numerical code written for spherical container, comparisons are realized with some of the references related to the inward solidification in spherical coordinates. However, all of the studies available have been done to find the total solidification time of a liquid PCM initially at the freezing temperature, and the specific heat and thermal conductivity values of liquid and solid phases of PCM have been taken equal in all of these studies. Therefore, although the spherical container program is able to take into account the change of specific heat and thermal conductivity values of liquid and solid PCM, and initial PCM temperatures higher than the freezing temperature, the comparisons are realized for the conditions mentioned above.

The dimensionless total solidification times for different Stefan and Biot numbers are found from the spherical container program and the results are compared with those of Ref [4] and [10] in the following figures.

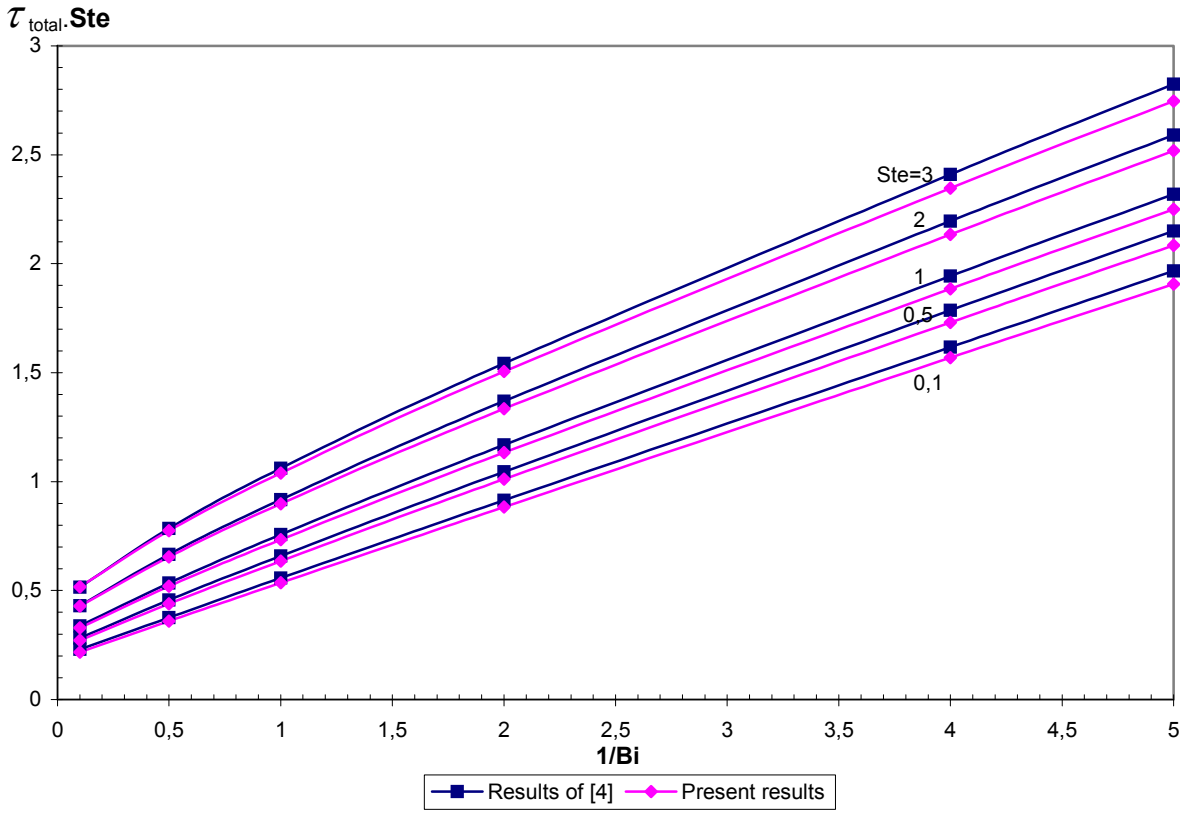

Fig 6.1 Comparison of the Total Solidification Time of a Sphere with Ref [4]

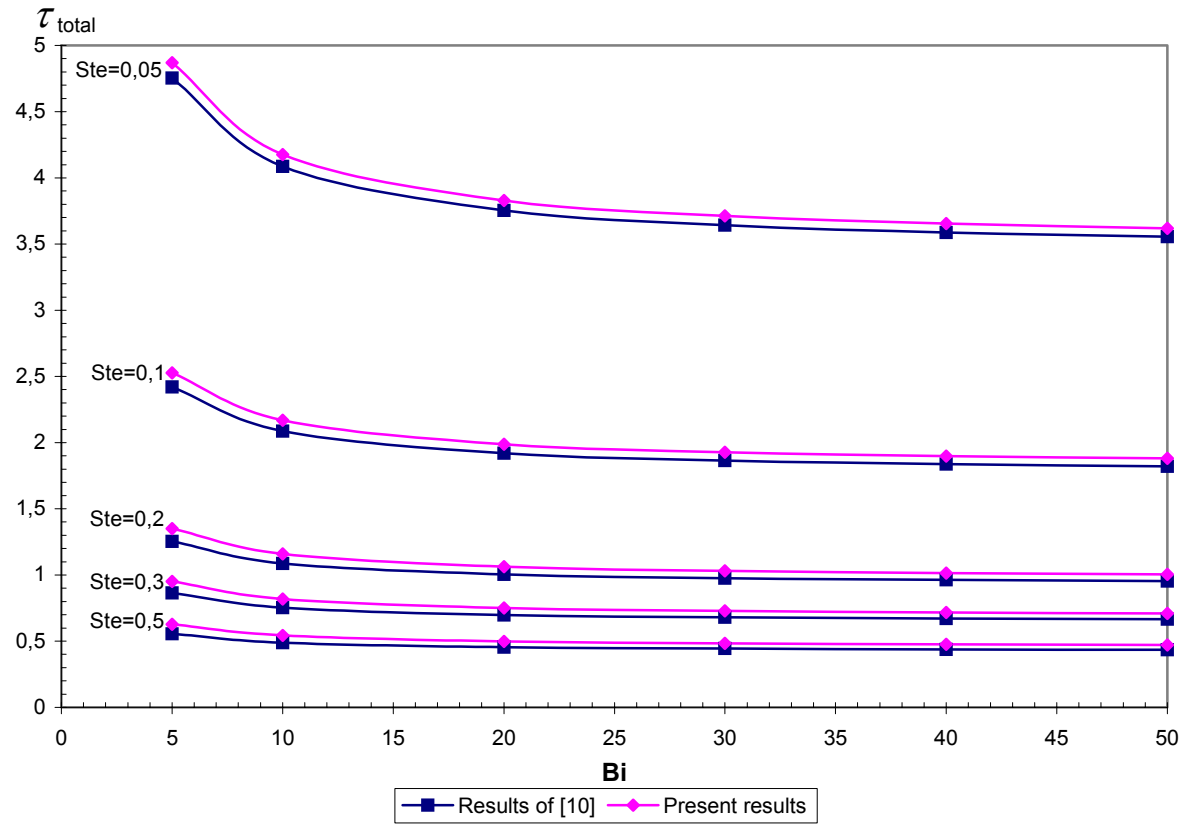

Fig 6.2 Comparison of the Total Solidification Time of a Sphere with Ref [10]

As seen from figures (6.1) and (6.2), there is a good agreement between the results of the spherical container program and the results due to ref [4] and [10].

After comparing the total solidification time for different parameters, the dimensionless phase change front position during solidification for determined Stefan and Biot numbers are also obtained from the program and compared with the available similar studies.

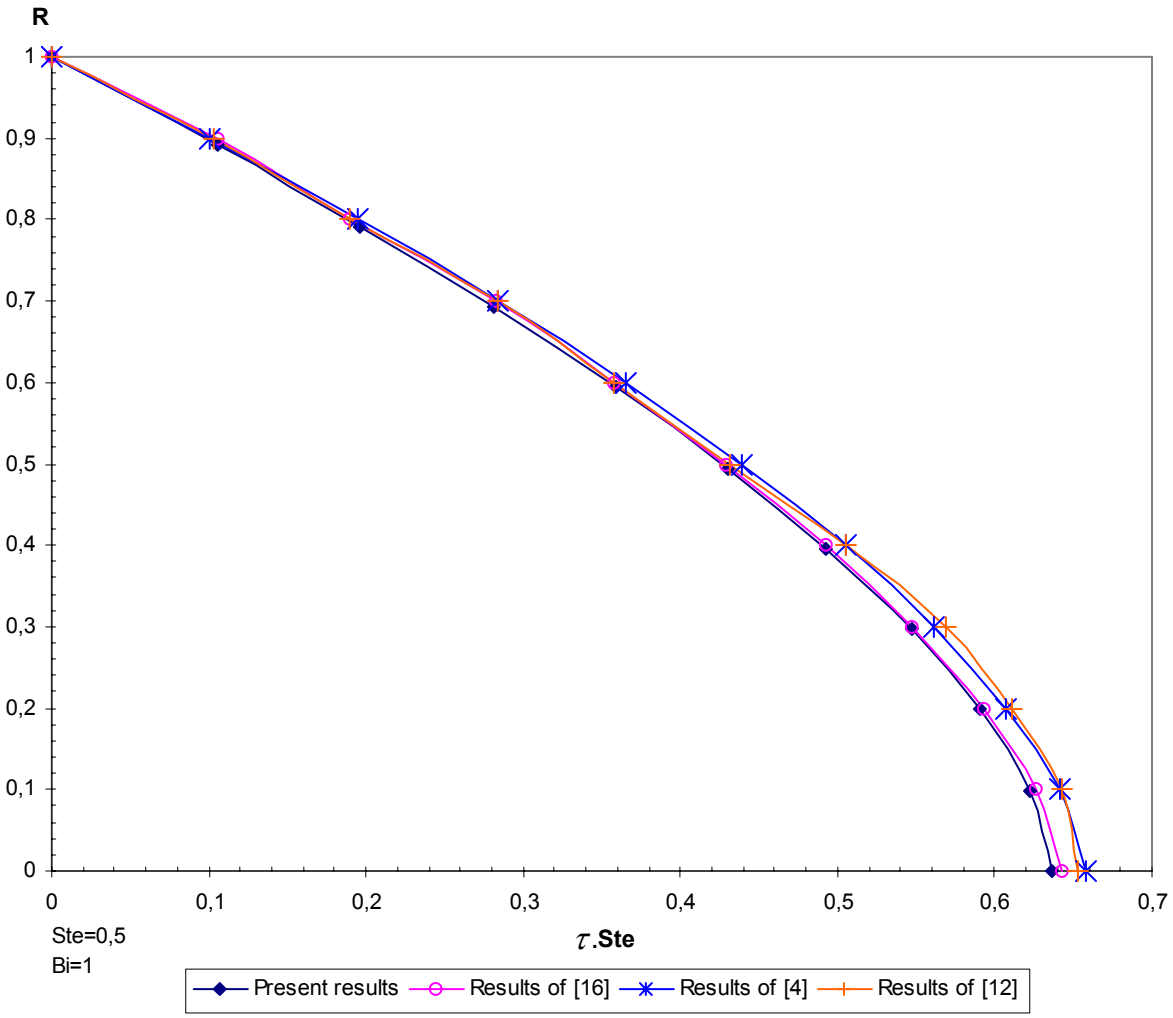

Fig 6.3 Comparison of the Phase Change Front Position in a Sphere with Refs [4,12,16]

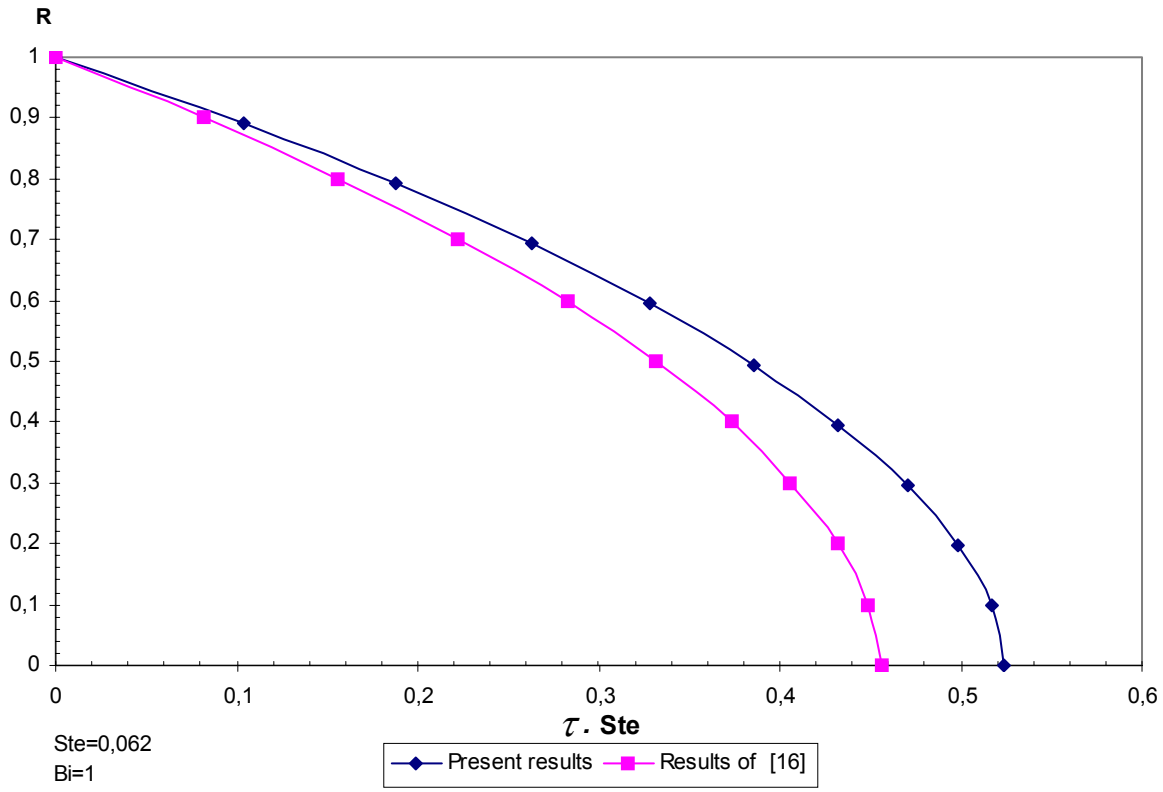

Fig 6.4 Comparison of the Phase Change Front Position in a Sphere with Ref [16]

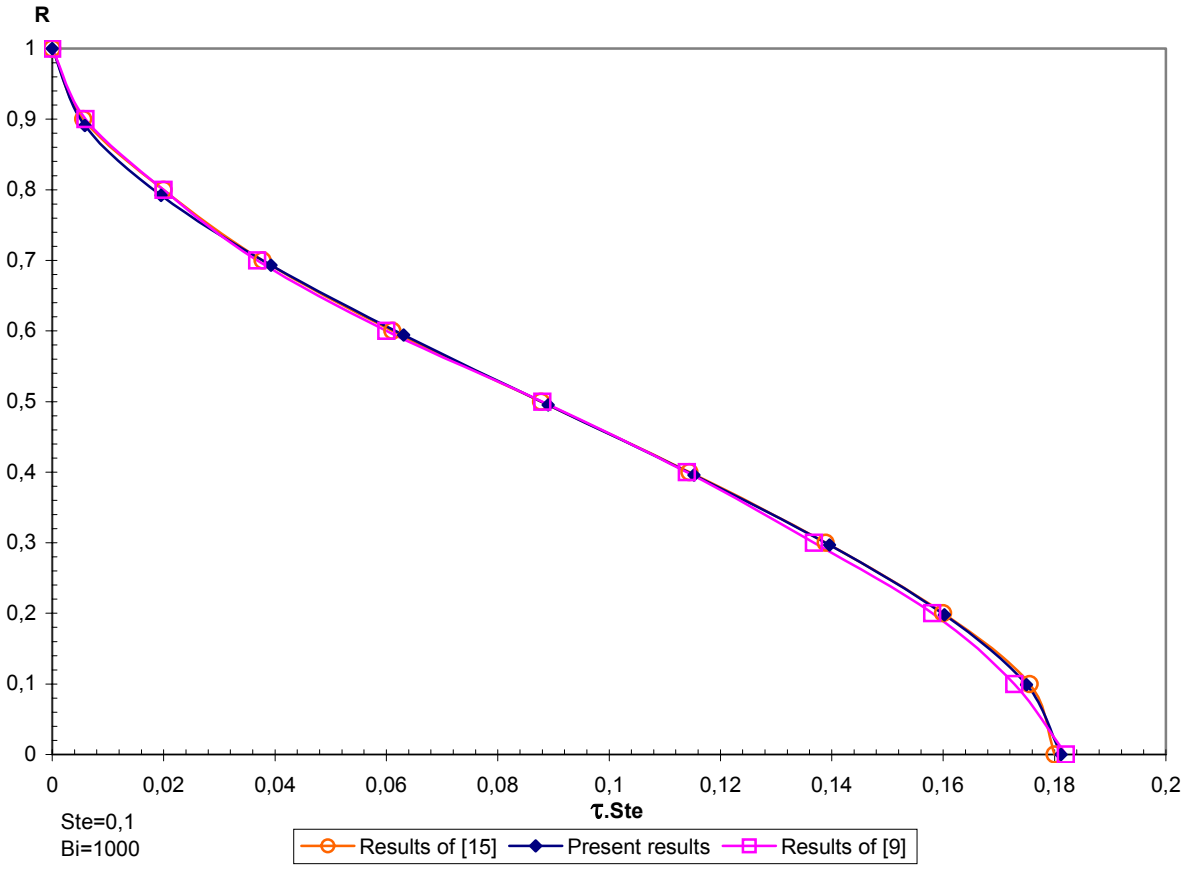

Fig 6.5 Comparison of the Phase Change Front Position in a Sphere with Refs [9,15]

In the references [9] and [15] the wall temperature of the sphere is assumed as constant, so Biot number is taken as 1000 to be able to compare the predictions of these references with the program. It is seen that taking Biot number greater than 1000 has negligible effects on results, so this value is considered appropriate for this comparison. The results of the comparison of phase change front position are also in good agreement as seen in figures (6.3), (6.4) and (6.5).

6.1.2 Verification of the Cylindrical Container Program

Some comparisons are made with some of the references about the inward solidification in cylindrical coordinates similar to the spherical case, to validate the program written for cylindrical container. But, unlike the spherical container, in this case all the comparisons are not done for the solidification of a liquid PCM initially at fusion temperature and which has equal thermal conductivity and specific heat values in solid and liquid phases. The PCM is initially superheated in [11], but it has equal physical properties for solid and liquid phases. In [17], it is also at an initial temperature higher than freezing temperature, and in addition the thermal conductivity and specific heat of solid and liquid phases are not taken equal. However, the other studies which are used in comparisons, except the ones mentioned above, assume that the PCM is initially at fusion temperature and have equal thermal conductivity and specific heat for both phases of PCM.

The dimensionless total solidification time obtained from the cylindrical container program are compared with Ref [4] and [10] for various Stefan and Biot numbers in the following figures.

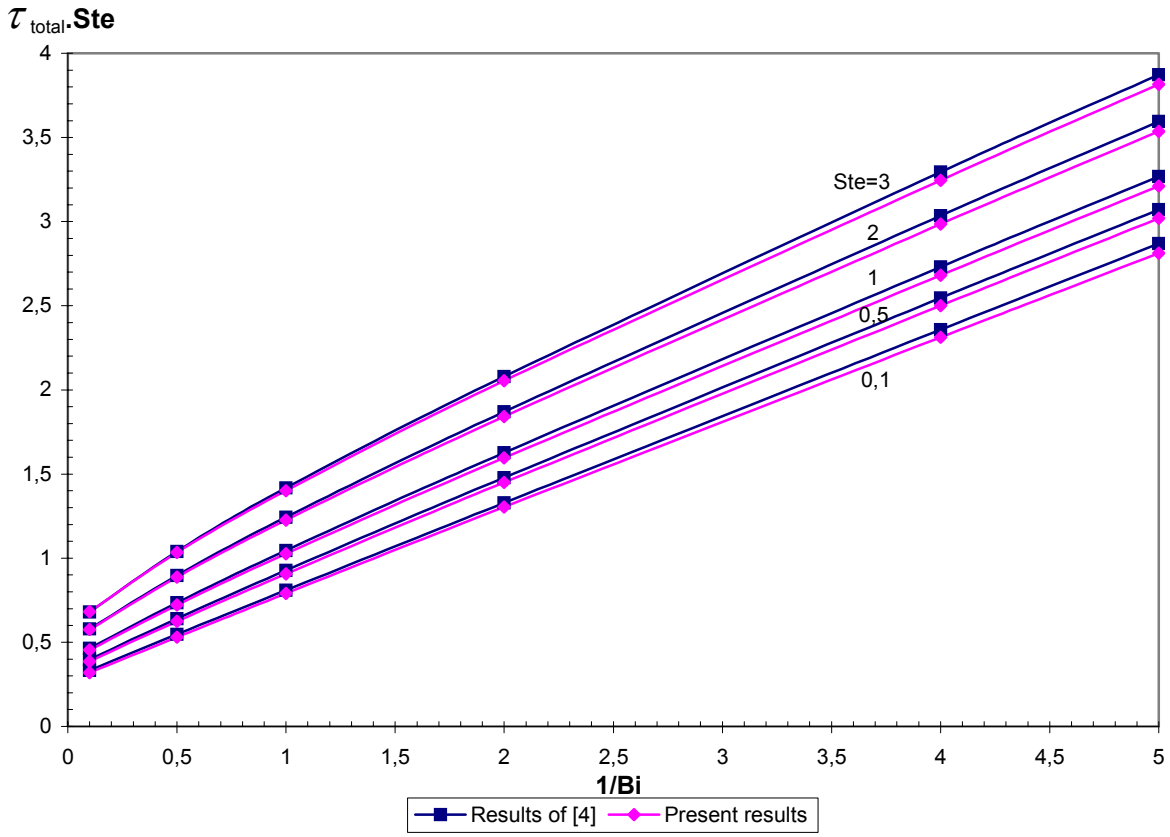

Fig 6.6 Comparison of the Total Solidification Time of a Cylinder with Ref [4]

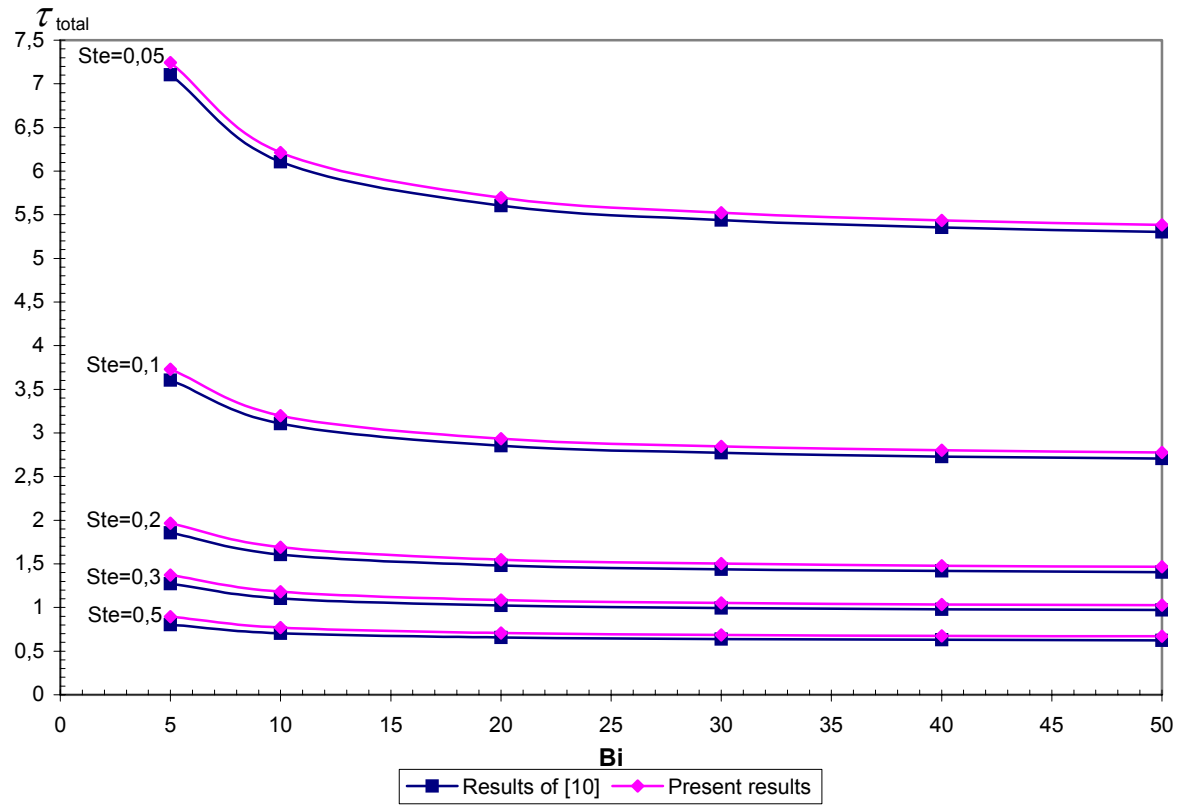

Fig 6.7 Comparison of the Total Solidification Time of a Cylinder with Ref [10]

It can be seen that there is a negligible difference between the results of Refs [4] and [10] and present results.

Figure (6.8) shows a comparison of dimensionless phase change front position between the present model and Refs [4] and [8] for two different Stefan and Biot numbers. The phase change front locations calculated from the cylindrical container program and taken from mentioned references are almost the same for the case in which Stefan and Biot numbers are 0.1 and 1, respectively, and they show a good agreement for the case in which Stefan and Biot numbers are both equal to 0.5.

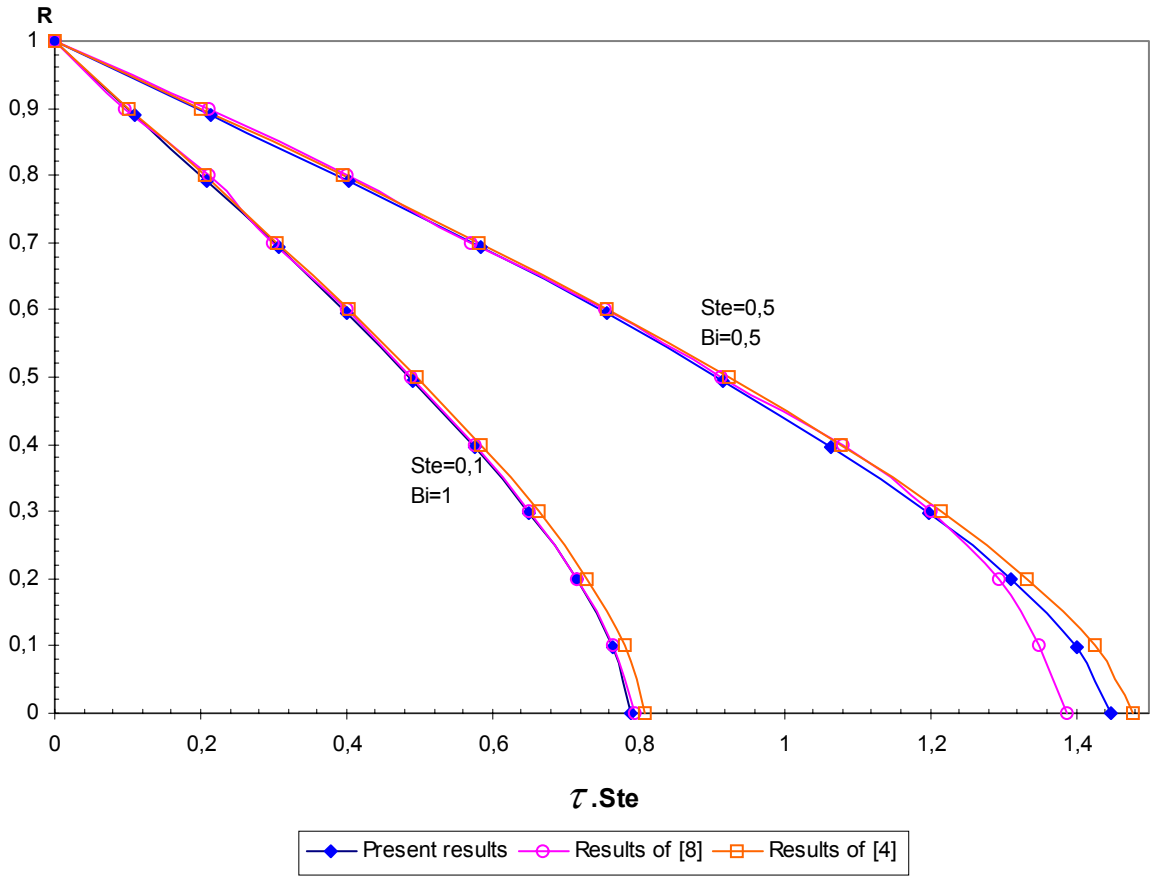

Fig 6.8 Comparison of the Phase Change Front Position in a Cylinder with Refs [4,8]

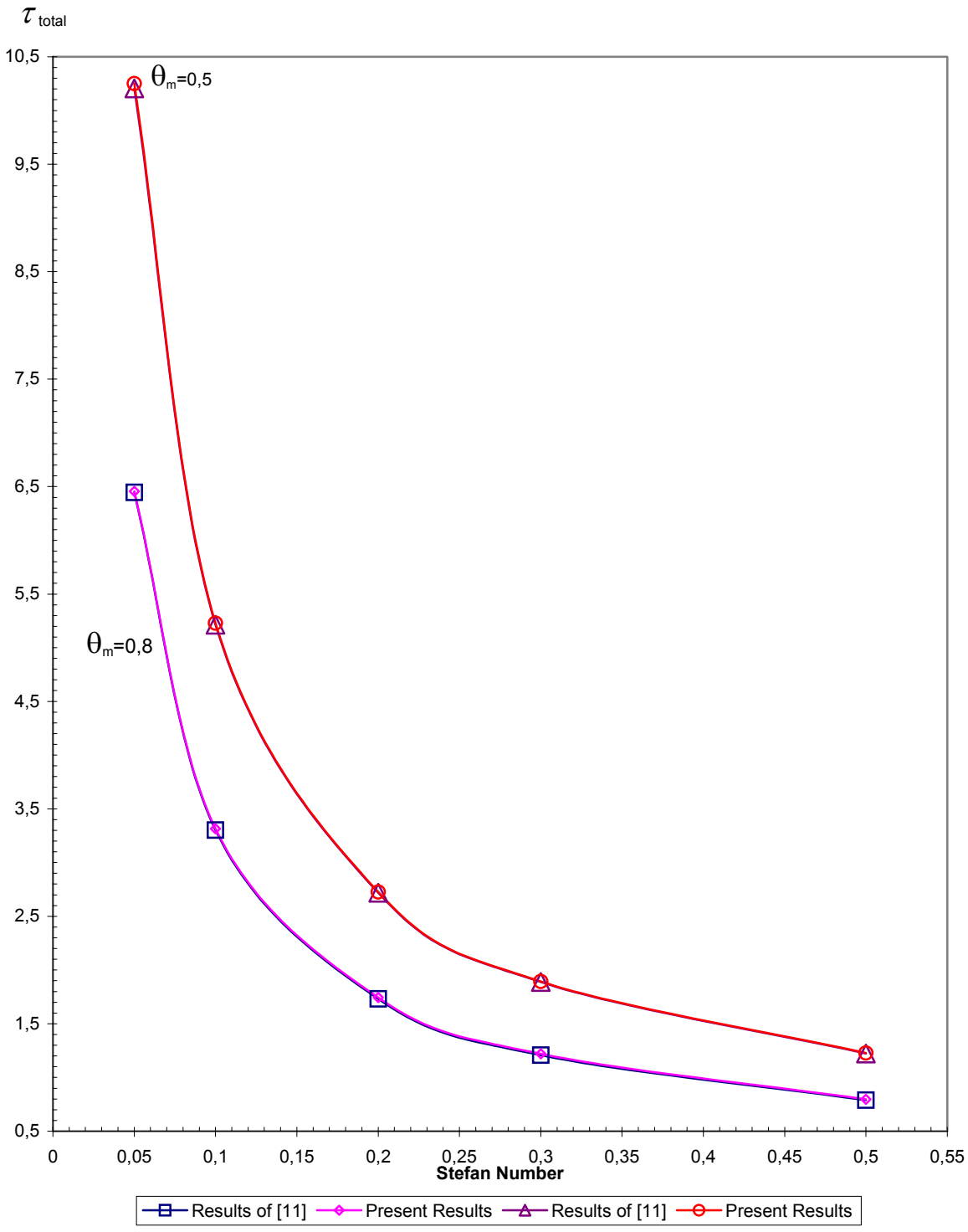

Fig 6.9 Comparison of the Total Solidification Time of a Cylinder with Ref [11]

In figure (6.9) it can be observed that the results of [11] and present results are almost same. The same method is used in this study and in [11] for the phase change problem inside the cylindrical container and a very good agreement is obtained between

the results. The results of [11] are valid for a cylinder with a first kind of boundary condition, so Biot number is taken as 1000 in comparison, because taking higher Biot numbers do not affect the results significantly.

In the following figures, freezing front position obtained from cylindrical container program is compared with ref [17]. $K^+ = 0.926$ and $C^+ = 1.147$ values are used in comparisons and freezing front position inside the cylindrical container for different θ_m, Biot and Stefan numbers is compared.

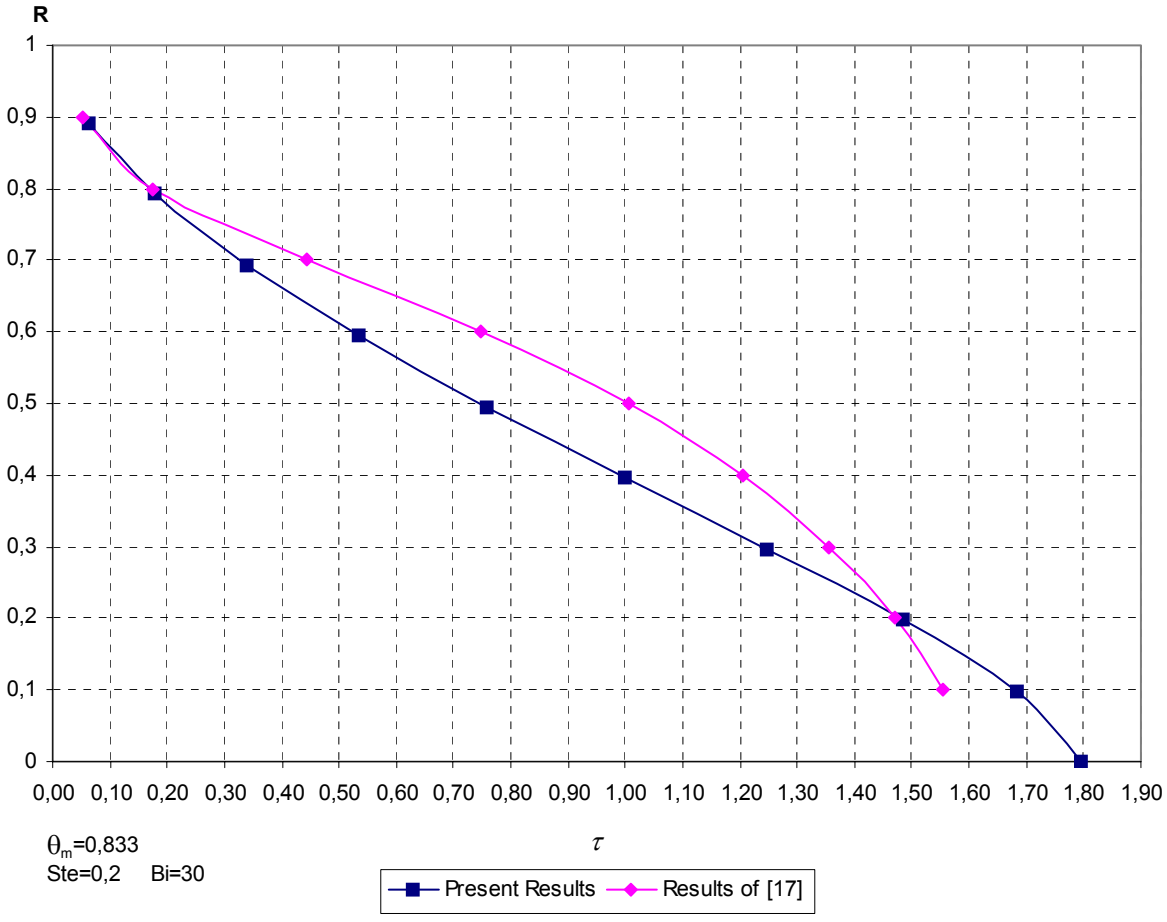

Fig 6.10 Comparison of the Freezing Front Position Inside the Cylinder for θ_m=0.833, Ste=0.2 and Bi=30 with Ref [17]

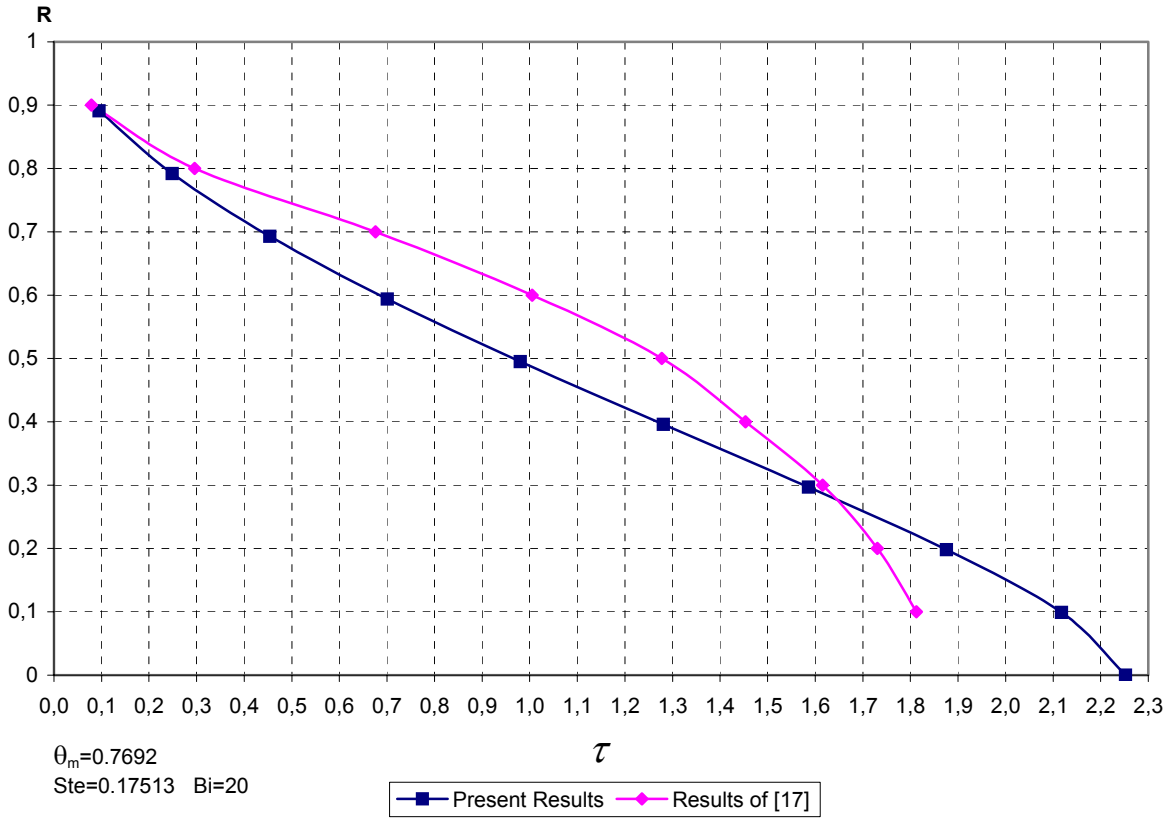

Fig 6.11 Comparison of the Freezing Front Position Inside the Cylinder for θ_m=0.7692, Ste=0.17513 and Bi=20 with Ref [17]

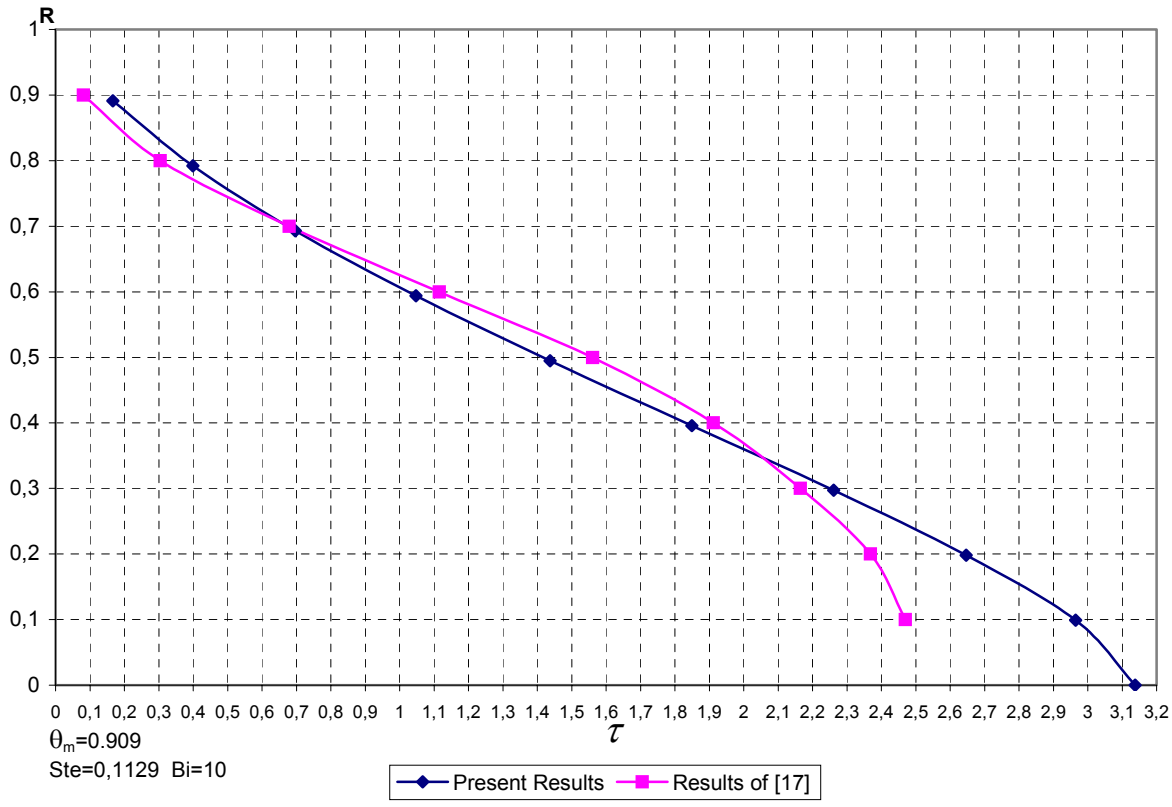

Fig 6.12 Comparison of the Freezing Front Position Inside the Cylinder for θ_m=0.909, Ste=0.1129 and Bi=10 with Ref [17]

It can be observed that for the case of taking nonequal thermal conductivity and specific heat values of the solid and liquid phase, satisfactory agreement is obtained. Especially in figure (6.12) it is seen that there are small differences between the results until R value reaches 0.2. In figure (6.10) and (6.11), it can be noticed that the differences between the results are higher than those in figure (6.12) until R value reaches 0.2. After the dimensionless phase change front position is equal to 0.2, the difference between the results increases in figure (6.12), but it is also seen that this difference is smaller in figure (6.10) and (6.11) than that in figure (6.12).

6.1.3 Verification of the Cool Storage Tank Program

The cool storage tank program is written to find the total solidification time of the spherical containers of the last layer and the charging time of a cool storage tank. These values are calculated for different working fluid inlet temperatures, different volumetric flow rates of working fluid and different spherical shell materials, while other parameters such as cool storage tank diameter and height, diameter of the spherical containers, initial temperature etc. are kept constant. The values of the parameters used in this calculation are taken the same as those of ref [23] to compare its numerical and experimental results with the cool storage tank program results.

In ref [23] a cool storage tank of cylindrical form of 0.92m in diameter and 1.54m in height is simulated. The tank is full with spherical containers of 77mm in diameter and 2mm in thickness. These containers form 20 regular layers in the storage tank and there are 132 containers in each layer. The phase change material inside the containers is water. The working fluid considered is ethylene glycol of 30% volumetric concentration and the initial storage tank temperature is considered $20\,°C$ for all the cases simulated. The working fluid inlet temperature is varied from –3 to $-15\,°C$ while the volumetric flow rate is varied from 0.5 to 1.5 m^3/h. The material of the spherical shell simulated is copper, aluminium, PVC, acrylic and polyethylene with thermal conductivity values of 372, 204, 0.15, 0.184 and 0.35 W/mK, respectively.

Firstly, the effect of working fluid inlet temperature on the complete solidification and complete charging time is investigated. The comparison of the results of the cool storage tank program and ref [23] are given in the following figures. For these figures the volumetric flow rate of working fluid is kept at 1 m^3/h and spherical shell material is polyethylene.

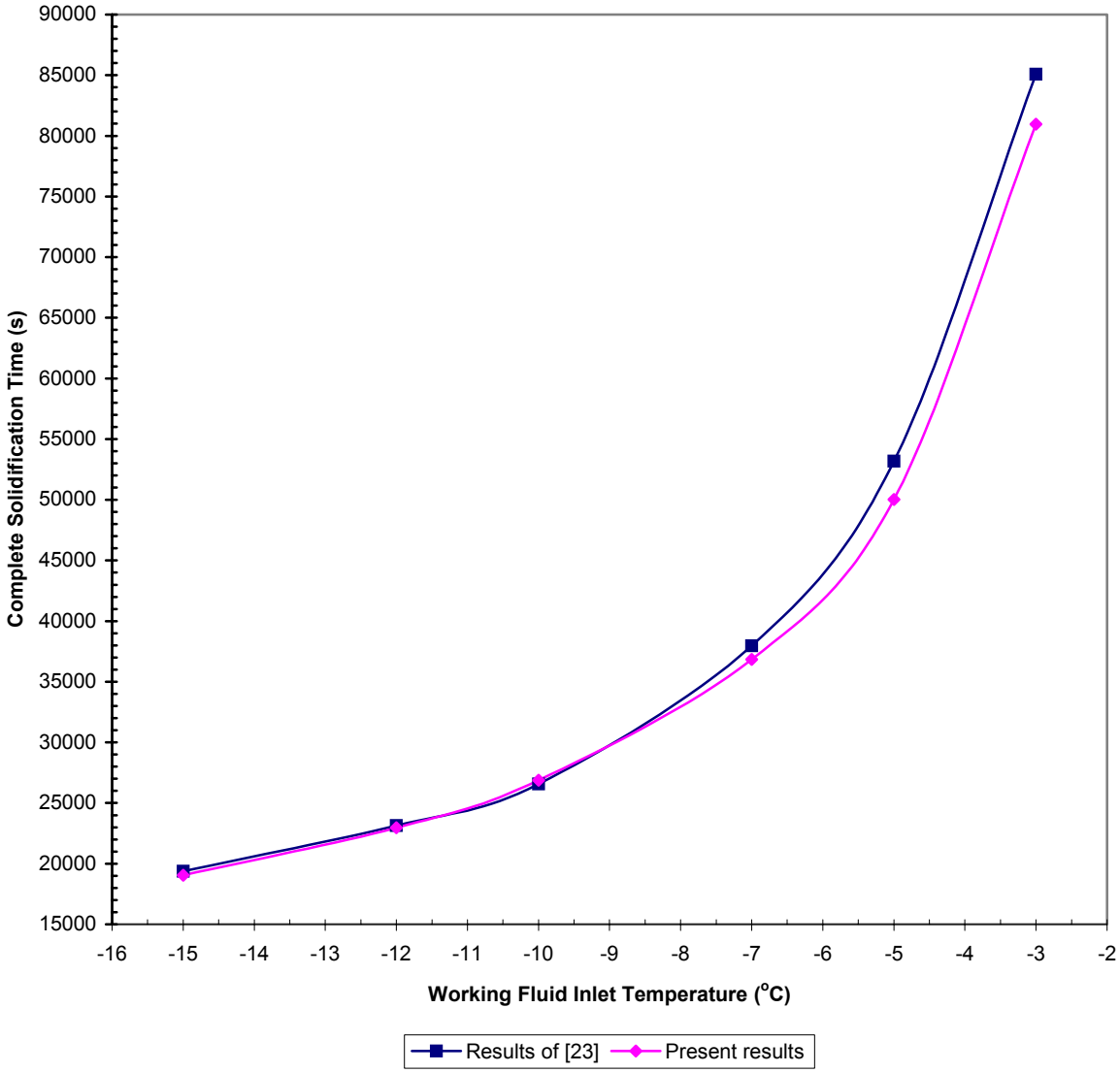

Fig 6.13 Comparison of Complete Solidification Time for Various Working Fluid Inlet Temperatures with Ref [23]

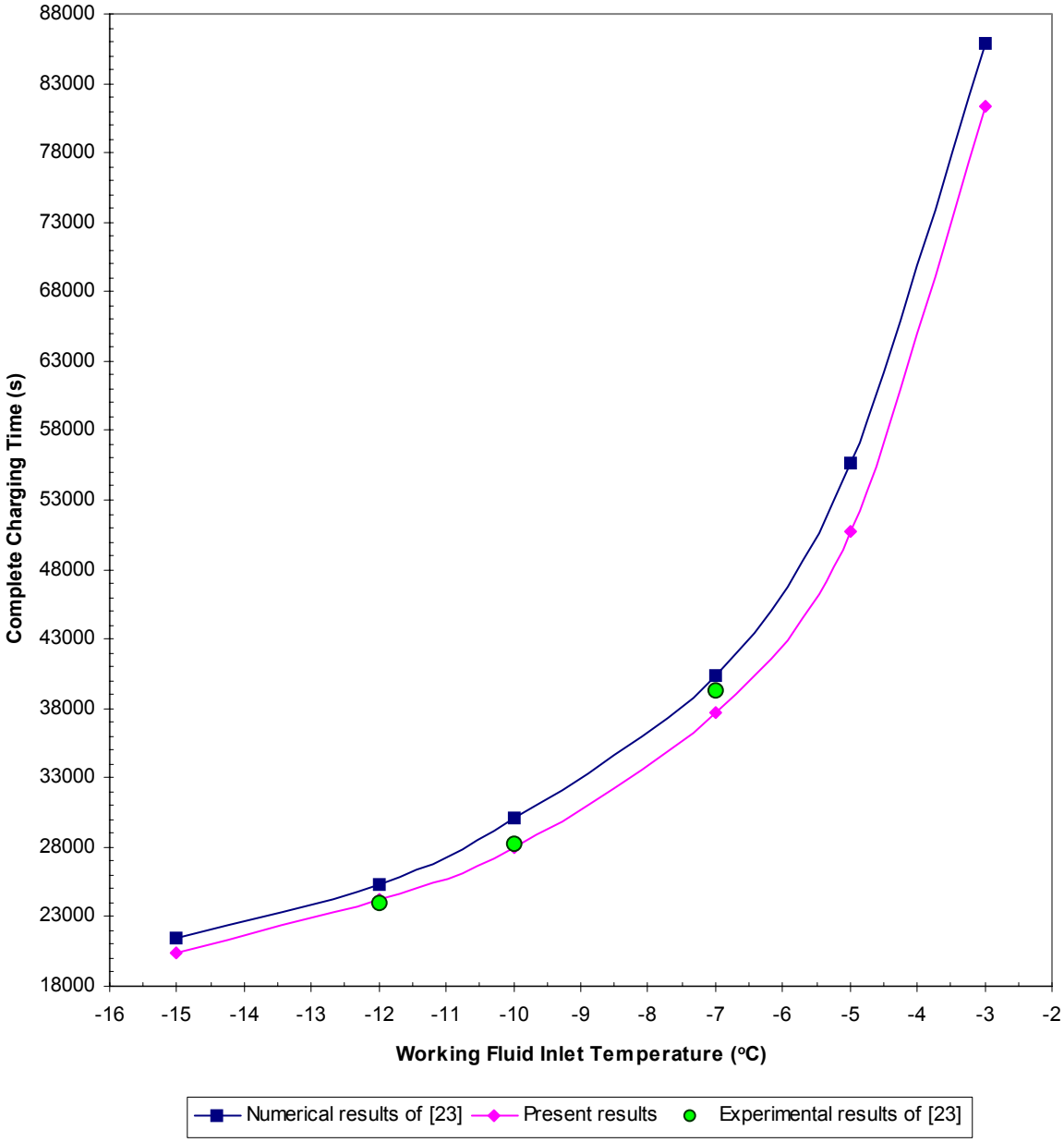

Fig 6.14 Comparison of Complete Charging Time for Various Working Fluid Inlet Temperatures with Ref [23]

Secondly, the volumetric flow rate of working fluid is changed and complete solidification and charging time of the tank is calculated with the cool storage tank program. At this trial working fluid inlet temperature is kept constant at –10 $°C$ and spherical shell material is taken as polyethylene.

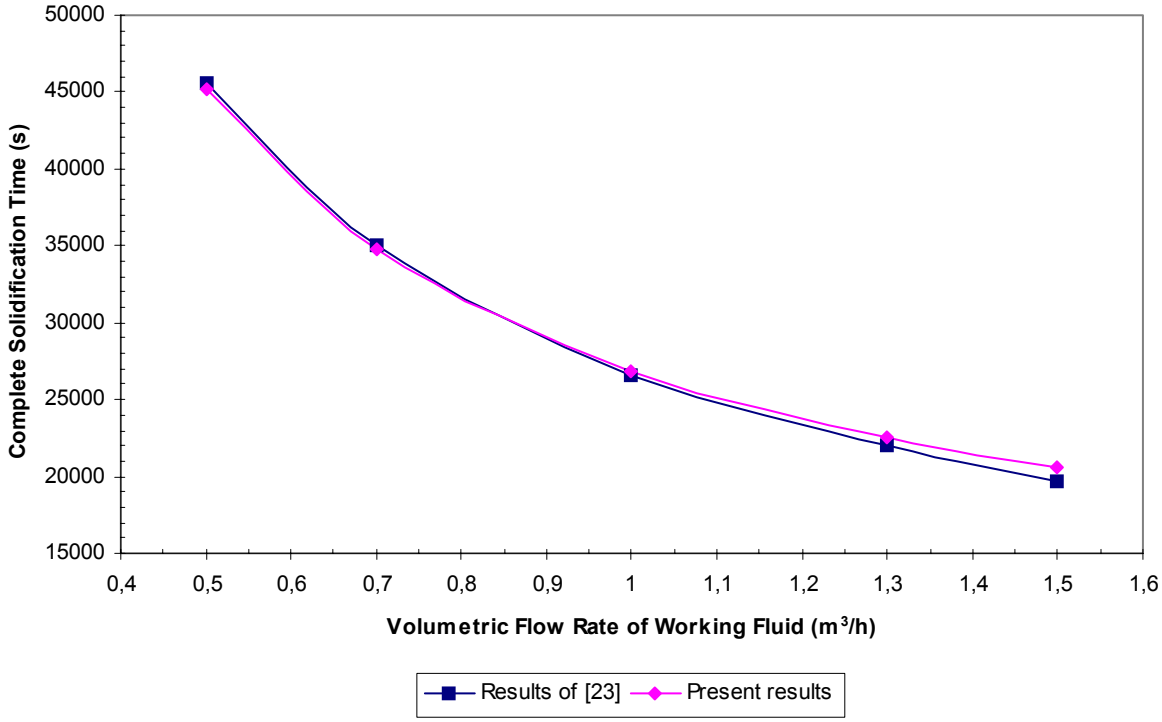

Fig 6.15 Comparison of Complete Solidification Time for Various Volumetric Flow Rate of Working Fluid with Ref [23]

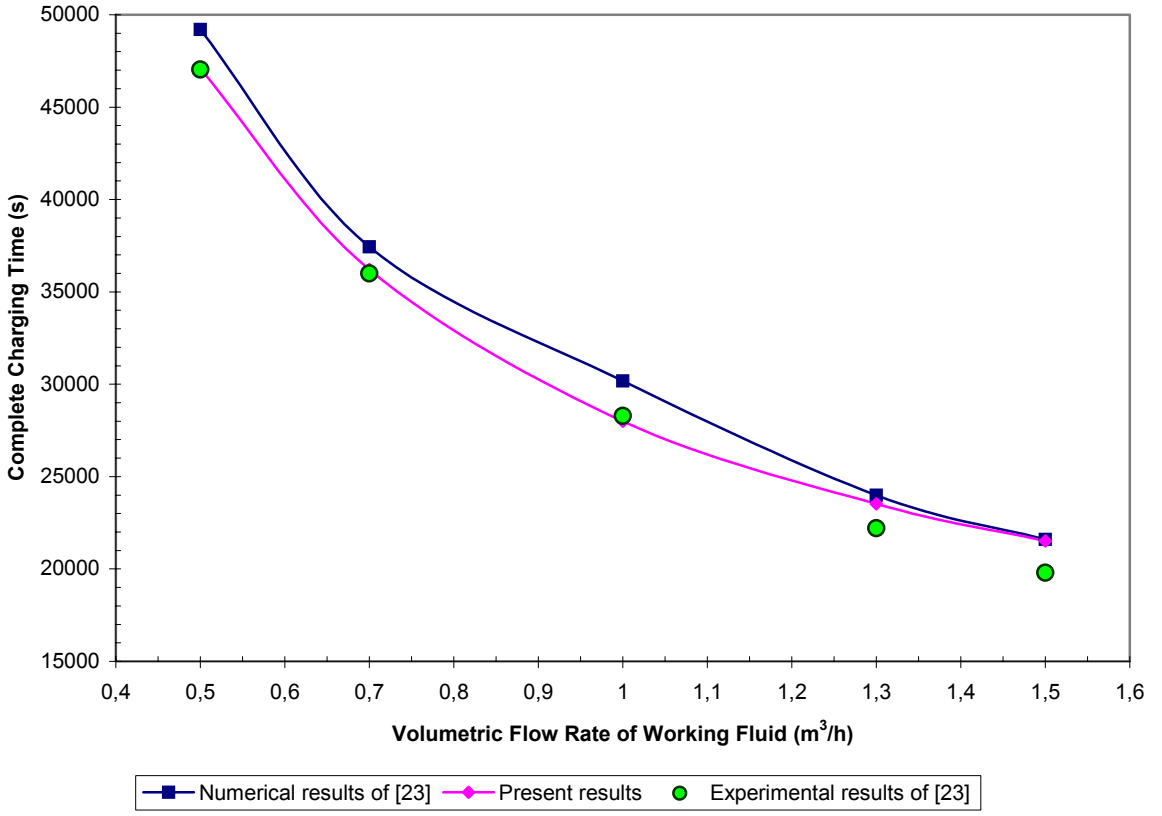

Fig 6.16 Comparison of Complete Charging Time for Various Volumetric Flow Rate of Working Fluid with Ref [23]

Finally, the complete solidification and charging time of the cool storage tank is calculated for different spherical shell materials while inlet temperature and volumetric flow rate of working fluid are kept at $-10\,°C$ and 1 m^3/h, respectively.

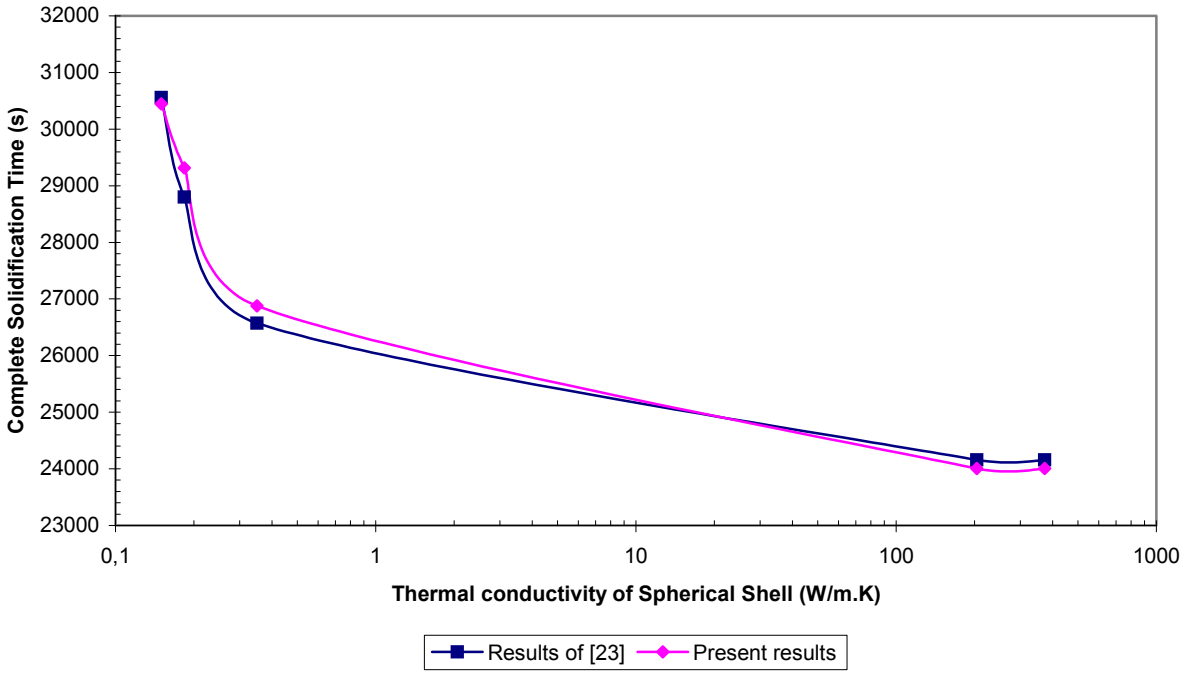

Fig 6.17 Comparison of Complete Solidification Time for Various Thermal Conductivity Values of Spherical Shell with Ref [23]

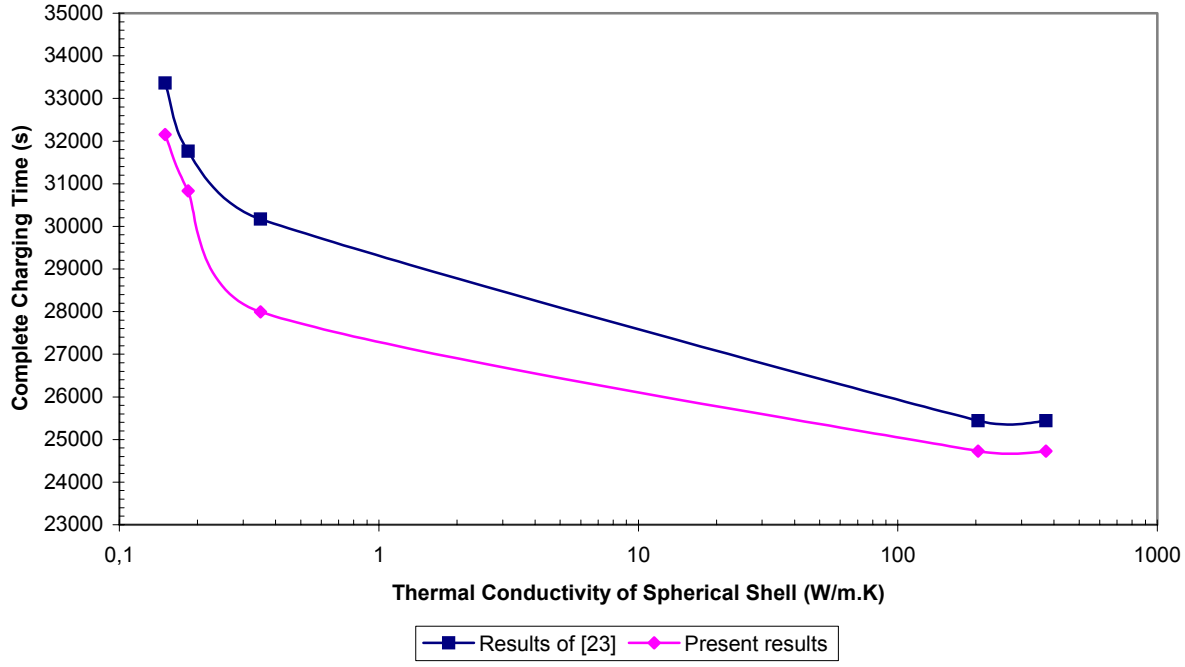

Fig 6.18 Comparison of Complete Charging Time for Various Thermal Conductivity Values of Spherical Shell with Ref [23]

As seen from the figures, the results of the cool storage tank program agree with the numerical and experimental results of ref [23]. Since in the cool storage tank program the solidification problem inside the spherical containers is solved by taking different specific heat and thermal conductivity values for liquid and solid phases of water and the results of the cool storage tank program are in agreement with numerical and experimental results of [23], it can be said that the method used in the solution of the solidification problem inside the spherical containers is also valid for the case of nonequal specific heat and thermal conductivity values for liquid and solid PCM.

6.2 CORRELATIONS FOR THE DIMENSIONLESS TOTAL SOLIDIFICATION TIME OF A PHASE CHANGE MATERIAL INSIDE A SPHERICAL AND CYLINDRICAL CONTAINER

When nondimensional form of heat conduction equations for liquid and solid regions and energy balance equation for the solid-liquid interface which express phase change problems are considered it can be seen that dimensionless total solidification time of a PCM held in a spherical or cylindrical container can be expressed as;

$$\tau_{total} = f(Bi, Ste, \theta_m, K^+, C^+) \tag{6.1a}$$

In this study, it is aimed to find correlations which give the dimensionless total solidification time in spherical and cylindrical containers in terms of these affecting parameters.

It is decided to find correlations for the case of equal specific heat and thermal conductivity values of liquid and solid phases $\left(K^+ = 1,\ C^+ = 1\right)$ and for water, which is one of the most common phase change materials $\left(K^+ = 0.3016,\ C^+ = 2.0637\right)$. So the correlations to be found are in the form of;

$$\tau_{total} = a \times \left(Ste\right)^b \times \left(Bi\right)^c \times \left(\theta_m\right)^d \tag{6.1b}$$

To find the coefficients a, b, c and d, the spherical container and the cylindrical container programs are run for different Stefan, Biot and θ_m values and data sets are

obtained for the dimensionless total solidification time found for these values, then the correlations in the form given by equation (6.1b) are obtained by applying multiple regression analysis.

6.2.1 The Applicability Range of the Correlations

The data sets are obtained by varying Biot number from 1 to 50, Stefan number from 0.01 to 0.5 and θ_m value from 0.2 to 1. The increase in Biot number is 1, in Stefan number 0.025 and in θ_m 0.1 while the data sets are created. The θ_m value is kept at 0.2 and Stefan number is kept at 0.01 while Biot number is changed from 1 to 50, then Stefan number is increased to 0.025 and Biot number is varied again from 1 to 50. When Stefan number reaches the value of 0.5, the θ_m value is increased to 0.3 and the same variation for Biot and Stefan numbers is repeated. This process is continued until θ_m value reaches 1 and for each of these variations the dimensionless total solidification time is calculated from the programs.

The values of the parameters while the data sets are created are;

$$\theta_m = \underbrace{0.2, 0.3, 0.4, 0.5, 0.6, 0.7, 0.8, 0.9 \, and \, 1}_{9 \, values}$$

$$Ste = \underbrace{0.01, 0.025, 0.05, 0.075, 0.1, 0.125, 0.15, ..., 0.45, 0.475 \, and \, 0.5}_{21 \, values}$$

$$Bi = \underbrace{1, 2, 3, 4, 5, ..., 47, 48, 49 \, and \, 50}_{50 \, values}$$

So, a total of 9450 values are calculated for the dimensionless total solidification time for each of the data sets and the applicability range of the correlations to be found by using these data sets are;

$$0.2 \le \theta_m \le 1,$$
$$0.01 \le Ste \le 0.5, \qquad (6.2)$$
$$1 \le Bi \le 50$$

6.2.2 Correlations Found for the Dimensionless Total Solidification Time

(a) for the case of equal thermal conductivity and specific heat values of solid and liquid phases of PCM

After obtaining the data sets as described above, the correlations for the dimensionless total solidification time of a PCM inside a spherical and cylindrical container for the case of equal specific heat and thermal conductivity in solid and liquid phases are found by using multiple regression analysis as;

- for a spherical container;

$$\tau_{total} = 0.4527292 \times (Ste)^{-0.9355889} \times (Bi)^{-0.194888} \times (\theta_m)^{-0.9368148} \quad (6.3)$$

The correlation coefficient: R = 0.9969049

- for a cylindrical container;

$$\tau_{total} = 0.6496729 \times (Ste)^{-0.9439889} \times (Bi)^{-0.194324} \times (\theta_m)^{-0.9548947} \quad (6.4)$$

R = 0.9970823

(b) for water

The correlations obtained for the dimensionless total solidification time of water inside a spherical and cylindrical container are as follows;

- for a spherical container;

$$\tau_{total} = 0.5012181 \times (Ste)^{-0.9070384} \times (Bi)^{-0.1864788} \times (\theta_m)^{-0.9843633} \quad (6.5)$$

R = 0.9964224

- for a cylindrical container;

$$\tau_{total} = 0.7192535 \times (Ste)^{-0.9107597} \times (Bi)^{-0.188035} \times (\theta_m)^{-1.010093} \quad (6.6)$$

R = 0.9964247

The correlation coefficients (R) for each of the correlations are higher than 0.996 and this means that the correlations found as the result of multiple regression analysis represent the dimensionless total solidification time found from the programs very well, and they can be used in the applicability range given in equation (6.2).

6.3 PARAMETRIC STUDY FOR THE COOL STORAGE TANK

6.3.1 Dimensions of the Cool Storage Tank Used in Parametric Study

A parametric study is realized for the storage tank having the same dimensions as those of the ref [23] by varying the working fluid volumetric flow rate and inlet temperature. Spherical containers with various diameters are used in the parametric study. The diameter and the height of the cool storage tank are 0.92m and 1.54m, respectively, and the working fluid is ethylene glycol of 30% volumetric concentration.

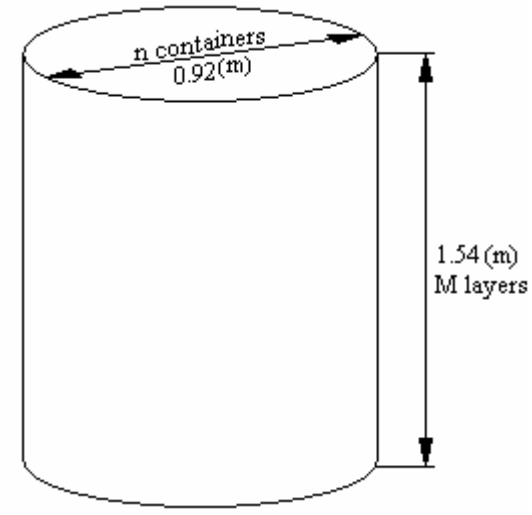

Fig 6.19 Dimensions of the Cool Storage Tank

As indicated in figure (6.19), n containers are placed on the diameter of the cool storage tank and they constitute M layers in 1.54 m, the height of the storage tank. So, the relation between the number of the containers on the diameter of the cool storage tank and the number of layers is as follows;

$$n \times d_{ex} = 920(mm) \tag{6.7a}$$

$$M \times d_{ex} = 1540(mm) \tag{6.7b}$$

$$n = 0.5974025974 \times M \tag{6.7c}$$

After finding this relation, the diameter of the spherical containers to be used in the parametric study and the total layers they form in the cool storage tank are determined as given in Table 6.1;

Table 6.1 The External Diameter of Spherical Containers and Total Layer Numbers

Total number of layers (M)	Number of containers on the diameter of the cool storage tank (n)	External diameter of spherical containers (d_{ex}) (mm)
10	6	153
15	9	102
22	13	70
30	18	51
40	24	38

The thickness of the spherical shell for each case is taken as 2 mm and its material is selected as polyethylene with a thermal conductivity value of 0.35 W/m.K. The number of spherical containers in a layer (spcl) for each of the cases is determined by drawing the containers inside the cross section of the cool storage tank. These drawings are given in figure (6.20).

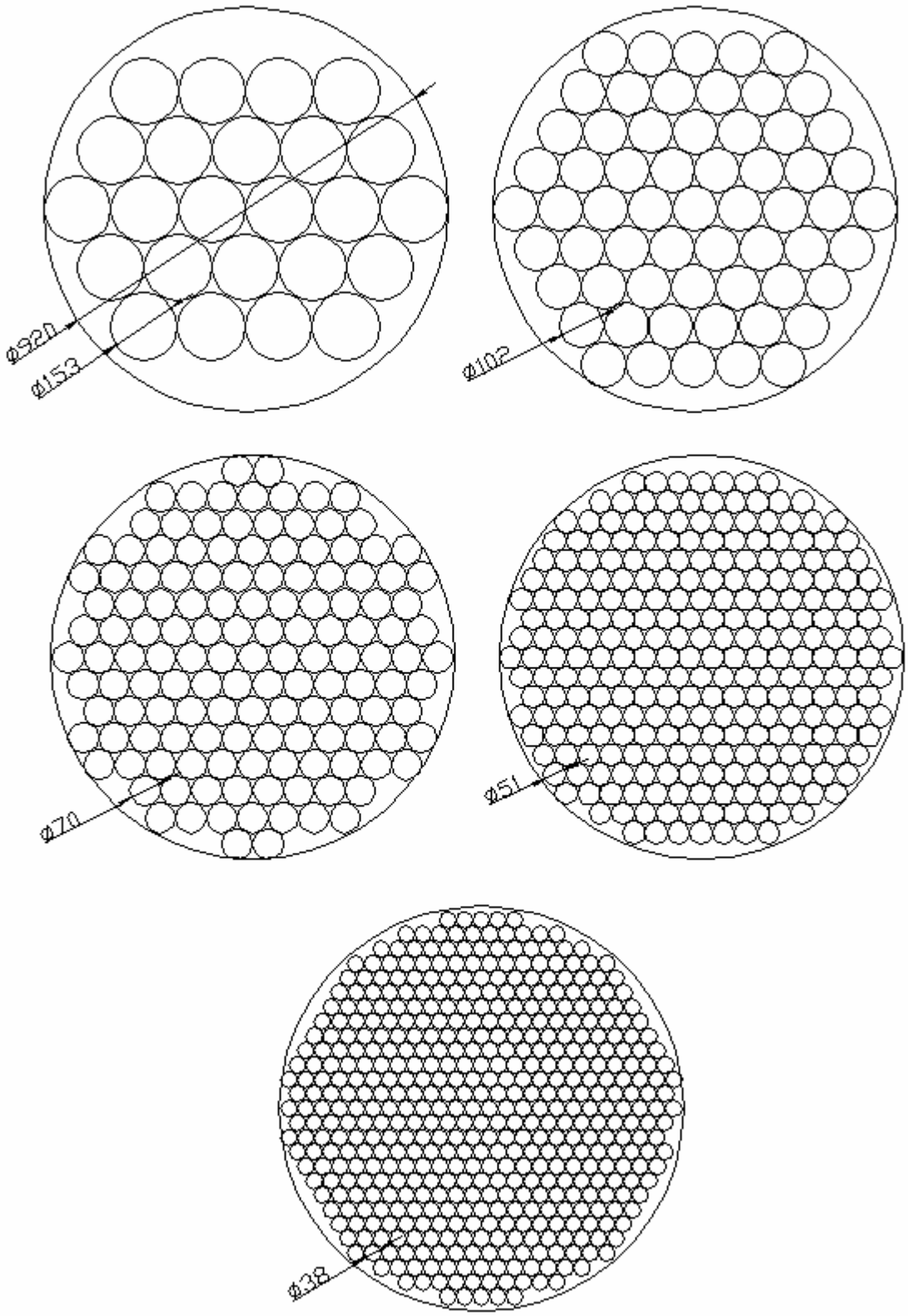

Fig 6.20 Spherical Containers in a Layer

The total number of containers in a layer for each case is determined as given in Table 6.2;

Table 6.2 The Number of Spherical Containers in a Layer

External diameter of spherical containers (d_{ex}) (mm)	The number of spherical containers in a layer (spcl)
153	24
102	61
70	139
51	268
38	486

6.3.2 Varying the Volumetric Flow Rate of Working Fluid

The volumetric flow rate of working fluid is varied from 0.5 to 5 m^3/h while the entry temperature is constant at $-10\,°C$. The initial temperature of the cool storage tank is $20\,°C$ for all of the cases.

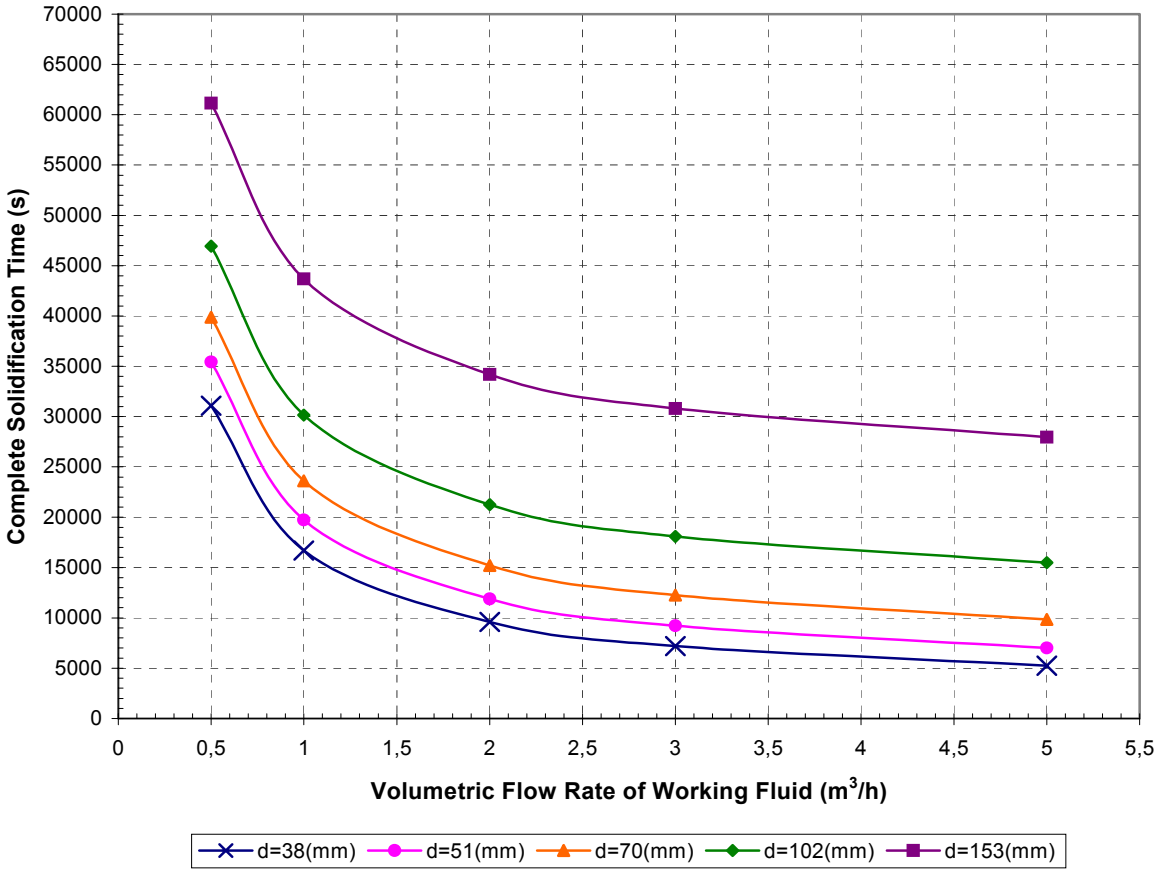

Fig 6.21 Complete Solidification Time of the Cool Storage Tank for Different Flow Rates

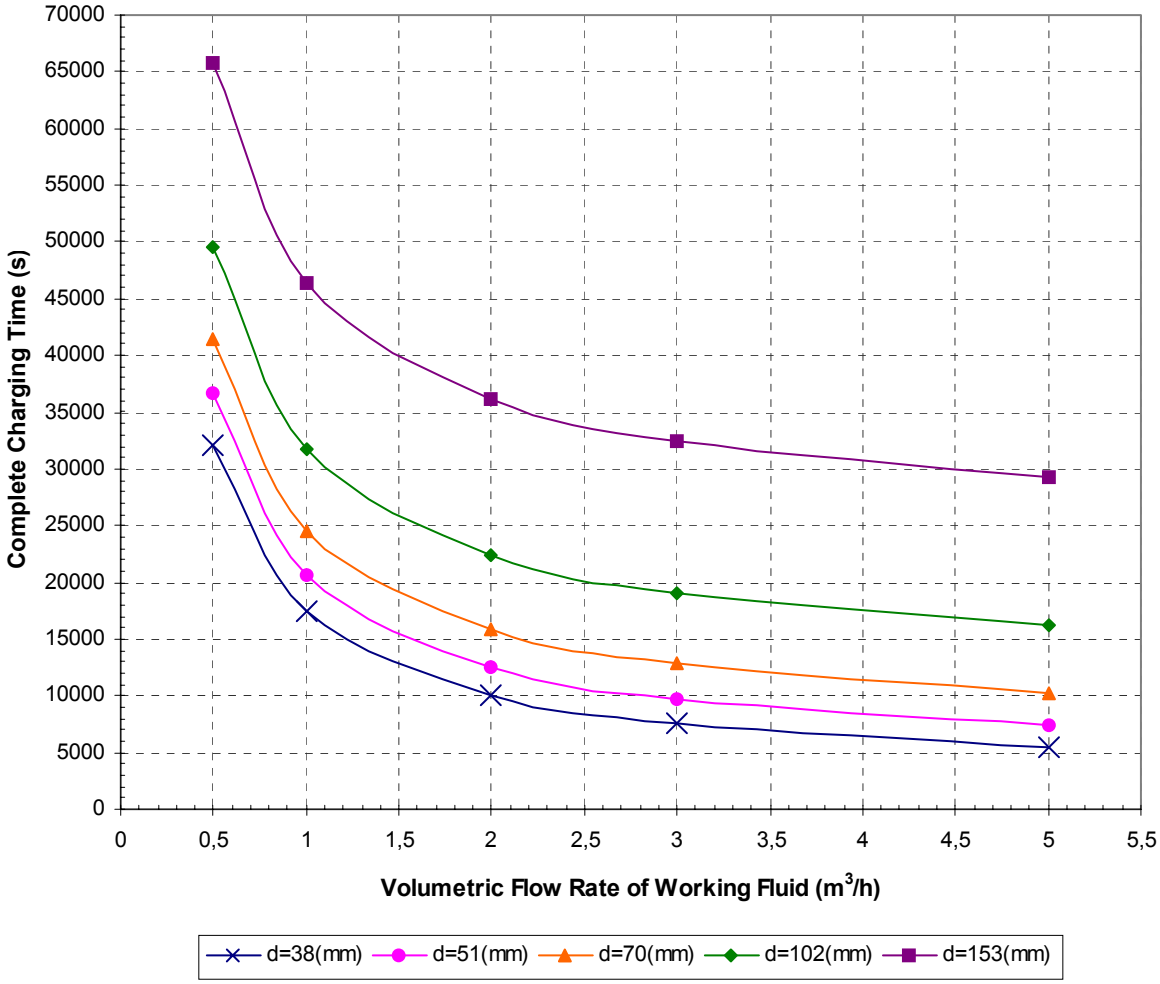

Fig 6.22 Complete Charging Time of the Cool Storage Tank for Different Flow Rates

Figure (6.21) and (6.22) indicate that increasing volumetric flow rate of working fluid leads to a decrease in complete solidification and charging time of the cool storage tank. The effect of increasing volumetric flow rate from 0.5 m^3/h to 2 m^3/h is more dominant as can be seen from the figures, while varying it from 2 m^3/h to 5 m^3/h results in less change in solidification and charging time. Another observation is that the time required for complete solidification and charging increases as bigger containers are used. The difference between the complete charging and complete solidification time for constant container diameter decreases as the volumetric flow rate increases and this difference increases for constant flow rate as the diameter of the container increases. The numerical values of the complete solidification and charging time of the cool storage tank are given in Table 6.3.

Table 6.3 Complete Solidification and Charging Time for Different Volumetric Flow Rates of Working Fluid

Volumetric Flow Rate (m^3/h)	d_{ex}(mm)	Complete Solidification Time (s)	Complete Charging Time (s)	Difference between complete solidification and charging time (s)
0,5	38	31091,31	32087,98	996,67
0,5	51	35444,89	36733,5	1288,61
0,5	70	39880,07	41456,36	1576,29
0,5	102	46955,54	49577,31	2621,77
0,5	153	61156,36	65808,12	4651,76
1	38	16706,01	17383,31	677,3
1	51	19734,5	20687,74	953,24
1	70	23607,92	24580,34	972,42
1	102	30163,07	31766,56	1603,49
1	153	43674,48	46395,39	2720,91
2	38	9602,43	10012,87	410,44
2	51	11869,89	12495,83	625,94
2	70	15202	15890,8	688,8
2	102	21250,35	22367,82	1117,47
2	153	34191,34	36074,27	1882,93
3	38	7205,155	7518,848	313,693
3	51	9204,639	9666,774	462,135
3	70	12266,26	12848,83	582,57
3	102	18102,38	19048,04	945,66
3	153	30812,46	32410,04	1597,58
5	38	5246,199	5495,831	249,632
5	51	7006,408	7367,69	361,282
5	70	9821,886	10311,76	489,874
5	102	15468,62	16269,77	801,15
5	153	27962,76	29292,06	1329,3

6.3.3 Varying the Inlet Temperature of Working Fluid

After investigating the effect of varying the volumetric flow rate of working fluid, a similar study is done for the working fluid inlet temperature. The entry temperature is changed from –3 to –15 $°C$. The volumetric flow rate is 1 m^3/h and the initial temperature is 20 $°C$ for all cases.

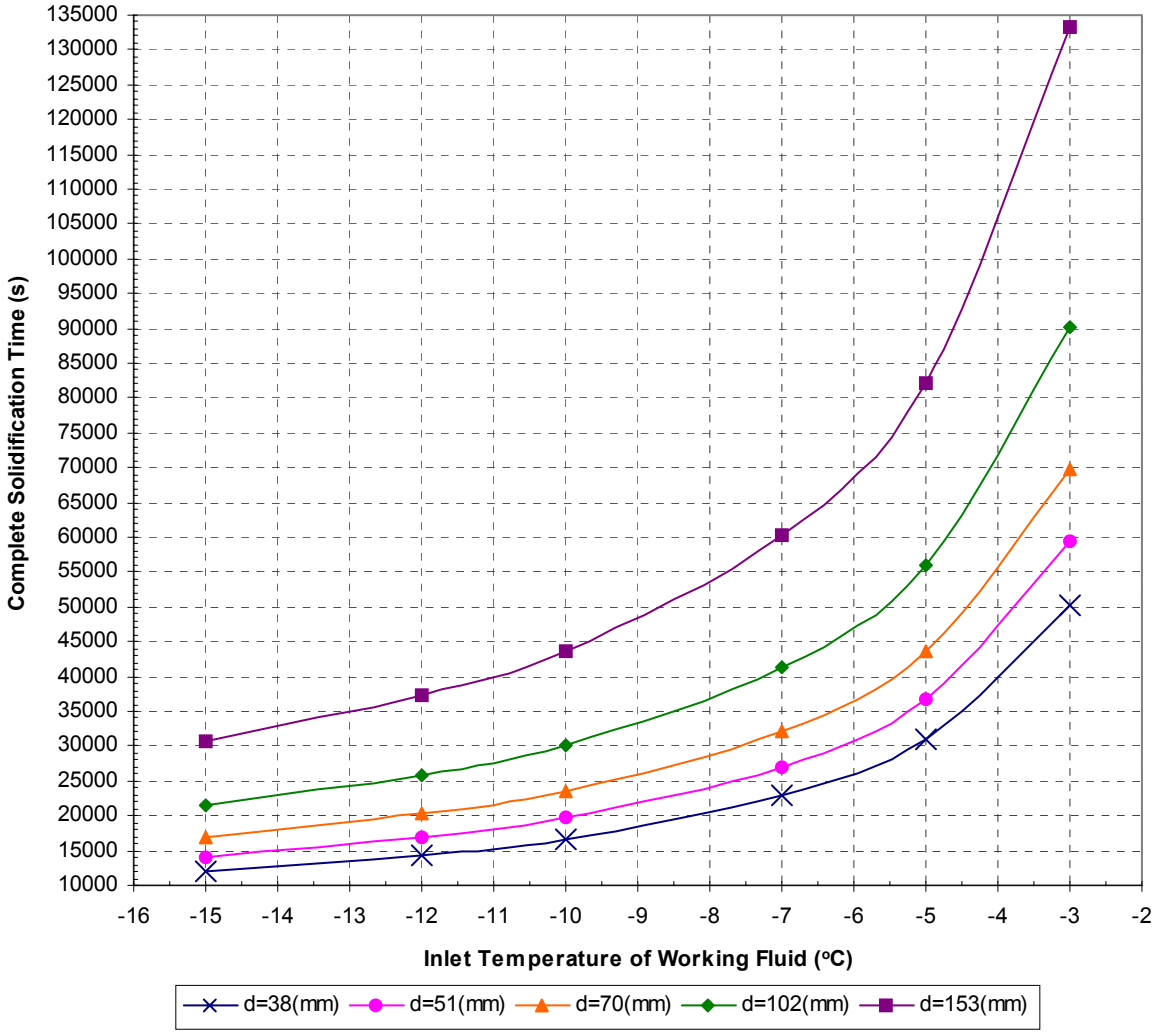

Fig 6.23 Complete Solidification Time of the Cool Storage Tank for Different Working Fluid Inlet Temperatures

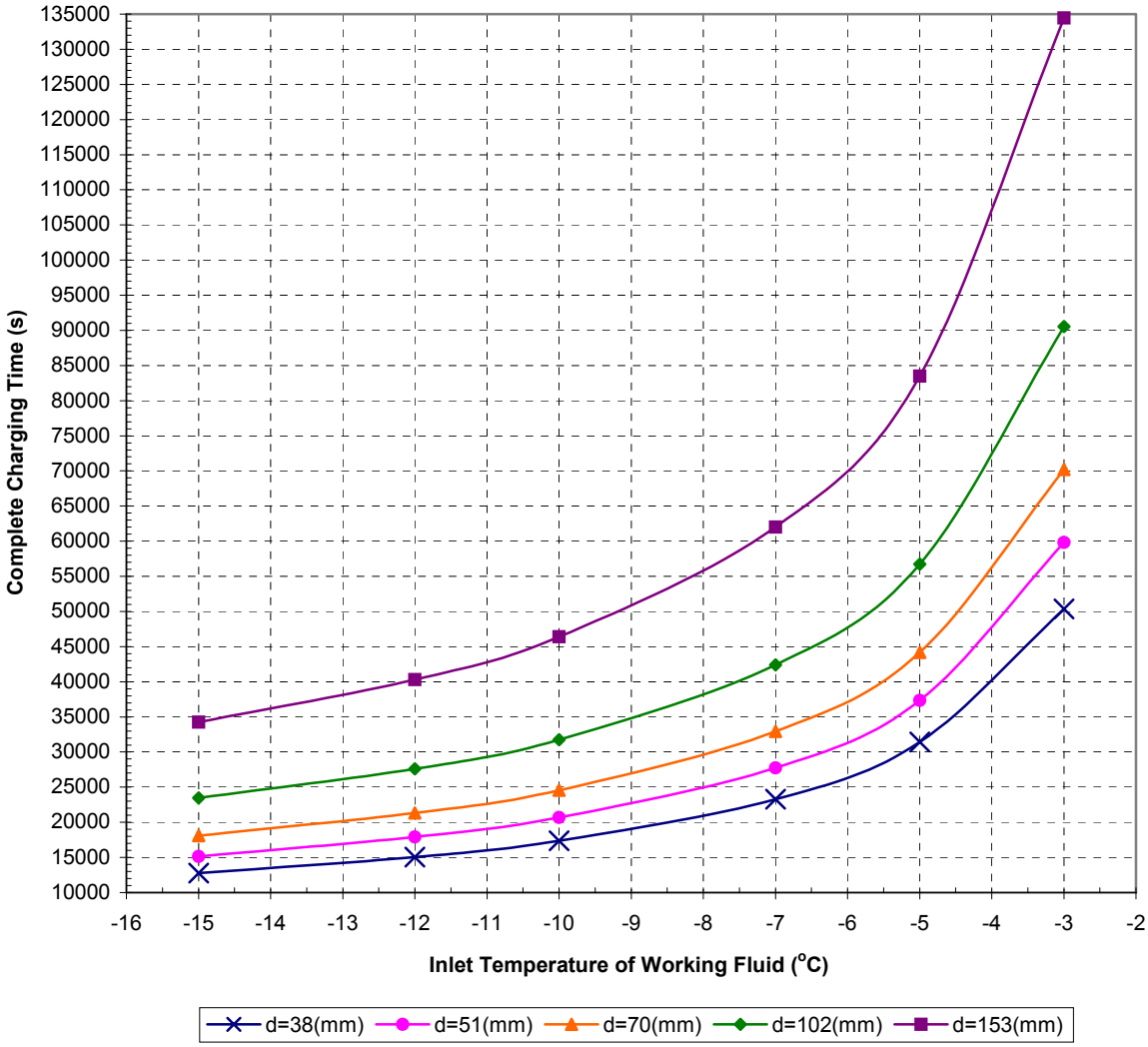

Fig 6.24 Complete Charging Time of the Cool Storage Tank for Different Working Fluid Inlet Temperatures

It is observed from figures (6.23) and (6.24) that the solidification and charging time of the cool storage tank decrease significantly when the inlet temperature of the working fluid decrease gradually from –3 to $-10\,^{\circ}C$. The effect of varying the inlet temperature from –10 to $-15\,^{\circ}C$ is not so remarkable. Similar to the variation of volumetric flow rate, it is clearly seen that for the cool storage tank with bigger spherical containers it takes longer to reach the complete solidification and charging for all of the cases simulated. It should be noted that for constant container diameter, the difference between complete solidification and charging time increases with decreasing the inlet temperature. This difference for constant inlet temperature increases with

increasing the container diameter. The values of the complete charging and solidification are given in Table 6.4

Table 6.4 Complete Solidification and Charging Time for Different Working Fluid Inlet Temperatures

Inlet Temperature (^oC)	d_{ex} (mm)	Complete Solidification Time (s)	Complete Charging Time (s)	Difference between complete solidification and charging time (s)
-3	38	50112,66	50354,55	241,89
-3	51	59485,09	59815,05	329,96
-3	70	69875,97	70219,59	343,62
-3	102	90111,5	90527,01	415,51
-3	153	133380,9	134462,5	1081,6
-5	38	30998,47	31414,32	415,85
-5	51	36735,21	37355,67	620,46
-5	70	43506,75	44152,24	645,49
-5	102	55863,7	56738,23	874,53
-5	153	82230,88	83474,1	1243,22
-7	38	22828,73	23301,66	472,93
-7	51	27019,48	27732,07	712,59
-7	70	32171,77	32913,06	741,29
-7	102	41245,78	42411,21	1165,43
-7	153	60166,02	61994,02	1828
-10	38	16706,01	17383,31	677,3
-10	51	19734,5	20687,74	953,24
-10	70	23607,92	24580,34	972,42
-10	102	30163,07	31766,56	1603,49
-10	153	43674,48	46395,39	2720,91
-12	38	14359,27	15045,91	686,64
-12	51	16891,93	17900,62	1008,69
-12	70	20252,15	21325,9	1073,75
-12	102	25807,24	27594,92	1787,68
-12	153	37197,95	40295,51	3097,56
-15	38	12015,46	12759,65	744,19
-15	51	14086,78	15147,38	1060,6
-15	70	16875,12	18084,41	1209,29
-15	102	21414,9	23454,55	2039,65
-15	153	30674,71	34264,36	3589,65

CHAPTER 7

CONCLUSIONS

In this study, the inward solidification of a phase change material in a spherical and cylindrical container is analyzed as a first step. Programs written in Basic language for spherical and cylindrical containers are used to determine the dimensionless total solidification time of the PCM held inside the containers. The accuracy of the programs is checked by comparing their results with similar available studies and a good agreement is achieved. The programs are run for many times by changing the affecting parameters and data sets are obtained for the dimensionless total solidification time. These data sets are then used to find correlations which express the dimensionless total solidification time in terms of affecting parameters. A total of four correlations are derived (two for spherical and two for cylindrical container), two of which are for the case of equal specific heat and thermal conductivity values of liquid and solid PCM and the others are for water as the PCM. As a result, the correlations, which are given by equations (6.3, 6.4, 6.5 and 6.6), with high correlation coefficients are obtained.

The second step of the study is the analysis of a cool storage tank which is filled with spherical containers containing PCM. The analyses are performed by a program written in Basic language. This program is used to find the complete solidification and complete charging time of the cool storage tank. The outputs of the program are compared with a similar study which gives numerical and experimental results of complete solidification and charging time. It is seen that there is an agreement between the results of the program and the numerical and experimental data given by the mentioned similar study. Since in the comparison the specific heat and thermal conductivity values of the PCM (water for this case) inside the containers are not taken equal, the validation of the method used for the solidification problem in spherical coordinates for the case of non equal PCM physical properties is also made.

The analysis made for the cool storage tank for the case of constant working fluid inlet temperature indicates that the complete solidification and complete charging time decrease with increasing volumetric flow rate of working fluid. It is also seen that using containers with greater diameter inside the cool storage tank leads to an increase in complete solidification and charging time. Another conclusion for the case of

constant working fluid inlet temperature is that the complete charging and solidification time get closer for constant container diameter when volumetric flow rate of working fluid is increased, but the difference between them increases for constant volumetric flow rate when the diameter of the containers increases.

A similar analysis is performed for the case of constant working fluid volumetric flow rate and it is observed that the complete solidification and charging time of the cool storage tank decrease as the working fluid inlet temperature is lowered. Similar to the previous analysis, using containers with greater diameter results in greater complete solidification and charging time. When the container diameter is kept constant, it is found that the difference between complete solidification and charging time becomes larger as working fluid inlet temperature is lowered while this difference increases with increasing container diameter for constant working fluid inlet temperature.

REFERENCES

[1] C.H. Dorgan, J.S. Elleson, *Design Guide for Cool Thermal Storage*, ASHRAE, 1993

[2] S.M. Hasnain, "Review on Sustainable Thermal Energy Storage Technologies, Part II: Cool Thermal Storage", Energy Convers. Mgmt., Vol.39, No.11, 1139-1153, 1998

[3] İ. Dinçer, M.A. Rosen, *Thermal Energy Storage Systems and Applications,* John Wiley and Sons Ltd., 2001

[4] L.C. Tao, "Generalized Numerical Solutions of Freezing a Saturated Liquid in Cylinders and Spheres", A.I.Ch.E. Journal, Vol.13, No.1, 165-169, 1967

[5] S.H. Cho, J.E. Sunderland, "Phase Change of Spherical Bodies", International Journal of Heat and Mass Transfer, Vol.13, 1231-1233, 1970

[6] D.S. Riley, F.T. Smith and G. Poots, "The Inward Solidification of Spheres and Circular Cylinders", International Journal of Heat and Mass Transfer, Vol.17, 1507-1516, 1974

[7] Y.K. Chuang and J. Szekely, "The Use of Green's Functions for Solving Melting or Solidification Problems in the Cylindrical Coordinate System", International Journal of Heat and Mass Transfer, Vol.15, 1171-1174, 1972

[8] Y.P. Shih and S.Y. Tsay, "Analytical Solutions for Freezing a Saturated Liquid Inside and Outside Cylinders", Chemical Engineering Science, Vol.26, 809-816, 1971

[9] R.I. Pedroso, G.A. Domoto, "Inward Spherical Solidification – Solution by the Method of Strained Coordinates", International Journal of Heat and Mass Transfer, Vol.16, 1037-1043, 1973

[10] A.D. Solomon, "On the Melting Time of a Simple Body with a Convection Boundary Condition", Letters in Heat and Mass Transfer, Vol.7, 183-188, 1980

[11] V.R. Voller and M.Cross, "Estimating the Solidification/Melting Times of Cylindrically Symmetric Regions", International Journal of Heat and Mass Transfer, Vol.24, No.9, 1457-1462, 1981

[12] J.M. Hill and A. Kucera, "Freezing a Saturated Liquid Inside a Sphere", International Journal of Heat and Mass Transfer, Vol.26, No.11, 1631-1637, 1983

[13] L.F. Milanez, "Simplified Relations for the Phase Change Process in Spherical Geometry", International Journal of Heat and Mass Transfer, Vol.28, No.4, 884-885, 1985

[14] M. Prud'Homme, T.H. Nguyen, D.L. Nguyen, "A Heat Transfer Analysis for Solidification of Slabs, Cylinders and Spheres", Journal of Heat Transfer, Vol.111, 669-705, 1989

[15] J.D. Caldwell, C.C.Chan, "Spherical Solidification by the Enthalpy Method and Heat Balance Integral Method", Applied Mathematical Modelling, 24, 45-53, 2000

[16] K.A.R. Ismail, J.R. Henriquez, "Solidification of PCM Inside a Spherical Capsule", Energy Conversion and Management, 41, 173-187, 2000

[17] H. Günerhan, Faz Değişimli ve Değişimsiz Isı İletim Problemlerinin Sonuçları Arasındaki İlişkiler Üzerine Bir Araştırma, Ph.D. Thesis, Ege University, İzmir, Turkey, 1998

[18] T. Saitoh and K. Hirose, "High Performance Phase-Change Thermal Energy Storage Using Spherical Capsules", Chem. Eng. Comm., 41, 39-58, 1986

[19] T.F. Green, G.C. Vliet, "Transient Response of a Latent Heat Storage Unit: An Analytical and Experimental Investigation", ASME Journal of Solar Energy Engineering, Vol.103, 275-280, 1981

[20] D.E. Beasley, C. Ramanarayanan and H. Torab, "Thermal Response of a Packed Bed of Spheres Containing a Phase Change Material", International Journal of Energy Research, Vol.13, 253-265, 1989

[21] S.L. Chen, C.L. Chen, C.C. Tin, T.S. Lee, M.C. Ke, "An Experimental Investigation of Cold Storage in an Encapsulated Thermal Storage Tank", Experimental Thermal and Fluid Science, 23, 133-144, 2000

[22] K. Cho, S.H. Choi, "Thermal Characteristics of Paraffin in a Spherical Capsule During Freezing and Melting Processes", International Journal of Heat and Mass Transfer, 43, 3183-3196, 2000

[23] K.A.R. Ismail, J.R. Henriquez, "Numerical and Experimental Study of Spherical Capsules Packed Bed Latent Heat Storage System", Applied Thermal Engineering, 22, 1705-1716, 2002

[24] S.V. Patankar, *Numerical Heat Transfer and Fluid Flow*, Hemisphere Publishing Corporation, 1980

[25] F.P. Incropera, D.P. Dewitt, *Introduction to Heat Transfer*, Third Edition, John Wiley and Sons, Inc.,1996

[26] G.E. Bell, "On the Performance of the Enthalpy Method", International Journal of Heat and Mass Transfer, Vol.25, No.4, 587-589, 1982

[27] V. Voller, M. Cross, “Accurate Solutions of Moving Boundary Problems Using the Enthalpy Method”, International Journal of Heat and Mass Transfer, Vol. 24, 545-556, 1981

[28] V.R. Voller and C.R. Swaminathan, “Treatment of Discontinuous Thermal Conductivity in Control Volume Solutions of Phase Change Problems”, Numerical Heat Transfer, Part B, Vol.24, 161-180, 1993.

APPENDICES

APPENDIX A

SPHERICAL CONTAINER PROGRAM

```
CLS
INPUT "BI="; BI
INPUT "STE="; STE
INPUT "C="; C
INPUT "K="; K
INPUT "TM="; TM
INPUT "N="; N
DR = 1 / (N - .5)
INPUT "DTOU="; DTOU

DIM H(N), T(N), OLDH(N), K(N)

FOR I = 1 TO N
T(I) = 1
H(I) = (1 / STE) + (C * (1 - TM))
K(I) = K
NEXT I

TOU = 0

10  TOU = TOU + DTOU

FOR I = 1 TO N
OLDH(I) = H(I)
NEXT I

H(1) = H(1) + ((3 * DTOU / (DR ^ 2)) * (K(1) + K(2)) * (T(2) - T(1)))

H(2) = H(2) + ((3 * DTOU / (3.25 * (DR ^ 2))) * (((1.5 ^ 3) * K(2) * K(3) *
                (T(3) - T(2)) / ((.5 * K(2)) + K(3))) - ((K(1) + K(2)) * (.5 ^ 2) *
                (T(2) - T(1)) / 2)))

FOR I = 3 TO N - 1
H(I) = H(I) + ((3 * DTOU / (((3 * (I ^ 2)) - (6 * I) + 3.25) * (DR ^ 2))) * ((((I - .5) ^ 3)
               * K(I + 1) * K(I) * (T(I + 1) - T(I)) / ((.5 * (I - 1) * K(I)) + (.5 * I *
               K(I + 1)))) - (((I - 1.5) ^ 3) * K(I) * K(I - 1) * (T(I) - T(I - 1)) /
               ((.5 * (I - 2) * K(I - 1)) + (.5 * (I - 1) * K(I))))))
NEXT I

H(N) = H(N) + ((3 * DTOU / (DR + ((N - 1.5) * (DR ^ 2)) + (((N - 1.5) ^ 2) *
                 (DR ^ 3)))) * ((-2 * BI * K(N) * T(N) / ((2 * K(N)) + (BI * DR))) -
                 (((N - 1.5) ^ 3) * K(N) * K(N - 1) * DR * (T(N) - T(N - 1)) /
                 ((.5 * (N - 2) * K(N - 1)) + (.5 * (N - 1) * K(N))))))
```

```
    FOR I = 1 TO N
    IF H(I) < 0 THEN T(I) = H(I) + TM
    IF H(I) >= 0 AND H(I) <= (1 / STE) THEN T(I) = TM
    IF H(I) > (1 / STE) THEN T(I) = ((H(I) - (1 / STE)) / C) + TM
    NEXT I

    FOR I = 2 TO N
    IF H(I) < (((I - .5) ^ 3) + (3 * ((I - .5) ^ 2) * (I - 1.5)) + (3 * (I - .5) * ((I - 1.5) ^ 2)) –
            (7 * ((I - 1.5) ^ 3))) / (8 * STE * (((I - .5) ^ 3) - ((I - 1.5) ^ 3))) THEN
            K(I) = 1 ELSE K(I) = K
    NEXT I

    FOR I = N TO 2 STEP -1
    IF H(I) < (((I - .5) ^ 3) + (3 * ((I - .5) ^ 2) * (I - 1.5)) + (3 * (I - .5) * ((I - 1.5) ^ 2)) –
            (7 * ((I - 1.5) ^ 3))) / (8 * STE * (((I - .5) ^ 3) - ((I - 1.5) ^ 3)))
    AND OLDH(I) > (((I - .5) ^ 3) + (3 * ((I - .5) ^ 2) * (I - 1.5)) + (3 * (I - .5) *
                    ((I - 1.5) ^ 2)) - (7 * ((I - 1.5) ^ 3))) / (8 * STE * (((I - .5) ^ 3) –
                    ((I - 1.5) ^ 3))) THEN GOTO 20
    NEXT I

    IF H(1) < 0 AND OLDH(1) > 0 THEN I = 1
    IF H(1) < 0 AND OLDH(1) > 0 THEN GOTO 20

    GOTO 10

20  S = 1 - ((N - I + .5) * DR)

    IF S > .00001 THEN X = (((((I - .5) ^ 3) + (3 * ((I - .5) ^ 2) * (I - 1.5)) + (3 * (I - .5) *
                                ((I - 1.5) ^ 2)) - (7 * ((I - 1.5) ^ 3))) / (8 * STE *
                                (((I - .5) ^ 3) - ((I - 1.5) ^ 3)))) - OLDH(I)) /
                                (H(I) - OLDH(I))

   IF ABS(S) < .00001 THEN X = (OLDH(I) / (OLDH(I) - H(I)))

   PRINT "DIMENSIONLESS PHASE CHANGE FRONT POSITION="; S,
         "DIMENSIONLESS TIME="; TOU + ((X - 1) * DTOU)

   IF ABS(S) < .00001 THEN GOTO 30

   GOTO 10

30  END
```

APPENDIX B

CYLINDRICAL CONTAINER PROGRAM

```
CLS
INPUT "BI="; BI
INPUT "STE="; STE
INPUT "C="; C
INPUT "K="; K
INPUT "TM="; TM
INPUT "N="; N
DR = 1 / (N - .5)
INPUT "DTOU="; DTOU

DIM H(N), T(N), OLDH(N), K(N)

FOR I = 1 TO N
T(I) = 1
H(I) = (1 / STE) + (C * (1 - TM))
K(I) = K
NEXT I

TOU = 0

10  TOU = TOU + DTOU

FOR I = 1 TO N
OLDH(I) = H(I)
NEXT I

H(1) = H(1) + ((2 * DTOU / (DR ^ 2)) * (K(1) + K(2)) * (T(2) - T(1)))

H(2) = H(2) + ((DTOU / (DR ^ 2)) * ((1.5 * K(2) * K(3) * LOG(2) * (T(3) - T(2)) /
                ((K(2) * LOG(2 / 1.5)) + (K(3) * LOG(1.5)))) - ((K(1) + K(2)) *
                (T(2) - T(1)) / 4)))

FOR I = 3 TO N - 1
H(I) = H(I) + ((DTOU / ((I - 1) * (DR ^ 2))) * ((K(I + 1) * K(I) * LOG(I / (I - 1)) *
               (I - .5) * (T(I + 1) - T(I)) / ((K(I) * LOG(I / (I - .5))) + (K(I + 1) *
               LOG((I - .5) / (I - 1))))) - (K(I) * K(I - 1) * LOG((I - 1) / (I - 2)) *
               (I - 1.5) * (T(I) - T(I - 1)) / ((K(I - 1) * LOG((I - 1) / (I - 1.5))) +
               (K(I) * LOG((I - 1.5) / (I - 2)))))))
NEXT I

H(N) = H(N) + ((DTOU / ((N - 1) * (DR ^ 2))) * ((-2 * BI * K(N) * T(N) /
                ((2 * K(N)) + (BI * DR))) - (K(N) * K(N - 1) * LOG((N - 1) / (N - 2))
                (N - 1.5) * (T(N) - T(N - 1)) / ((K(N - 1) * LOG((N - 1) / (N - 1.5)))
                + (K(N) * LOG((N - 1.5) / (N - 2)))))))
```

```
    FOR I = 1 TO N
    IF H(I) < 0 THEN T(I) = H(I) + TM
    IF H(I) >= 0 AND H(I) <= (1 / STE) THEN T(I) = TM
    IF H(I) > (1 / STE) THEN T(I) = ((H(I) - (1 / STE)) / C) + TM
    NEXT I

    FOR I = 2 TO N
    IF H(I) < (((I - .5) ^ 2) + (2 * (I - .5) * (I - 1.5)) - (3 * ((I - 1.5) ^ 2))) / (4 * STE *
            (((I - .5) ^ 2) - ((I - 1.5) ^ 2))) THEN K(I) = 1 ELSE K(I) = K
    NEXT I

    FOR I = N TO 2 STEP -1
    IF H(I) < (((I - .5) ^ 2) + (2 * (I - .5) * (I - 1.5)) - (3 * ((I - 1.5) ^ 2))) / (4 * STE *
            (((I - .5) ^ 2) - ((I - 1.5) ^ 2)))
    AND OLDH(I) > (((I - .5) ^ 2) + (2 * (I - .5) * (I - 1.5)) - (3 * ((I - 1.5) ^ 2))) /
                    (4 * STE * (((I - .5) ^ 2) - ((I - 1.5) ^ 2))) THEN GOTO 20
    NEXT I

    IF H(1) < 0 AND OLDH(1) > 0 THEN I = 1
    IF H(1) < 0 AND OLDH(1) > 0 THEN GOTO 20

    GOTO 10

20  S = 1 - ((N - I + .5) * DR)

    IF S > .00001 THEN X = (((((I - .5) ^ 2) + (2 * (I - .5) * (I - 1.5)) - (3 * ((I - 1.5) ^ 2)))
                            / (4 * STE * (((I - .5) ^ 2) - ((I - 1.5) ^ 2)))) - OLDH(I)) /
                            (H(I) - OLDH(I))

    IF ABS(S) < .00001 THEN X = (OLDH(I) / (OLDH(I) - H(I)))

    PRINT "DIMENSIONLESS PHASE CHANGE FRONT POSITION"; S,
          "DIMENSIONLESS TIME="; TOU + ((X - 1) * DTOU)

    IF ABS(S) < .00001 THEN GOTO 30

    GOTO 10

30  END
```

APPENDIX C

COOL STORAGE TANK PROGRAM

```
CLS
INPUT "VOLUMETRIC FLOW RATE OF WORKING FLUID="; VOLFRWF
INPUT "TOTAL NUMBER OF LAYERS IN THE COOL STORAGE TANK="; M
INPUT "TOTAL NUMBER OF SPHERICAL CONTAINERS IN A LAYER="; SPCL
INPUT "DIAMETER OF THE COOL STORAGE TANK="; DCST
PI = 3.141592654#
ACST = PI * (DCST ^ 2) / 4
INPUT "ENTRY TEMPERATURE OF WORKING FLUID="; TENWF
ROWF = (.0000001399# * (TENWF ^ 3)) - (.0024417249# * (TENWF ^ 2)) –
          (.2775594406# * TENWF) + 1051.7802564102#
MASSFRWF = ROWF * VOLFRWF
REM "PROPERTIES OF PCM INSIDE THE SPHERICAL CONTAINERS"
INPUT "LATENT HEAT OF PCM="; L
INPUT "DENSITY OF PCM="; RO
INPUT "SPECIFIC HEAT OF SOLID PCM="; CS
INPUT "SPECIFIC HEAT OF LIQUID PCM="; CL
INPUT "THERMAL CONDUCTIVITY OF SOLID PCM="; KS
INPUT "THERMAL CONDUCTIVITY OF LIQUID PCM="; KL
INPUT "SOLIDIFICATION TEMPERATURE="; TM
INPUT "INITIAL TEMPERATURE OF PCM="; TINITIAL
INPUT "TOTAL GRID NUMBERS IN A SPHERICAL CONTAINER="; N
INPUT "INTERNAL SHELL RADIUS="; RIN
INPUT "EXTERNAL SHELL RADIUS="; REX
DR = RIN / (N - .5)
INPUT "TIME INCREMENT="; DT
VOIDFR = ((2 * REX * M * ACST) - (M * SPCL * 4 * PI * (REX ^ 3) / 3)) /
            (2 * REX * M * ACST)
VELWF = MASSFRWF / (ROWF * VOIDFR * ACST)
VOLWF = (2 * REX * ACST) - (SPCL * 4 * PI * (REX ^ 3) / 3)
INPUT "THERMAL CONDUCTIVITY OF SPHERICAL SHELL="; KSHELL
DIM H(M, N), T(M, N), OLDH(M, N), K(M, N), TWF(M + 1), OLDTWF(M + 1),
      TS(M), TW(M)
FOR I = 1 TO M
FOR J = 1 TO N
T(I, J) = TINITIAL
H(I, J) = (CL * (TINITIAL - TM)) + L
K(I, J) = KL
NEXT J
NEXT I
TWF(1) = TENWF
FOR I = 2 TO M + 1
TWF(I) = TINITIAL
NEXT I
```

```
    FOR I = 1 TO M
    TS(I) = TINITIAL
    TW(I) = TINITIAL
    NEXT I
    T = 0
10  T = T + DT
    FOR I = 1 TO M
    FOR J = 1 TO N
    OLDH(I, J) = H(I, J)
    NEXT J
    NEXT I
    FOR I = 1 TO M + 1
    OLDTWF(I) = TWF(I)
    NEXT I
    FOR I = 1 TO M
    TFILM = (((OLDTWF(I) + OLDTWF(I + 1)) / 2) + TS(I)) / 2
    TCALC = TFILM
15  GOSUB 35
    RE = (ROWF * VELWF * 2 * REX) / MUWF
    NU = (3.22 * (RE ^ (1 / 3)) * (PRWF ^ (1 / 3))) + (.117 * (RE ^ .8) * (PRWF ^ .8))
    H = KWF * NU / (2 * REX)
    TF = (OLDTWF(I) + OLDTWF(I + 1)) / 2
    Q = (TW(I) - TF) / (((REX - RIN) / (4 * PI * KSHELL * REX * RIN)) +
        (1 / (4 * PI * H * (REX ^ 2))))
    TCALC = TF
20  GOSUB 35
    TWF(I + 1) = ((2 * MASSFRWF * DT * (OLDTWF(I) - OLDTWF(I + 1))) /
                 (ROWF * VOLWF)) + (2 * SPCL * Q * DT / (ROWF * CWF *
                 VOLWF)) + OLDTWF(I) + OLDTWF(I + 1) - TWF(I)
    H(I, 1) = H(I, 1) + ((3 * DT / (RO * (DR ^ 2))) * (K(I, 1) + K(I, 2)) *
                        (T(I, 2) - T(I, 1)))
    H(I, 2) = H(I, 2) + ((3 * DT / (3.25 * RO * (DR ^ 2))) * (((1.5 ^ 3) * K(I, 2) * K(I, 3)
                        (T(I, 3) - T(I, 2)) / ((.5 * K(I, 2)) + K(I, 3))) - ((K(I, 1) + K(I, 2))
                        * (.5 ^ 2) * (T(I, 2) - T(I, 1)) / 2)))
    FOR J = 3 TO N - 1
    H(I, J) = H(I, J) + ((3 * DT / (((3 * (J ^ 2)) - (6 * J) + 3.25) * RO * (DR ^ 2))) *
                        ((((J - .5) ^ 3) * K(I, J + 1) * K(I, J) * (T(I, J + 1) - T(I, J)) /
                        ((.5 * (J - 1) * K(I, J)) + (.5 * J * K(I, J + 1)))) - (((J - 1.5) ^ 3) *
                        K(I, J) * K(I, J - 1) * (T(I, J) - T(I, J - 1)) / ((.5 * (J - 2) *
                        K(I, J - 1)) + (.5 * (J - 1) * K(I, J))))))
    NEXT J
    H(I, N) = H(I, N) + (((3 * DT) / (((3 * (N ^ 2)) - (6 * N) + 3.25) * RO * (DR ^ 2))) *
                         ((2 * K(I, N) * ((N - .5) ^ 2) * (TW(I) - T(I, N))) –
                         ((((N - 1.5) ^ 3) * K(I, N) * K(I, N - 1) * (T(I, N) - T(I, N - 1))) /
                         ((.5 * (N - 2) * K(I, N - 1)) + ( .5 * (N - 1) * K(I, N))))))
    FOR J = 1 TO N
    IF H(I, J) < 0 THEN T(I, J) = (H(I, J) / CS) + TM
    IF H(I, J) >= 0 AND H(I, J) <= L THEN T(I, J) = TM
    IF H(I, J) > L THEN T(I, J) = ((H(I, J) - L) / CL) + TM
    NEXT J
```

```
    FOR J = 2 TO N
    IF H(I, J) < (L / 8) * ((((J - .5) ^ 3) + (3 * ((J - .5) ^ 2) * (J - 1.5)) + (3 * (J - .5) *
                ((J - 1.5) ^ 2)) - (7 * ((J - 1.5) ^ 3))) / (((J - .5) ^ 3) - ((J - 1.5) ^ 3)))
                THEN K(I, J) = KS
    NEXT J
    IF H(I, 1) < 0 THEN K(I, 1) = KS
    IF NOT I = M THEN GOTO 30
    IF SOLTIME > 0 THEN GOTO 30
    IF H(M, 1) < 0 AND OLDH(M, 1) > 0 THEN GOTO 25
    GOTO 30
25  X = OLDH(M, 1) / (OLDH(M, 1) - H(M, 1))
    SOLTIME = T + ((X - 1) * DT)
    PRINT "THE CONTAINERS AT THE LAST ROW OF THE COOL STORAGE
            TANK SOLIDIFIED"
    PRINT "SOLTIME="; SOLTIME
30  IF ABS(TWF(M + 1) - TENWF) < .01 THEN GOTO 31 ELSE 32
31  CHRGTIME = T
    PRINT "SOLTIME="; SOLTIME
    PRINT "CHARGE TIME"; CHRGTIME
    END
32  TF = (TWF(I) + TWF(I + 1)) / 2
    A = 2 * K(I, N) * RIN * ((KSHELL * RIN) + (REX * H * (REX - RIN)))
    B = H * KSHELL * (REX ^ 2) * DR
    TW(I) = ((A * T(I, N)) + (B * TF)) / (A + B)
    TS(I) = ((KSHELL * RIN * TW(I)) + (H * REX * (REX - RIN) * TF)) /
          ((KSHELL * RIN) + (REX * H * (REX - RIN)))
    NEXT I
    GOTO 10
35  ROWF = (.0000001399# * (TCALC ^ 3)) - (.0024417249# * (TCALC ^ 2)) –
            (.2775594406# * TCALC) + 1051.7802564102#
    MUWF = (-.000000037# * (TCALC ^ 3)) + (.000003635# * (TCALC ^ 2)) –
            (.0001578089# * TCALC) + .0041800699#
    KWF = (.0000000078# * (TCALC ^ 3)) - (.0000065035# * (TCALC ^ 2)) +
            (.0013500389# * TCALC) + .4290885781#
    CWF = (.000004662# * (TCALC ^ 3)) - (.0005361305# * (TCALC ^ 2)) +
            (2.8526806527# * TCALC) + 3588.578088578#
    PRWF = (CWF * MUWF) / KWF
    RETURN
```

APPENDIX D

MULTIPLE REGRESSION ANALYSIS

When $x_1, x_2, x_3, \ldots, x_n$ are defined as independent variables and $\hat{y}$ is defined as dependent variable, deriving a correlation in the form given by equation (D-1) is named as linear multiple regression analysis.

$$\hat{y} = a + b_1 x_1 + b_2 x_2 + b_3 x_3 + \ldots + b_n x_n \qquad \text{(D-1)}$$

$a, b_1, b_2, b_3, \ldots, b_n$ are the regression coefficients.

When the derivation of the square of the difference between the observed value of y and the expected value from the equation (D-1) is done in terms of each coefficient and these derivations are equalized to zero, the coefficients obtained give the minimum of the square of the deviations. This method is the modified version of the least square method used for two variables. When the mentioned derivations are done the following equation set is obtained;

$$\begin{aligned}
&N a + b_1 \sum x_1 + b_2 \sum x_2 + b_3 \sum x_3 + \ldots = \sum y \\
&a \sum x_1 + b_1 \sum x_1^2 + b_2 \sum x_1 x_2 + b_3 \sum x_1 x_3 + \ldots = \sum x_1 y \\
&a \sum x_2 + b_1 \sum x_1 x_2 + b_2 \sum x_2^2 + b_3 \sum x_2 x_3 + \ldots = \sum x_2 y \qquad \text{(D-2)} \\
&a \sum x_n + b_1 \sum x_1 x_n + b_2 \sum x_2 x_n + \ldots + b_n \sum x_n^2 = \sum x_n y
\end{aligned}$$

N is the total number of data. The correlation coefficients are found by solving this equation set.

Cerrelation Coefficient (R)

Correlation coefficient changes between 0 and 1. If the correlation coefficient is 0, there is a random relation between the expected and observed values while if it is 1,

the correlation represent perfectly the observed values. The correlation coefficient is defined as;

$$R = \left[\frac{a\, g_0 + \sum_{i=1}^{n} b_i\, g_i - N\, \bar{y}^2}{\sum y^2 - \left(\sum y\right)^2 / N} \right]^{1/2} \qquad \text{(D-3)}$$

where;

$g_0 = \sum y$

$g_1 = \sum x_1\, y$

$g_2 = \sum x_2\, y$

$g_n = \sum x_n\, y$

and $\bar{y}$ is the mean of y's.

Linearization

If the correlation to be found is in the form as;

$$\hat{y} = a\, x_1^{b_1}\, x_2^{b_2}\, x_3^{b_3} \ldots\ldots \qquad \text{(D-4)}$$

it can be linearized as follows;

$$\ln \hat{y} = \ln a + b_1 \ln x_1 + b_2 \ln x_2 + b_3 \ln x_3 + \ldots\ldots \qquad \text{(D-5)}$$

or

$$Y = A + b_1 X_1 + b_2 X_2 + b_3 X_3 + \ldots\ldots \qquad \text{(D-6)}$$

So, the procedure explained for equation (D-1) can also be applied for equation (D-6).

MULTIPLE REGRESSION ANALYSIS PROGRAM

The program written to find the correlations in the form of $\tau_{total} = a \times (Ste)^b \times (Bi)^c \times (\theta_m)^d$ is given as follows;

```
OPEN "C:DATA" FOR INPUT AS #1
WHILE NOT EOF(1)
INPUT #1, TM, STE, BI, SOLTIME
X1 = LOG(STE)
X2 = LOG(BI)
X3 = LOG(TM)
Y = LOG(SOLTIME)
N = N + 1
TY = TY + Y
TX1 = TX1 + X1
TX2 = TX2 + X2
TX3 = TX3 + X3
TX1K = TX1K + (X1 ^ 2)
TX1Y = TX1Y + (X1 * Y)
TX1X2 = TX1X2 + (X1 * X2)
TX1X3 = TX1X3 + (X1 * X3)
TX2K = TX2K + (X2 ^ 2)
TX2Y = TX2Y + (X2 * Y)
TX2X3 = TX2X3 + (X2 * X3)
TX3K = TX3K + (X3 ^ 2)
TX3Y = TX3Y + (X3 * Y)
TYK = TYK + (Y ^ 2)
WEND
YMEAN = TY / N
DIM A(4, 5)
A(1, 1) = N
A(1, 2) = TX1
A(1, 3) = TX2
A(1, 4) = TX3
A(1, 5) = TY
A(2, 1) = TX1
A(2, 2) = TX1K
A(2, 3) = TX1X2
A(2, 4) = TX1X3
A(2, 5) = TX1Y
A(3, 1) = TX2
A(3, 2) = TX1X2
A(3, 3) = TX2K
A(3, 4) = TX2X3
A(3, 5) = TX2Y
A(4, 1) = TX3
A(4, 2) = TX1X3
A(4, 3) = TX2X3
```

```
A(4, 4) = TX3K
A(4, 5) = TX3Y
DE = -(A(2, 1) / A(1, 1))
A(2, 1) = A(2, 1) + (DE * A(1, 1))
A(2, 2) = A(2, 2) + (DE * A(1, 2))
A(2, 3) = A(2, 3) + (DE * A(1, 3))
A(2, 4) = A(2, 4) + (DE * A(1, 4))
A(2, 5) = A(2, 5) + (DE * A(1, 5))
DE = -(A(3, 1) / A(1, 1))
A(3, 1) = A(3, 1) + (DE * A(1, 1))
A(3, 2) = A(3, 2) + (DE * A(1, 2))
A(3, 3) = A(3, 3) + (DE * A(1, 3))
A(3, 4) = A(3, 4) + (DE * A(1, 4))
A(3, 5) = A(3, 5) + (DE * A(1, 5))
DE = -(A(4, 1) / A(1, 1))
A(4, 1) = A(4, 1) + (DE * A(1, 1))
A(4, 2) = A(4, 2) + (DE * A(1, 2))
A(4, 3) = A(4, 3) + (DE * A(1, 3))
A(4, 4) = A(4, 4) + (DE * A(1, 4))
A(4, 5) = A(4, 5) + (DE * A(1, 5))
DE = -(A(3, 2) / A(2, 2))
A(3, 2) = A(3, 2) + (DE * A(2, 2))
A(3, 3) = A(3, 3) + (DE * A(2, 3))
A(3, 4) = A(3, 4) + (DE * A(2, 4))
A(3, 5) = A(3, 5) + (DE * A(2, 5))
DE = -(A(4, 2) / A(2, 2))
A(4, 2) = A(4, 2) + (DE * A(2, 2))
A(4, 3) = A(4, 3) + (DE * A(2, 3))
A(4, 4) = A(4, 4) + (DE * A(2, 4))
A(4, 5) = A(4, 5) + (DE * A(2, 5))
DE = -(A(4, 3) / A(3, 3))
A(4, 3) = A(4, 3) + (DE * A(3, 3))
A(4, 4) = A(4, 4) + (DE * A(3, 4))
A(4, 5) = A(4, 5) + (DE * A(3, 5))
D = A(4, 5) / A(4, 4)
C = (A(3, 5) - (A(3, 4) * D)) / A(3, 3)
B = (A(2, 5) - (A(2, 4) * D) - (A(2, 3) * C)) / A(2, 2)
A = (A(1, 5) - (A(1, 4) * D) - (A(1, 3) * C) - (A(1, 2) * B)) / A(1, 1)
R = (((A * TY) + (B * TX1Y) + (C * TX2Y) + (D * TX3Y) – (N * (YMEAN ^ 2))) /
     (TYK - ((TY ^ 2) / N))) ^ .5
LINA = EXP(A)
PRINT "TOTAL DATA NUMBER="; N
PRINT "REGRESSION COEFFICIENTS"
PRINT "-----------------------"
PRINT "A="; LINA, "B="; B, "C="; C, "D="; D
PRINT "CORRELATION COEFFICIENT"
PRINT "-----------------------"
PRINT "R="; R
END
```

APPENDIX E

PROPERTIES OF SOME PHASE CHANGE MATERIALS

The thermophysical properties of the phase change materials used in this study are given in Table E-1

Table E-1 Thermophysical Properties of Some Phase Change Materials

Property	H_2O (Water)	$Na_2HPO_4.12H_2O$ (Sodium Hydrogen Phosphate Dodecahydrate)
k_s (W/mK)	1.880	0.514
k_l (W/mK)	0.567	0.476
k_s/k_l	3.3157	1.080
k_l/k_s	0.3016	0.926
ρ_s (kg/m^3)	916.8	1520
ρ_l (kg/m^3)	999.8	1442
ρ_s/ρ_l	0.917	1.054
ρ_l/ρ_s	1.091	0.949
c_{p_s} (j/kgK)	2040	1700
c_{p_l} (j/kgK)	4210	1950
c_{p_s}/c_{p_l}	0.4846	0.872
c_{p_l}/c_{p_s}	2.0637	1.147
$\alpha_s.10^6$ (m^2/s)	1.005	0.199
$\alpha_l.10^6$ (m^2/s)	0.135	0.169
α_s/α_l	7.462	1.175
α_l/α_s	0.134	0.849
T_m $(°C)$	0	36
L (j/kg)	333500	265000

APPENDIX F

RESULTS OF COMPARISONS

Table F-1 Data for Figure 6.1

	1/BI	τ.STE (Ref [4])	τ.STE
STE=0,1	0,1	0,22979	0,2168816
	0,5	0,37644	0,3595699
	1	0,55724	0,53567
	2	0,91373	0,8830976
	4	1,61698	1,568807
	5	1,96611	1,906408
STE=0,5	0,1	0,28228	0,2712049
	0,5	0,45583	0,43918515
	1	0,65844	0,6359245
	2	1,04475	1,0107435
	4	1,78598	1,7303565
	5	2,14951	2,0835605
STE=1	0,1	0,33775	0,3284819
	0,5	0,53472	0,5194784
	1	0,75675	0,7342109
	2	1,16901	1,133106
	4	1,94339	1,884813
	5	2,3186	2,249735
STE=2	0,1	0,42977	0,4279168
	0,5	0,66703	0,6552574
	1	0,91766	0,8977022
	2	1,3694	1,333882
	4	2,19534	2,134484
	5	2,59062	2,51829
STE=3	0,1	0,51569	0,5166576
	0,5	0,78506	0,7742178
	1	1,06129	1,0394823
	2	1,54276	1,5062772
	4	2,40927	2,3473503
	5	2,82382	2,7466128

Table F-2 Data for Figure 6.2

	BI	τ (Ref [10])	τ
STE=0,05	5	4,754360967	4,870751
	10	4,0876943	4,175378
	20	3,754360967	3,827654
	30	3,643249856	3,71182
	40	3,5876943	3,653891
	50	3,554360967	3,619129
STE=0,1	5	2,421027633	2,527682
	10	2,0876943	2,168816
	20	1,921027633	1,98879
	30	1,865472078	1,928627
	40	1,8376943	1,89853
	50	1,821027633	1,880467
STE=0,2	5	1,254360967	1,349071
	10	1,0876943	1,158746
	20	1,004360967	1,062856
	30	0,976583189	1,030781
	40	0,9626943	1,014723
	50	0,954360967	1,005081
STE=0,3	5	0,865472078	0,9518051
	10	0,754360967	0,8185505
	20	0,698805411	0,7511086
	30	0,680286893	0,7285007
	40	0,671027633	0,717172
	50	0,665472078	0,7103673
STE=0,5	5	0,554360967	0,6291754
	10	0,4876943	0,5424098
	20	0,454360967	0,4981121
	30	0,443249856	0,4832029
	40	0,4376943	0,4757197
	50	0,434360967	0,4712206

Table F-3 Data for Figure 6.3

SPHERICAL CONTAINER PROGRAM	
τ.Ste	R
0	1
0,10595095	0,89108910
0,19650455	0,79207920
0,28104545	0,69306930
0,35908825	0,59405940
0,4299588	0,49504950
0,49288385	0,39603960
0,5468805	0,29702970
0,5905945	0,19801980
0,6218895	0,09900992
0,6359245	0,00000000

TAO [4]	
τ.Ste	R
0	1
0,10014	0,90000000
0,19503	0,80000000
0,28361	0,70000000
0,36523	0,60000000
0,43927	0,50000000
0,50511	0,40000000
0,56165	0,30000000
0,60772	0,20000000
0,64139	0,10000000
0,65844	0,00000000

ISMAIL & HENRIQUEZ [16]	
τ.Ste	R
0	1
0,1052632	0,90000000
0,1894737	0,80000000
0,2821053	0,70000000
0,3578947	0,60000000
0,4294737	0,50000000
0,4926316	0,40000000
0,5473684	0,30000000
0,5926316	0,20000000
0,6263158	0,10000000
0,6421053	0,00000000

HILL&KUCERA [12]	
τ.Ste	R
0	1
0,1031579	0,90000000
0,1894737	0,80000000
0,2842105	0,70000000
0,3578947	0,60000000
0,4315789	0,50000000
0,5052632	0,40000000
0,5684211	0,30000000
0,6105263	0,20000000
0,6421053	0,10000000
0,6526316	0,00000000

Table F-4 Data for Figure 6.4

SPHERICAL CONTAINER PROGRAM	
τ.Ste	R
0	1
0,103396532	0,8910891
0,1876275	0,7920792
0,262670254	0,6930693
0,328588654	0,5940594
0,38521065	0,4950495
0,432492718	0,3960396
0,470338882	0,2970297
0,498561902	0,1980198
0,516760638	0,0990099
0,523742272	0,0000000

ISMAIL & HENRIQUEZ [16]	
τ.Ste	R
0	1
0,081940397	0,90000000
0,156076965	0,80000000
0,22240968	0,70000000
0,283279693	0,60000000
0,331663556	0,50000000
0,373023949	0,40000000
0,405800112	0,30000000
0,432333198	0,20000000
0,44872128	0,10000000
0,456525126	0,00000000

Table F-5 Data for Figure 6.5

SPHERICAL CONTAINER PROGRAM	
τ.Ste	R
0	1
0,005839597	0,89108910
0,01954881	0,79207920
0,03928617	0,69306930
0,06311077	0,59405940
0,08907872	0,49504950
0,1152362	0,39603960
0,1396198	0,29702970
0,1602348	0,19801980
0,1749844	0,09900992
0,181179	0,00000000

PEDROSO&DOMOTO [9]	
τ.Ste	R
0	1
0,006	0,90000000
0,02	0,80000000
0,0368	0,70000000
0,06	0,60000000
0,088	0,50000000
0,114	0,40000000
0,1368	0,30000000
0,158	0,20000000
0,1728	0,10000000
0,182	0,00000000

CALDWELL&CHAN [15]	
τ.Ste	R
0	1
0,0055555	0,90000000
0,02	0,80000000
0,0377777	0,70000000
0,0611111	0,60000000
0,0877777	0,50000000
0,1144444	0,40000000
0,1388888	0,30000000
0,16	0,20000000
0,1755555	0,10000000
0,18	0,00000000

Table F-6 Data for Figure 6.6

	1/BI	τ.STE (Ref [4])	τ.STE
STE=0,1	0,1	0,33321	0,3199755
	0,5	0,54647	0,5303633
	1	0,80941	0,7898899
	2	1,32896	1,302873
	4	2,35751	2,311968
	5	2,86937	2,812818
STE=0,5	0,1	0,39662	0,3852325
	0,5	0,6401	0,6246235
	1	0,92755	0,9072015
	2	1,47884	1,4491865
	4	2,54567	2,5001165
	5	3,07131	3,0186355
STE=1	0,1	0,46348	0,4545256
	0,5	0,73606	0,7218229
	1	1,04547	1,025993
	2	1,62645	1,596645
	4	2,73015	2,681704
	5	3,26842	3,21163
STE=2	0,1	0,58046	0,5753008
	0,5	0,8971	0,8874926
	1	1,24326	1,2259334
	2	1,87012	1,841822
	4	3,03448	2,984992
	5	3,59451	3,536686
STE=3	0,1	0,68084	0,6830703
	0,5	1,03942	1,0330251
	1	1,41827	1,3999923
	2	2,07815	2,0538867
	4	3,29431	3,245928
	5	3,87353	3,815853

Table F-7 Data for Figure 6.7

	BI	τ (Ref [10])	τ
STE=0,05	5	7,105	7,244773
	10	6,105	6,212166
	20	5,605	5,69488
	30	5,43833333	5,522299
	40	5,355	5,435977
	50	5,305	5,384175
STE=0,1	5	3,605	3,728407
	10	3,105	3,199755
	20	2,855	2,93437
	30	2,77166667	2,84574
	40	2,73	2,801392
	50	2,705	2,774772
STE=0,2	5	1,855	1,965988
	10	1,605	1,689086
	20	1,48	1,549489
	30	1,43833333	1,502771
	40	1,4175	1,479376
	50	1,405	1,465328
STE=0,3	5	1,27166667	1,373259
	10	1,105	1,181225
	20	1,02166667	1,084015
	30	0,99388889	1,051416
	40	0,98	1,035078
	50	0,97166667	1,025263
STE=0,5	5	0,805	0,8937575
	10	0,705	0,770465
	20	0,655	0,707573
	30	0,63833333	0,6864003
	40	0,63	0,6757725
	50	0,625	0,6693824

Table F-8 Data for Figure 6.8

Ste=0,1 Bi=1	
CYLINDRICAL CONTAINER PROGRAM	
τ.Ste	R
0	1,000000
0,1093103	0,891089
0,2084223	0,792079
0,3059433	0,693069
0,4005981	0,594059
0,4910655	0,495050
0,5753248	0,396040
0,6511842	0,297030
0,7158075	0,198020
0,7650603	0,099010
0,7898899	0,000000
SHIH&TSAY [8]	
τ.Ste	R
0	1,000000
0,095	0,900000
0,2125	0,800000
0,3	0,700000
0,4	0,600000
0,4875	0,500000
0,575	0,400000
0,65	0,300000
0,715	0,200000
0,765	0,100000
0,795	0,000000
TAO [4]	
τ.Ste	R
0	1,000000
0,10235	0,900000
0,20473	0,800000
0,3056	0,700000
0,40357	0,600000
0,49707	0,500000
0,58423	0,400000
0,66283	0,300000
0,73001	0,200000
0,78165	0,100000
0,80941	0,000000

Ste=0,5 Bi=0,5	
CYLINDRICAL CONTAINER PROGRAM	
τ.Ste	R
0	1
0,2146489	0,8910891
0,4033388	0,7920792
0,584271	0,6930693
0,7560865	0,5940594
0,9171265	0,4950495
1,0652975	0,3960396
1,198055	0,2970297
1,311951	0,1980198
1,401071	9,90E-02
1,4491865	0,00E+00
SHIH&TSAY [8]	
τ.Ste	R
0	1,000000
0,2125	0,900000
0,4	0,800000
0,57	0,700000
0,755	0,600000
0,9125	0,500000
1,08	0,400000
1,2	0,300000
1,295	0,200000
1,35	0,100000
1,3875	0,000000
TAO [4]	
τ.Ste	R
0	1,000000
0,20006	0,900000
0,39415	0,800000
0,58062	0,700000
0,75775	0,600000
0,92374	0,500000
1,07664	0,400000
1,21386	0,300000
1,33195	0,200000
1,42507	0,100000
1,47884	0,000000

Table F-9 Data for Figure 6.9

	VOLLER & CROSS [11]			PRESENT RESULTS	
	STE	τ_{total}		STE	τ_{total}
θ_m=0,8	0,05	6,445625		0,05	6,456994
	0,1	3,3034375		0,1	3,315345
	0,2	1,732344		0,2	1,74513
	0,3	1,208647		0,3	1,21965
	0,5	0,7896875		0,5	0,79725
θ_m=0,5	0,05	10,205		0,05	10,25056
	0,1	5,215		0,1	5,228601
	0,2	2,72		0,2	2,725386
	0,3	1,888334		0,3	1,893433
	0,5	1,223		0,5	1,228487

Table F-10 Data for Figure 6.10

PRESENT RESULTS	
TOU	R
6,35E-02	0,891089
0,179092	0,792079
0,339443	0,693069
0,53499	0,594059
0,758376	0,49505
1,000159	0,39604
1,247358	0,29703
1,482919	0,19802
1,682245	9,90E-02
1,794355	0

GÜNERHAN [17]	
TOU	R
0,05323	0,9
0,17343	0,8
0,442	0,7
0,74835	0,6
1,00415	0,5
1,20561	0,4
1,35472	0,3
1,47129	0,2
1,55485	0,1

Table F-11 Data for Figure 6.11

PRESENT RESULTS	
TOU	R
9,48E-02	0,891089
0,248801	0,792079
0,453972	0,693069
0,700471	0,594059
0,98015	0,49505
1,280832	0,39604
1,586298	0,29703
1,875493	0,19802
2,11803	9,90E-02
2,252331	0

GÜNERHAN [17]	
TOU	R
0,07888	0,9
0,29601	0,8
0,67586	0,7
1,0054	0,6
1,27757	0,5
1,45347	0,4
1,6156	0,3
1,73066	0,2
1,81231	0,1

Table F-12 Data for Figure 6.12

PRESENT RESULTS	
TOU	R
0,166866	0,891089
0,399191	0,792079
0,696459	0,693069
1,04714	0,594059
1,43718	0,49505
1,849137	0,39604
2,261341	0,29703
2,646356	0,19802
2,964879	9,90E-02
3,1376	0

GÜNERHAN [17]	
TOU	R
0,081075	0,9
0,304043	0,8
0,679338	0,7
1,115322	0,6
1,5606	0,5
1,9117	0,4
2,164597	0,3
2,368048	0,2
2,470108	0,1

Table F-13 Data for Figure 6.13

	COMPLETE SOLIDIFICATION TIME (s)	
TENWF $(°C)$	ISMAIL&HENRIQUEZ [23]	COOL STORAGE TANK PROGRAM
-3	85090,91	80956,82
-5	53181,82	50038,66
-7	37963,64	36842,48
-10	26571,43	26877,75
-12	23142,86	22974,54
-15	19371,43	19048,11

Table F-14 Data for Figure 6.14

	COMPLETE CHARGING TIME (s)		
TENWF $(°C)$	ISMAIL&HENRIQUEZ [23]		COOL STORAGE TANK PROGRAM
	Numerical	Experimental	
-3	85909,09		81355,51
-5	55636,36		50715,85
-7	40418,18	39272,73	37695,11
-10	30171,43	28285,71	27997,14
-12	25371,43	24000	24204,41
-15	21428,57		20425,43

Table F-15 Data for Figure 6.15

	COMPLETE SOLIDIFICATION TIME (s)	
VOLFRWF (m^3/h)	ISMAIL&HENRIQUEZ [23]	COOL STORAGE TANK PROGRAM
0,5	45600	45241,01
0,7	35040	34794,03
1	26571,43	26877,75
1,3	22080	22556,07
1,5	19680	20613

Table F-16 Data for Figure 6.16

	COMPLETE CHARGING TIME (s)		
VOLFRWF	ISMAIL&HENRIQUEZ [23]		COOL STORAGE TANK PROGRAM
	Numerical	Experimental	
0,5	49200	47040	47095,84
0,7	37440	36000	36203,96
1	30171,43	28285,71	27997,14
1,3	24000	22200	23521,09
1,5	21600	19800	21510,58

Table F-17 Data for Figure 6.17

	COMPLETE SOLIDIFICATION TIME (s)	
KSHELL (W/m.K)	ISMAIL&HENRIQUEZ [23]	COOL STORAGE TANK PROGRAM
0,15	30560	30444,89
0,184	28800	29316,27
0,35	26571,43	26877,75
204	24160	24006,95
372	24160	24004,57

Table F-18 Data for Figure 6.18

	COMPLETE CHARGING TIME (s)	
KSHELL (W/m.K)	ISMAIL&HENRIQUEZ [23]	COOL STORAGE TANK PROGRAM
0,15	33360	32156,83
0,184	31760	30830,83
0,35	30171,43	27997,14
204	25440	24727,76
372	25440	24725,57